ABSTRACT

Title of Document: EFFECTS OF DEGENERATION AND LOAD HISTORY ON NUCLEUS PULPOSUS BEHAVIOR

David Hwang, Doctor of Philosophy, 2011

Directed By: Associate Professor Adam H. Hsieh, Fischell Department of Bioengineering

The nucleus pulposus (NP) plays a critical role in resisting loads placed on the spine, and therefore, the intervertebral disc. The function of the NP is to generate a hydrostatic pressure to evenly disperse the load within the disc. This ability hinges on the hydration of the disc, which is affected by age, health and even prior load history. This dissertation aims to elucidate key points about how the disc functions and reacts, both mechanically and biologically, to different sets of axial loading. We demonstrate our ability to create a degenerate disc model using trans-annular puncture in caudal rat discs and verify using viscoelastic analysis and histologic examination. Using a custom miniature fiber-optic pressure sensor, we determined the loss of pressurization in a degenerate versus a healthy disc. This compromised ability to generate an intradiscal pressure is essential, and indicates that a degenerate disc inadequately distributes the load and may lead to pain, injury and lack of function. We then investigated the influence of load history on the NP. Using a

preload placed on a disc beforehand, we change the hydrated state of the disc before the exertion load is applied. The viscoelastic creep response was analyzed and showed changes due to the addition of the preload. We also directly observed this change by using the miniature pressure sensors to measure intradiscal pressure during the loading regime. To further track changes caused by the introduction of a preload, we examined the gene expression of several associated extracellular matrix proteins after loading. The results demonstrate changing gene expression contrary to the expected outcome, given the understood pressurized cellular environment. We speculate that instead of a hydrostatic pressure driven response, the tonic environment dictated genetic upregulation. Using collaborative efforts, we assessed the ability to use Pneumatic Artificial Muscles as the actuating element in a long term loading device for caudal rat discs. In conclusion, we gathered new reactions from the NP given a variety of changed states, both diseased and loaded. Our new findings will help complete the picture to fully understand how the disc functions, specifically the response of the NP

EFFECTS OF DEGENERATION AND LOAD HISTORY ON NUCLEUS PULPOSUS BEHAVIOR

By

David Hwang

Dissertation submitted to the Faculty of the Graduate School of the
University of Maryland, College Park, in partial fulfillment
of the requirements for the degree of
Doctor of Philosophy
2011

Advisory Committee:
Associate Professor Adam H. Hsieh, Chair
Dr. Douglas Powell
Assistant Professor Sameer B. Shah
Professor Norman M. Wereley
Assistant Professor Ian M. White
Associate Professor Miao Yu

© Copyright by
David Hwang
2011

Acknowledgements

I first would like to thank my advisor Dr. Adam Hsieh who gave me the opportunity to join his lab after I was homeless, in the graduate school sense of the word. I am really appreciative of his guidance, through all the frustrations and struggles I put him through. I would like to thank Dr. Miao Yu for her generous support in the development and production of the pressure sensors. I would like to thank Dr. Norman Wereley for his patience with my slow moving development of using his PAM systems. I also want to thank the rest of my committee, Dr. Sameer Shah, Dr. Ian White and Dr. Doug Powell for their time, brain power and support of my efforts.

A big thank you of course goes out to the Orthopaedic Mechanobiology Lab: Hyunchul Kim for sticking with me and working things out with me the whole way. Alvin Yew for numerous doses of life saving Matlab "help." Anshu Rastogi, Julianne Twomey and Pratiksha Thakore for constant support and scientific soundboard. And also other members both past and present for the small things that get you through grad school.

I am also very grateful of my time spent in Intelligent Optics Lab, specifically Yuxiang Liu, Hyungdae Bae, Haijun Liu, and Felix Stief for hours of fiber optics help and letting me into the lab both earlier and later than they wanted to. I also want to thank the Smart Structures Laboratory, specifically Ryan Robinson for his quick construction to our needy demands to so many little PAM devices. I also want to thank Dawn Jackson and the veterinary staff for care of our rats, especially the surgery ones, and handling our constant rat orders. I am thankful for my short time

with Dr. Ghandehari and his lab. I also owe thanks to my previous mentor Dr. Tom Caperna who provided me with experience, and more recently, assay help and donating animal tissue.

I want to thank my family and friends who have been with me all along the way: All my boys from college who are already doctors of some kind. Andrew Dietrich, who despite my warnings, still went off the grad school. Jonny Lee, my PhD buddy who beat me to the finish (but I'm still trying to beat in page length). All my grad school buddies who have experienced the same hardships as me. A small thanks also goes out to PHD comics, whose humor has made grad school just tolerable enough to finish. And of course my girlfriend Carol Wong, for being there for me and especially for all the food she brought to feed me while I struggled with this dissertation.

Really, thank you to everyone who has been with me through this endeavor.

And most importantly, thank you to my funding sources who paid me and made it all possible: National Institutes of Health AR054051 (AHH) and Institutional support from the University of Maryland.

Table of Contents

List of Tables

List of Figures

Chapter 1 Introduction

The intervertebral disc (IVD) is a cartilaginous joint in the body responsible for flexibility and absorbing loads in the spine. The often described joint is referred to as a motion segment, consisting of two adjacent vertebrae with the IVD sandwiched between them. The disc is divided into three main portions: the nucleus pulposus (NP), the annulus fibrosus (AF) and the endplates. Unlike the more commonly thought of articular cartilage, the IVD has a very complex design. The NP makes up the gelatinous core, which consists of a viscous gel composed mainly of type II collagen and proteoglycans, primarily aggrecan[1]. The NP is then surrounded circumferentially by layers of fibrocartilage called the AF. The AF forms concentric lamellar rings, made with a greater concentration of type I collagen, around the NP[1]. The endplates form cartilaginous caps on the proximal and distal region of the disc and are considered path for nutrient transport. Due to the avascular nature of the disc, it must rely on simple transport phenomenon to diffuse nutrients from a relatively far distance. Much like the intricate nature of the structure, the cellular content of the disc is equally complex. The NP consists of chondrocytic cells as well as another type of cell of notochordal nature that begin to die off during human adolescence[1]. The AF contains cells that begin like chondrocytes in the areas towards the inner portion of the disc and become more and more fibroblastic as you radiate towards the outer edges.

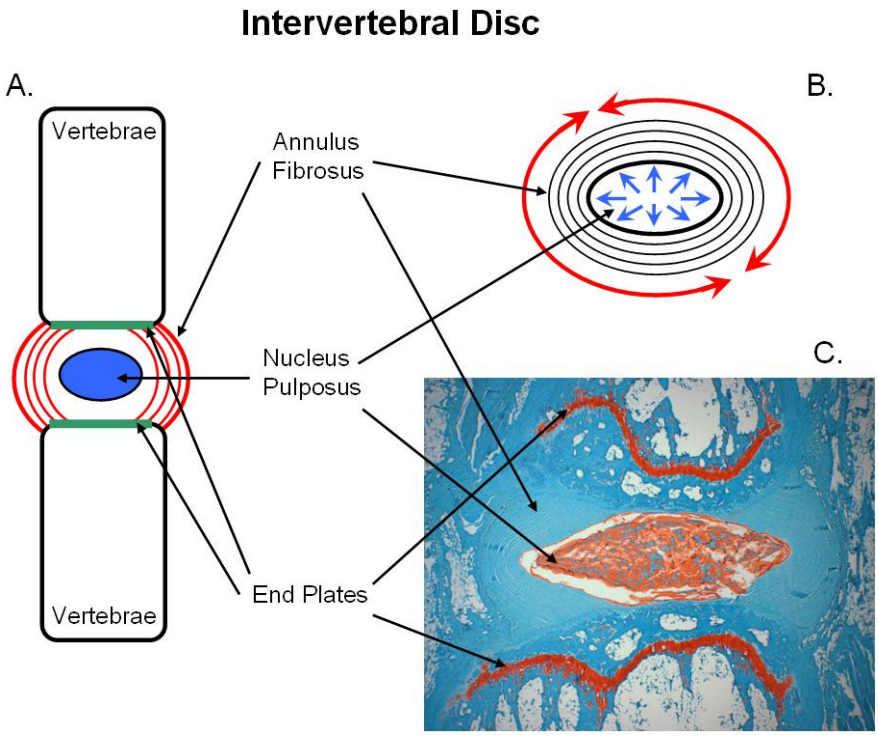

Figure 1.1 A front or sagital view of a caudal rat motion segment is shown in A. with the vertebrae, NP, AF and end plates labeled. In B. a transverse view of the disc shows the direction of the hydrostatic swelling pressure of the NP (blue) and the circumferential tension of the AF (red). Lastly, C. is a histological section of a caudal rat disc stained with Safranin O and Fast green. Proteoglycans are stained red, while collagen is counterstained blue and nuclei stained black.

The ability for the disc to resist loading is dependent on the disc's complicated structure. The gelatinous NP generates a hydrostatic pressure that evenly distributes the applied load equally in all directions. The lamellar rings of the AF then acts in tension, surrounding the NP and keeping the outward pushing force further diverted circumferentially. This unique structural function is dependent on the ability for each part to perform its job. Importantly, the NP must remain hydrated to be able to generate an intradiscal hydrostatic pressure. Hydration of the NP is dependent on extracellular matrix, as the NP is proteoglycan rich[1]. The glycosaminoglycans

abundantly attached to proteoglycans such as aggrecan, use its long, negatively charged, tightly packed nature to attract water molecules to help the NP swell.

As mentioned, this intricate joint system is dependent on the function of many parts, which are not without issues of health and age. Degenerate disc disease is an age related breakdown of the cartilage components in the disc. Beginning as early as adolescence[2], the human disc begins to slowly degenerate. Though not yet found as a direct cause, a high incidence of degenerate disc disease has been linked with nondescript low back pain. A condition that affects people from all walks of life, throughout the world[3]. This disease stems from a breakdown of both the AF and the NP. The AF under degeneration becomes more and more fibrous, and loses tensile properties. The lamellar rings that define the AF begin to crack and lose definition. This loss of structure causes severe impact on the function. Cellularly, the inner portion of the AF has displayed properties of both fibroblasts and chondrocytes, however, as the breakdown begins, even cells directly adjacent with the nucleus fibrosus become very fibroblastic. The NP almost undergoes a phase change, as the viscous gelatinous material firms up and becomes a more solid fibrous material. The extracellular matrix breaks down, as the proteoglycans are broken down, with the glycosaminoglycan chains cleaved[2]. The type II collagen nature of the NP begins to shift towards a type I collagen dominance. Because of the proteoglycan breakdown, the swelling capacity of the NP is severely damaged. Instead of a hydrostatic pressure that evenly distributing load, the NP has a more solid core, which creates uneven pressure peaks throughout, which are notably higher and cause uneven loading[4]. As a representative figure, in juveniles, the proteoglycan accounts for 70%

dry weight of the NP, but falls dramatically to 20% in mature adults[5]. Using this loss in hydration, MRI's have been used as a detection tool, imaging the water concentration in the disc and quantifying the intensity or lack thereof as an early sign that can be detected without invasive procedures[6-9]. As a part of the degenerating NP, the presence of notochordal cells lessens as chondrocytes take over, but also slowly die off until the NP becomes acellular. It is unclear whether notochordal cells die off due to degeneration or that their disappearance is the cause of degeneration. Mechanically, the loss of hydration stiffens the disc significantly, does not allow the disc to swell and respond to applied pressures. Overall, the breakdown compromises all aspects of the disc and changes how the disc is able to function. Studies suggest that the stiffer NP may even transfer the load to the AF, changing the circumferential tensile rings to more of an axial loaded column[10]. As it is briefly mentioned, the process of degeneration is complicated and is not fully understood. In conjunction with understanding disc degeneration and breakdown, further research must also be done to more thoroughly investigate the behavior of the healthy disc as well.

One lesser understood phenomenon regarding disc mechanics is the concept of load history and its effects on how the disc responds after certain loading scenarios. In the past, most loading experiments that track past loading are part of long term force application using cyclic loading[11-14]. However, the concept of load history considers that a prior load will affect how the next load is responded to on the basis of constant changing hydration of the disc. Early exploration of this concept was only in extreme cases, as the behavior of hydrated, superhydrated and dehydrated discs were compared[15]. Only after a number of dynamic loading experiments

presented unexpected gene expression results was it suggested that load history, specifically immediate prior loading conditions, may be a significant factor to consider[16]. Hydration in the disc may be lessened or compromised after even a small load, will affect the disc's response to a larger load after, unless there is ample time for recovery. While the concept is simple in nature, the biological components of the disc make it more than trivial to fully understand.

It is clear that the NP is an important aspect of the disc, and while the general mechanics and abilities of the NP is understood, many of the nuances and causes for responses are not yet known. Further research is necessary to fully understand the individual aspects of the disc and what it is responsible for biologically. Without this understanding, we have an incomplete picture of what the disc, or NP does. A unifying theme was presented to us for exploration, as the concept of specifically NP hydration was omnipresent in all aspects of disc function and behavior. The breakdown of the extracellular matrix caused by protease breakdown as well as lack of production all lead to the compromise of the disc's swelling capacity. The retention of water after prior loading is the cause of differing mechanical response of the disc given equal loading scenarios.

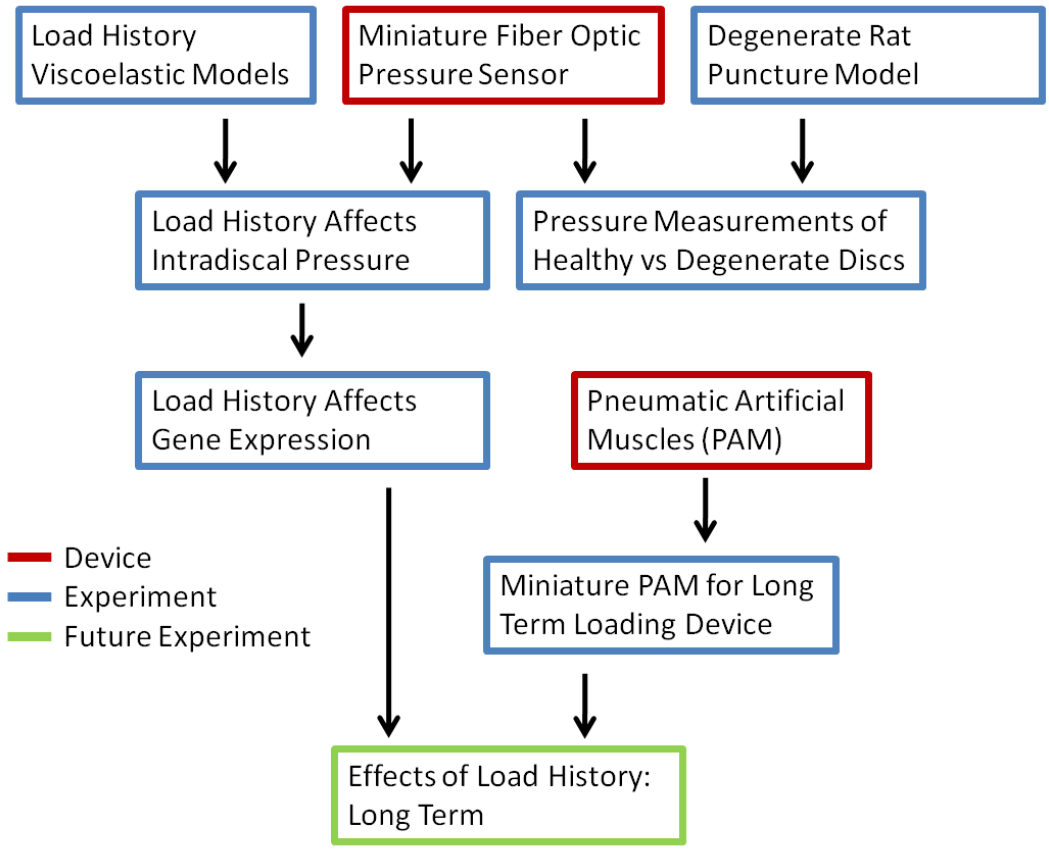

Figure 1.2 A general flow of the experiments. The new technologies are represented in red show collaboration with an existing lab with a unique device that was adapted for our purposes. Blue represents completed experiments that will result in publication. Green represents potential experimental pursuits.

To this end, the hydration is the focus of the studies that compose this dissertation. We began by establishing a degenerate disc model using a trans-annular puncture in a rat tail disc. Analysis of the viscoelastic creep response and the overall histology of the disc, degeneration was verified for each experimental method. The verification of our degenerate model allowed for further investigation of the degenerative process and effects on hydration and mechanics. In conjunction with the Intelligent Optics Lab, a miniature fiber-optic interference based pressure sensor was developed to measure the intradiscal pressure generated in the NP. Using our

verified degenerate disc model, and our uniquely small pressure sensor, we were able to measure the pressure generation of the disc under loading conditions. With this, we were able to compare the applied load to the generated pressure, for both healthy and degenerate discs. This further verified our degenerate model, as results paralleled past human and pig studies. Additionally, further knowledge was gained about the pressurization of the disc, allowing the possibility to predict the intradiscal pressure during specific loading conditions. To gain a better grasp of the hydration and load history, a study was performed to monitor the mechanics of the disc given specific load histories. This study then discovered subtle changes in behavior by fitting the standard solid viscoelastic model to the creep response caused by prior load history. In addition, a fluid transport model, created specifically to model disc behavior also showed changes in response, due to load history. This model suggested physical parameters that played critical roles in this changing behavior, one of which was the importance of the intradiscal pressure. To further pursue this point, another intradiscal pressure experiment was conducted to measure the effects of load history. After having documented the pressurization response in the NP given specific loading regimes, the biological response of these load histories were also investigated. By knowing key information about the physical environment the cells were exposed to, learned in previous experiments, the biological response through gene expression could be linked to these environmental factors. The loading regimes for the differing load histories were limited to short durations due to the *in vivo* nature and the time limit on anesthesia, so a long term *in vivo* loading device was developed. In order to create a lightweight, appropriately sized apparatus, the Smart Structures Laboratory

developed a mini-pneumatic artificial muscle to function as the actuating component in our loading device. Experiments were done to characterize and optimize components for the *in vivo* loading device, which will be used in the future to apply long term loading regimes on caudal rat discs. The aims of this set of experiments is to further enlighten the function and behavior, both mechanically and biologically of the disc. The general outline of research is shown in Figure 1.2. The central theme of hydration is shown to be the dictating cause of disc behavior, for healthy and degenerate discs, as well as those with differing load histories.

The presented research will offer another critical step in filling the gap of knowledge towards fully understanding the disc. Load history is a critical aspect that has only begun to be explored, but has a huge impact on what we know about the disc. The NP serves as a main portion of the puzzle that needs to be solved, and further exploration of how cells dictate and regulate the extracellular environment will also play a pivotal role in the future advancement of IVD therapies. The field of IVD research lags behind the overall study of cartilage and joints; and is currently stalled. We currently have a superficial understanding of the main components of the disc, and while some research has moved on towards more direct application of that knowledge in the form of implants, procedures and therapies, they have been met with only marginal success by researching the specific point they need. Basic scientific research about the details of function, response and behavior needs to reach a critical point before it completes a picture and allow for research to move on. The knowledge gained about the NP in this research shows the impact of the changing hydration. This impact affects the general intradiscal response, the cellular

production and the interactions with other parts of the disc. Research is incremental, and this provides another step of knowledge in completing the picture, and providing better methods and a more holistic approach for developing IVD therapies.

Chapter 2 Degenerative Changes Induced by Intervertebral Disc Puncture are Associated with Sufficiency of Biomechanical Function[1]

Numerous studies have been performed to outline the ability to induce degeneration in a variety of animal models. These studies have shown a varying degree of success using a wide variety of procedures. The motivation behind this experiment was to establish reliable procedures in our laboratory to induce degeneration in a caudal disc in the rat model. We will investigate our puncture method and link the degenerative cascade to a compromise in the biomechanical function. Secondarily, through changes in biomechanical function after puncture, we hoped to further elucidate the effects on the disc given smaller punctures, as many other procedures call for the injection or insertion into the disc.

2.1 Introduction

A variety of diagnostic, therapeutic, and basic research strategies to study degenerative disc disease (DDD) involve experimental procedures that compromise the integrity of the anulus fibrosus (AF), as well documented in a review by Elliott *et al.*[17] For instance, stress profilometry has been performed in human discs *in vitro*[18-21] and *in vivo* intradiscal pressure has been measured in both humans[22-29] and animals,[30-35] including rodents. Since the biomechanical function of individual disc subregions are inter-related, the act of sensor insertion must not induce compromise the ability

[1] As published in AH Hsieh, D Hwang, DA Ryan, AK Freeman, and H Kim. Degenerative Changes Induced by Intervertebral Disc Puncture are Associated with Sufficiency of Biomechanical Function. SPINE (2009). 34(10): 998-1005.

for the disc to pressurize. Importantly, in human studies minimization of AF injury should be considered so as not to alter disc mechanics.

Similarly, efforts to explore potential therapies, such as growth factor injection,[36-39] gene therapy,[40-43] and introduction of stem cells,[44-49] all require a trans-anular approach. While most of these *in vivo* studies utilize rabbit models, several have used rodents.[39, 40, 48, 49] Because the efficacy of all such regenerative therapies could be affected by the cells' mechanical exposure, the ability for the disc to pressurize to physiologic levels may be desired.

Finally, anular injury has been used to induce simulated degeneration in various *in vivo* animal models, to investigate the etiology and mechanisms of DDD. Trans-anular approaches have been used to inject enzymatic agents for chemonucleolysis in several animal species,[33, 50-58] including rodents.[59-61] It has been suggested that digestion of proteoglycans induces nucleus pulposus (NP) depressurization and loss of tensional stress in the AF, resulting in altered disc mechanics[33, 51, 62, 63] and, subsequently, degeneration. Another approach to effect degeneration has been partial or full anular stab injury, which also has been used in a variety of species.[64-72] While both single and multiple stabs have been employed,[67, 70, 72-74] it remains unclear whether degenerative changes are caused by the act of injury itself, or by the resultant change in the disc's biomechanical function.

Motivated by this lingering question and by the need to establish limits on needle size for intradiscal procedures in rats, we sought to determine in this study the impact of anular injury size on the initiation of degeneration and biomechanical function of rat caudal discs. Specifically, we used a combination of histologic

observation from *in vivo* experiments and *in vitro* characterization of disc creep behavior before and after hypodermic needle puncture of the AF. Since disc mechanics depends on interstitial fluid flow, osmotic pressure, and intrinsic viscoelasticity of the extracellular matrix,[75-79] we hypothesized that alteration in disc mechanics would depend on injury size. Furthermore, since experimental studies have found that different sized anular injuries produce varying degrees of degeneration,[67, 70] we secondarily hypothesized that there is a relationship between biomechanical function and susceptibility to disc degeneration. This study found that puncturing discs with an 18g needle significantly compromised the behavior of the disc due apparently to extrusion of the nucleus pulposus, and this was statistically associated with induction of degenerative anular changes *in vivo*. Our results will be important for reconciling findings from other studies that use a trans-anular approach in rats, and for our experiments that involve invasive techniques to measure intradiscal pressure.[34, 35]

2.2 Methods

2.2.1 Surgical procedure

Forty-eight retired breeder (6-9 mo) Sprague-Dawley rats (Taconic Farms, Germantown, NY) were obtained and sacrificed, following approval from the Institutional Animal Care and Use Committee at the University of Maryland, College Park. Of the 36 rats used for *in vivo* disc degeneration experiments, twelve were allocated for 18g needle puncture, nine for 22g puncture, and twelve for 26g puncture. These were then evenly distributed among three time points (1, 2, and 4

weeks). The remaining three rats were used for a 4 week sham control group. Rats were anesthetized using isoflurane and the c6-7 motion segment identified, marked, and confirmed using radiography. The diameters of the tail at the puncture site were measured with calipers to determine the necessary depth of needle insertion, and then the site of puncture was scrubbed with betadine and isopropyl alcohol. Sterile hypodermic needles of the appropriate sizes were carefully inserted with the taper of the needle along the axial direction of the tail. Film radiographs were taken after puncture to ensure proper insertion (Faxitron, Wheeling, IL). For sham surgeries, needles were inserted to a shallow depth in order to puncture the skin but leave the disc uninjured. After surgery, rats were revived and returned to normal cage activity with daily observation for pain and distress, which were absent for all rats.

2.2.2 Mechanical testing

The remaining 12 rats were euthanized, and coccygeal motion segments c6-7 and c8-9 were carefully dissected free of all surrounding soft tissues to expose the intervertebral discs, yielding a total of 24 specimens. Specimens were immediately frozen and maintained at -20°C. Six specimens were allocated to each of four groups: 18g, 22g, and 26g anular puncture, and a non-puncture control group. On the day of testing, motion segments were thawed at room temperature in a PBS bath containing protease inhibitors. Using custom-made fixtures, vertebrae were then embedded in cement (Fastray, Harry J. Bosworth Co., Skokie, IL) and mounted on a Bose Electroforce materials testing system (LM-1, Bose Corp., Eden Prarie, MN). Once

mounted, specimens were submerged in a room temperature protease inhibitor solution.

Specimens first underwent a compressive tare load of 0.003 MPa (0.04 N) until equilibrium was reached (900 sec). They were then subjected to identical intact preconditioning procedures by exposing discs to six consecutive creep compression cycles, each consisting of a 15 minute 0.3 MPa loading phase followed by a 30 minute 0.003 MPa relaxation phase. This protocol was designed based on using load levels approximating 1x body weight and on pilot experiments demonstrating reproducible creep behavior after 6 cycles of loading. For each specimen, the 7^{th} cycle of creep represented the mechanical behavior before anular puncture. Following the 7^{th} cycle of creep and relaxation, the position of the motion segment was held constant for 5 minutes. During these 5 minutes, the PBS bath was drained, and the AF was punctured, in a similar manner as *in vivo* studies, to a depth equal to one-half the measured disc diameter using a micrometer. The PBS solution was immediately replaced. Control motion segments were subjected to the same static phase and PBS removal/replacement. An 8^{th} and final cycle of creep and relaxation was subsequently performed to measure the effects of anular puncture. Representative data are shown in Figure 2.1.

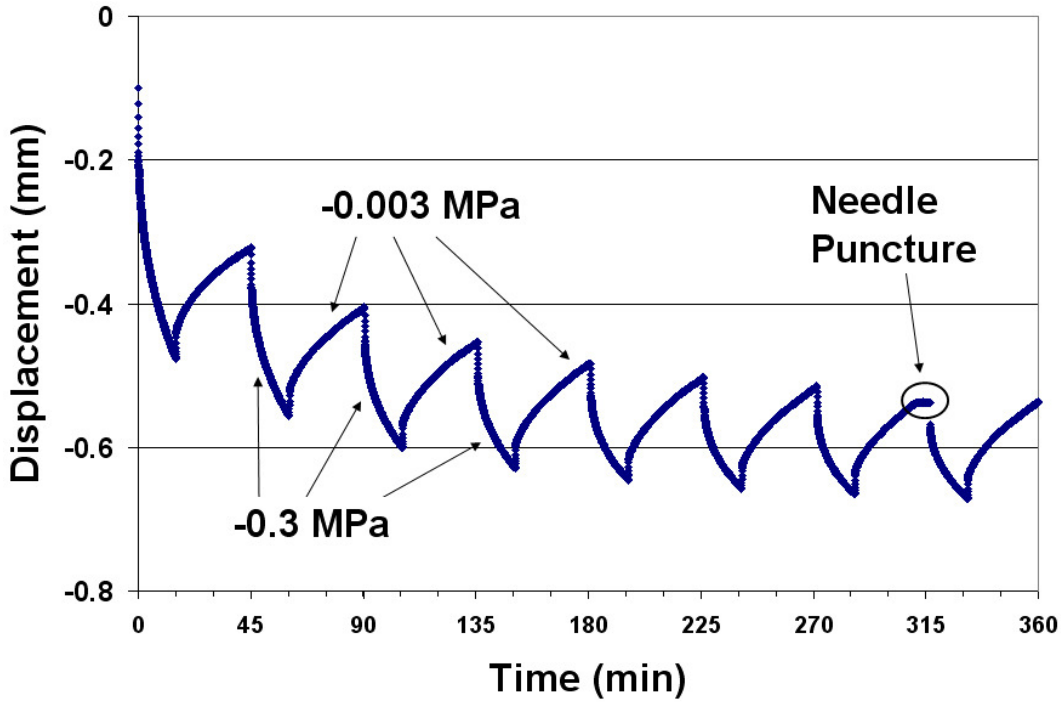

Figure 2.1 A representative graph of compressive creep displacement illustrating the seven 15 minute creep-30 minute recovery cycles. Following the 7th recovery period, the displacement was held fixed while the disc was punctured. The specimens were then subjected to an 8th cycle of creep-recovery.

2.2.3 Histology

Following euthanasia (in vivo experiments) and mechanical testing (in vitro experiments), specimens were fixed in formalin, decalcified in a solution containing 10% (w/v) sodium citrate and 20% formic acid, then processed for paraffin embedding. Tissues were then sectioned at 6μm using a microtome. A series of sagittal sections were stained with Safranin O/Fast green and inspected under light microscopy (Olympus America Inc., Center Valley, PA). The existence of anular degenerative changes were assessed by three independent observers.

2.2.4 Data analysis

Experimental data were fit to two different analytical solutions that have previously been used to describe creep compression. The first is a stretched exponential function:[80, 81]

$$\varepsilon(t) = \varepsilon_\infty + (\varepsilon_0 - \varepsilon_\infty) \times \exp\left[-\left(\frac{t}{\tau} \right)^\beta \right] \qquad (1)$$

where the stretched parameter, β, and time constant, τ, are used to describe the transient compressive behavior, and ε_0 and ε_∞ are the initial and equilibrium displacements, respectively. We calculated a value, ε_{eff}, to represent the difference between ε_0 and ε_∞ and corrected for estimated vertebral body deformations.[81]

The second is a model developed from fluid transport phenomena in different disc subregions:[82]

$$\varepsilon(t) = \varepsilon_0 + \left(\frac{\sigma_0 - P_0}{D} - \frac{h_i G}{2kD^2} \right) \times \left[1 - \exp\left(-\frac{2kDt}{h_i} \right) \right] + \frac{G}{D} t \qquad (2)$$

where the compaction of the nucleus pulposus is represented by D, the contribution of anular tension by G, and the permeability of the endplate by k. Constants were the initial disc height, h_i, applied creep load $\sigma_0 = 0.3$ MPa, and estimated nucleus swelling pressure $P_0 = 0.1$ MPa. Parameters were obtained for each of the eight cycles of every specimen by curve fitting the experimental data with Equations (1) and (2) using MATLAB (The Mathworks, MA). To account for inter-specimen variability, two ratios were calculated comparing the behavior of cycle 7 (before puncture) to cycle 6 (end of pre-conditioning), and comparing cycle 8 (after puncture) to cycle 7 (before puncture).

2.2.5 Statistical analysis

Ratio data were logarithmically transformed to improve normality, and the transformed data statistically analyzed using a General Linear Model and Fisher's LSD post-hoc tests in SPSS 14.0 (SPSS, Inc., Chicago, IL). In all analyses, critical significance levels were set to $\alpha = 0.05$. For all graphs, data are expressed as mean ± SEM. To test whether there was an association between change in biomechanical function and degeneration, we established two categorical variables indicating the presence or absence of biomechanical effect and presence or absence of AF degenerative changes. A 2x2 contingency table was then constructed based on histologic observation of *in vivo* experiments. A Fisher's exact test for independence[83] – suitable for small population data sets – was used to test whether an association exists between puncture size and degenerative change.

2.3 Results

2.3.1 Anular degenerative changes induced by anular puncture

Histology of punctured discs demonstrated marked differences in anular appearance among needle sizes (Figure 2.2). In 18g specimens, obvious needle tracks, accompanied by inward bulging of the AF on the side of puncture, presence of multiple-cell chondrons, and NP extrusion into the intralamellar space were evident in 1 week specimens and persisted through 2 weeks (Figure 2.3). At 2 weeks, increased Safranin-O stained chondrons were present in the inner half of the AF, together with

increasing lamellar disorganization. By 4 weeks, evidence of needle tracks was almost non-existent, and chondrocyte-like cell population and lamellar disorganization were enhanced. In two of the 12 specimens (one at 2 weeks, one at 4 weeks), no evidence of needle tracks or degenerate changes were observed. Punctures with needle sizes of 22g and 26g showed faint signs of needle tracks at 1 week, but no discernable signs by 2 weeks. Very little change in the lamellar appearance of the AF was observed over the course of 4 weeks except in 3 of the 21 specimens. In all of the degenerate specimens, the NP possessed large voids, even at 4 weeks. Presumably, these voids represent NP tissue that had extruded out and filled with other cells/tissues, which were lost in the fixation, processing, and sectioning steps. Interestingly, the small portions of NP tissue that remained appeared to contain morphologically healthy chondrocyte-like cells.

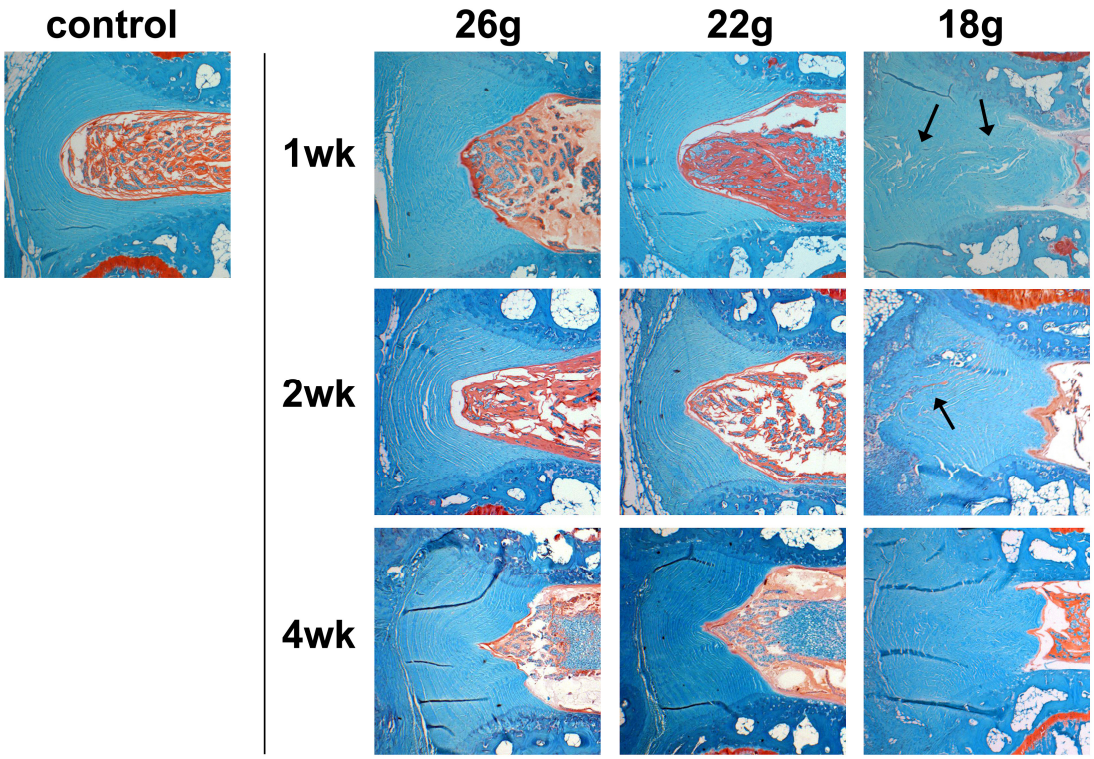

Figure 2.2 Overview of morphologic observations of AF in punctured discs. Except in three discs, all 22 and 26g punctured discs resembled those shown. No needle tracks could be definitively identified at any time point. Loss of significant amounts of nucleus pulposus in 18g punctures led to inward bulging within 1 week, resulting in degenerative changes in the AF. Needle tracks were evident in 1 and 2 week specimens, but not at 4 weeks.

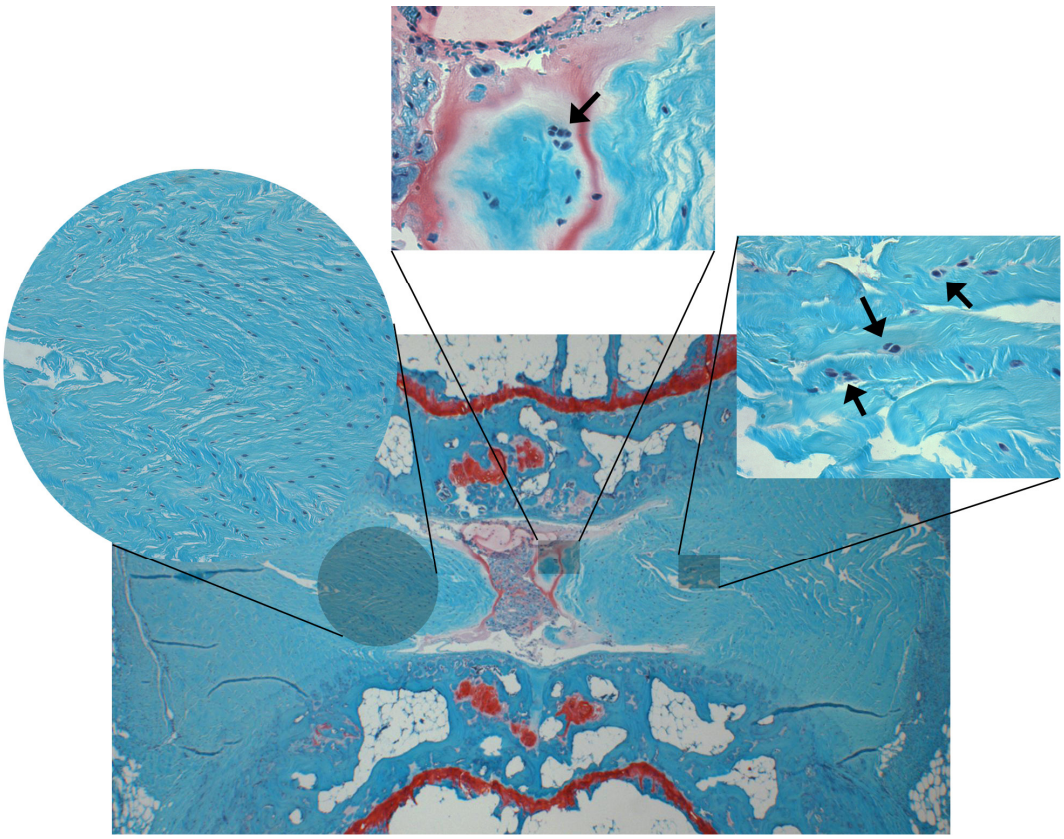

Figure 2.3 Higher magnification of selected areas in the 18g punctured disc, showing inward anular bulging, distinct needle track, presence of multiple-cell chondrons in the margins of the NP and within the AF (arrows), and disruption of lamellar structure (circular inset).

2.3.2 In vitro biomechanical testing

During preconditioning (cycles 1-6), each parameter exhibited progressive changes that leveled off by the 6th cycle (Table 2.1), consistent with our pilot experiments. Between preconditioning and the first test cycle (cycle 7), ratios of values for each parameter were close to unity, indicating very little change (Figure 2.4). No statistical differences among groups were detected ($p > 0.25$).

After puncture, there were statistically significant effects due to treatment (Figure 2.5) for parameters τ ($p < 0.005$), ε_{eff} ($p < 0.05$), G ($p < 0.005$), and k ($p < 0.01$). Pairwise comparisons revealed that, for all four parameters, differences were

statistically significant between the 18g group and every other group. No combinations of control, 26g, and 22g pairwise comparisons possessed any statistically significant differences ($p > 0.25$). The most profound changes were in parameters τ and k, which decreased and increased approximately 80%, respectively. Parameter D exhibited trends of decreasing values with increasing puncture size, while β did not show any identifiable trends.

Table 2.1 Average parameter values obtained from creep data during preconditioning for all motion segments tested (n = 24)

Parameter	Cycle 1	Cycle 2	Cycle 3	Cycle 4	Cycle 5	Cycle 6
β	0.537 ± 0.008	0.551 ± 0.007	0.545 ± 0.008	0.542 ± 0.007	0.533 ± 0.007	0.531 ± 0.007
τ (x10^3 sec)	3.186 ± 0.337	5.573 ± 0.499	5.283 ± 0.413	5.109 ± 0.415	5.472 ± 0.459	5.224 ± 0.389
ε_{eff}	0.296 ± 0.011	0.358 ± 0.016	0.366 ± 0.019	0.369 ± 0.019	0.376 ± 0.021	0.378 ± 0.022
D (N/mm)	1.999 ± 0.078	3.111 ± 0.124	3.608 ± 0.146	3.954 ± 0.171	4.346 ± 0.202	4.554 ± 0.220
G (x10^{-4} mm^2/s)	3.383 ± 0.045	3.913 ± 0.065	3.881 ± 0.051	3.805 ± 0.067	3.867 ± 0.065	3.877 ± 0.065
k (x10^{-4} $mm^3/N.s$)	18.54 ± 0.741	11.91 ± 0.536	10.49 ± 0.547	9.623 ± 0.513	9.152 ± 0.521	8.961 ± 0.549

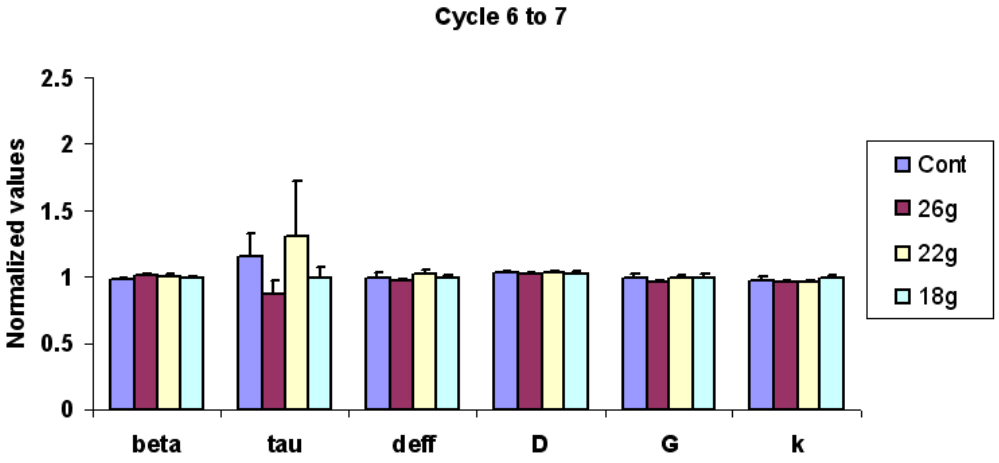

Figure 2.4 Changes in parameter values from preconditioning to the pre-puncture cycle expressed as a ratio of cycle 7:cycle 6. For the most part, changes in parameter values were small, with the exception of τ, which exhibited the highest sensitivity in curve fitting procedures. Statistical analyses found no significant differences among groups in any of the parameters. Data are represented as mean ± SEM.

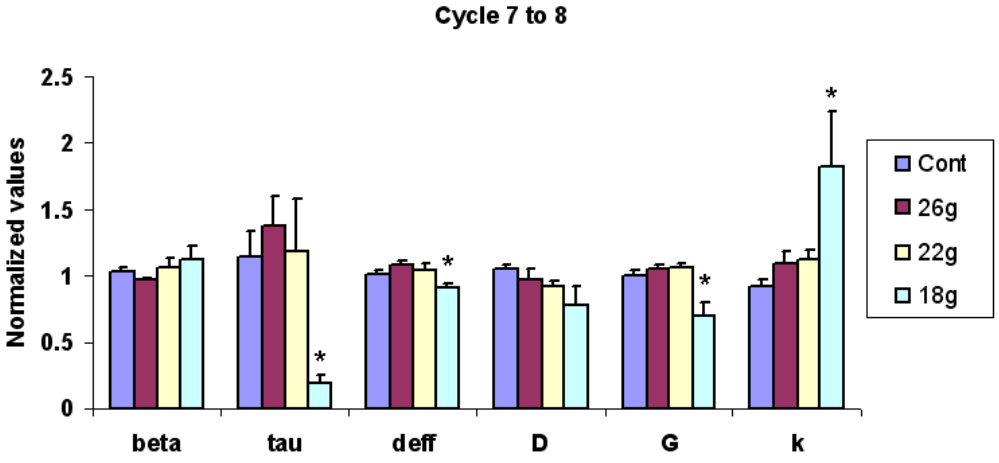

Figure 2.5 Changes in parameter values with puncture expressed as a ratio of cycle 8:cycle 7. Dramatic changes were induced in creep behavior after puncture using 18g needles, as illustrated by the large changes in parameters. Statistical analyses found no significant differences among groups in any of the parameters. Data are represented as mean ± SEM.

Histology of motion segments after testing provided information on extent of anular damage and extrusion of NP with creep compression. Non-punctured control discs possessed an intact NP with some damage to parts of the AF that likely occurred during testing (Figure 2.6a). With 26g punctures, only small voids in the nucleus were observed, and needle tracks were found to have collapsed presumably under loading (Figure 2.6b). A greater loss of nuclear material, collapse of disc height, and more anular damage were evident for punctures using 22g needles (Figure 2.6c). The most dramatic effects were found for 18g needle punctures, in which the majority of nucleus was extruded, and wide needle tracks were clearly present (Figure 2.6d).

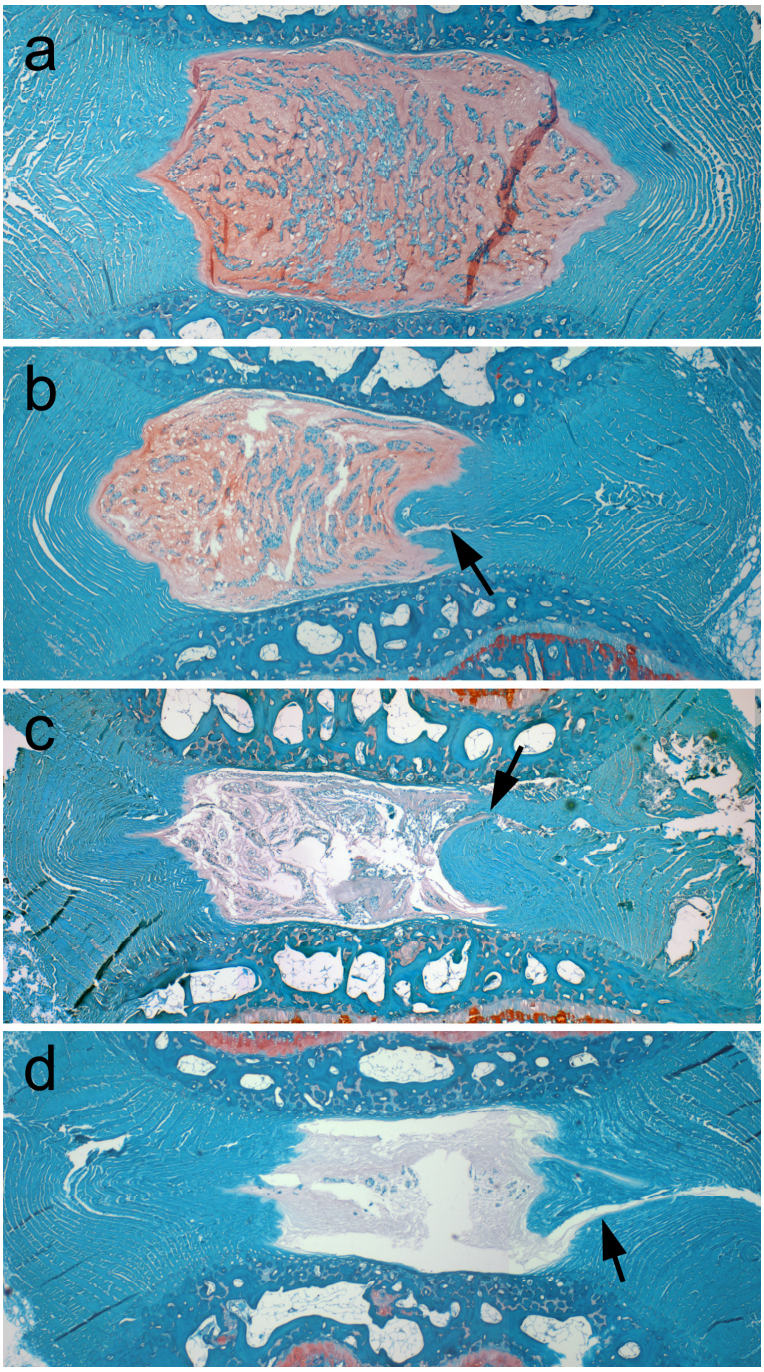

Figure 2.6 Histological sections of the tested motion segments provided insight into the potential mechanisms of altered biomechanics. The nucleus was intact for (a) control specimens. With anular puncture using (b) 26g, (c) 22g, and (d) 18g hypodermic needles, progressively increasing amounts of anular damage and loss of nuclear material were observed. Arrows point to needle tracks caused by anular puncture.

2.3.3 Test for association between compromised biomechanics and degenerative changes in AF

A contingency table was created (Table 2.2), where degeneration status of the AF of each disc was categorized according to the ability of the needle size to influence biomechanical function. Analysis revealed a statistically significant association between induction of degenerative changes in the AF and needle puncture sizes that compromised biomechanical function ($p = 0.00016$).

Table 2.2 Contingency table used for testing statistical association between biomechanical effect and induction of degenerative changes in AF

Biomechanical effect?	**Degenerate changes in AF?**		
	No	**Yes**	**Totals**
No (22g, 26g)	18	3	21
Yes (18g)	2	10	12
Totals	20	13	33

Fisher's exact test for association; $p = 0.00016$

2.4 Discussion

This study demonstrated that hypodermic needle puncture in rat caudal discs can lead to morphologic changes in the AF, and that induction of these changes depended on the size of the defect being large enough to affect disc creep behavior. Statistical tests found significant association between degenerative AF changes and needle sizes that affected biomechanical function. Our findings reinforce recent opinions about the importance of impaired biomechanics in contributing to degeneration.[84]

Observations of puncture size-dependent alterations in creep could be reconciled by histology of discs after biomechanical testing. The striking disruption of the AF with 18g puncture showed NP herniation with low loads, and likely increased transport characteristics as well, resulting in increased effective permeability, k, and decreased τ. Collapsed needle tracks found in disc histology effectively sealed 22 and 26g punctured AF and minimized NP loss, suggesting that the NP's ability to pressurize had not been compromised. Interestingly, the graded decrease in parameter D, which represents a diminishing role of swelling pressure of the NP, is consistent with needle size, in agreement with previous studies on partial and full nucleotomy of ovine discs.[85] The capability for collapse of puncture wounds may explain why needle tracks could not be found in 22 and 26g punctured discs at one week *in vivo*. Perhaps closely apposed tissue is more readily repaired than a larger defect that contains extruded NP.

Our results also suggest puncture size is an important determinant of AF degenerative changes; trans-anular injury, alone, is not sufficient. This size-dependence is consistent with other reported studies on the effects of AF injury. Three separate groups recently reported that 18g and larger hypodermic needles were required to induce degeneration in rabbit lumbar discs.[67, 70, 72] One of these studies also found that performing three simultaneous 21g needle punctures or manual NP aspiration through a 21g needle could generate similar degrees of degeneration.[67] Their use of a 23g needle puncture for injecting an apoptosis-inducing agent had no effect.

Biomechanically, Cowgill and colleagues reported that the force needed to cause NP extrusion after anular puncture of rabbit spinal discs varied inversely with needle size for 16, 18, and 20g needles in a graded fashion.[86] While their average stress for herniation was 0.7 MPa for 18g punctures (as computed based on rabbit disc cross-sectional areas published elsewhere),[87] we found NP extrusion in 18g discs at only 0.3 MPa creep compression. Size, species, anatomic location,[88] and loading profiles are several differences that may have contributed to our smaller extrusion loads.

These observations of herniation are consistent with the notion posed by Elliott and colleagues, that the ratio of puncture size to disc height may be a determining factor for altered mechanical properties.[17] However, we observed no effect for 22 and 26g needles, where they found that smaller 27g needles led to significantly lower compressive, tensile, and neutral zone stiffness in rat lumbar discs. Outer diameters for 22 and 26g needles are, respectively, greater than and equal to 40% of our measured average caudal disc height of 1.16mm, over the suggested threshold for biomechanical effect. A large part of the discrepancy in our results may be due to testing procedure. Allowing specimens to swell with extended incubation in PBS followed by cyclic loading prior to testing may lead to larger effects due to needle puncture.

Another study by Korecki *et al*. examined the effects of 14g and 25g needle puncture of bovine caudal discs in organ culture.[89] In contrast to both studies, they found marked changes in disc mechanics not only for 14g but also for 25g needles, which are only approximately 8% of disc height. For both puncture sizes, the needle

track remained evident in the tissue after 6 days and mechanical response was exacerbated with culture duration. Interestingly, no changes on cell viability, water content, or GAG loss were observed. Greater compressive stress (0.6 MPa time-averaged sinusoidal loads) as well as incubation and loading treatment after puncture may partially account for differences. Taken together, these data suggest that the immediate biomechanical stability of the injured disc, and not its performance under repetitive loading post-trauma, may be a good indicator the development of degenerative changes in the AF.

To the authors' knowledge, this is the first reported study that statistically links the biomechanical consequences of puncture alone to biological outcome *in vivo*. Specifically, our data suggest that immediate stability of the punctured motion segment may be important for the ability of the disc to retain NP and exhibit functional healing. An advantage for using rat caudal discs in this study is that the influence of injury is less likely to be confounded by *in vivo* loads, which could be greater in the spine and in larger species. However, this analysis is limited by not using the same specimens for *in vivo* studies and biomechanical testing. Our rationale for using separate specimens was not to exacerbate the injury artificially by external forces. With these experiments as a baseline, we can look more closely at these potential interactions between injury and loading *in vivo*, and potentially use intradiscal pressure as a way to validate our theory that pressurization of the NP is critical for AF homeostasis. Another limitation is the mode of mechanical testing, which was greatly simplified as axial creep compression. Motion segment bending is likely of equal, if not more, importance in rat caudal discs. Having the puncture on

the convex side of bending would likely facilitate NP herniation. Despite these limitations, results from this study provide a context for interpreting previous studies and a framework for the design of future experiments involving trans-anular procedures.

Chapter 3 Intradiscal Pressure Generation in a Degenerated Intervertebral Caudal Rat Disc Model

The changes described in a degenerate disc are well documented, in both histology and viscoelastic behavior. The pressure generation in human and large animal models such as the pig has also been explored, for both healthy and degenerate specimens; however, the intradiscal pressure generation within small animal models such as the caudal rat disc has long eluded researchers due to the small size and a lack of properly sized pressure sensors. Our recent development of a miniature fiber optic pressure sensor has granted us the ability to investigate the intradiscal pressure within a caudal rat disc. This study measures real physical observations of pressurization in the disc, between the more common rat model and the more physically relevant larger animal models. This comparison between the rat model and the pig or human model is able to bridge the gap between the more widely studied basic science learned from the rat model and pressure measurements and physical relevance of the human disc.

3.1 Introduction

The intervertebral disc (IVD) is an important component in the spine, responsible for the much of the body's flexibility and load bearing, specifically in the spine. As a part of a spinal motion segment, the disc acts as a flexible cushion that is able to absorb loads place on the spine. This load bearing property, also the flexibility to an extent, is dependent on the relative health and ultimately hydration of the disc. Concerns of disc degeneration stem from deteriorating extracellular matrix

(ECM) within the IVD, including disarray of the annulus fibrosus (AF), as well as stiffening of the nucleus pulposus (NP). Degenerate disc disease is a condition that affects people all over the world, most often experienced as generic low back pain. The IVD is one of the few avascular parts of your body, so the cells present in the disc do not have sufficient nutrient flow. In this regard, they are then unable maintain, remodel and rebuild the slow breakdown of the extracellular matrix as well as continue to support cell growth. Researchers are still unsure the true cause of this degeneration, so it is important to continue to investigate how it begins before we will be able to prevent it.

One critical aspect of the biomechanics of the IVD is the ability to resist loads. This property stems from the gelatinous core, the NP. The NP is able to generate an intradiscal hydrostatic pressure which absorbs and evenly distributes the load within the confines of the AF,. Many researchers have focused on intradiscal pressure generation as it a critical property that is required to dispersing the load. Without the hydrostatic pressure generation, uneven pressure spikes are created within the disc and result in irregular pressures and shears that may cause injury[90]. A loss in pressurization is also closely related to the degeneration of the disc, and may be one of the biggest factors towards a disc's failing mechanics. Early on, this pressure has been documented by Nachemson et al. monitoring pressure generation in human discs with patients in specific postures[91, 92]. Other investigations have followed, monitoring the intradiscal pressure within pigs, rabbits and rats[32, 93-95]. Progress in these research models have linked pressure generation with biomechanical function. Additionally, pressure generation has been seen to be

heavily dependent on hydration, which again, is associated with the breakdown of extracellular matrix, and therefore disc degeneration[75, 96]. This pressure generation is a critical part of healthy disc function, and decreases greatly as degeneration occurs[4]. Compromised IDP generation has long been documented within the human disc[10, 91]. As the NP stiffens, the overall pressure generation decreases, while increasing certain areas with pressure spikes of uneven pressure, which lead to other problems, such as bulging and herniation[97].

Several different animal models have been developed for studying the initiating factors involved in degenerative disc disease. While human samples provide greater relevance to the etiology of disc degeneration, source material is often limited, are suitable only for certain types of studies, and cannot provide mechanistic insight into the early stages of degeneration. Many animal models have also been used to induce degeneration, both large animals, such as goats, cows, sheep and pigs, as well as small animals, such as dogs, rabbits, rats, and mice[98-105]. The larger animal models offer a size advantage, more closely resembling the geometry of a human disc, and have a natural tendency to degenerate, also like human discs. The benefit of smaller animal models is that they allow fast metabolic changes, and can be easily induced to begin the degenerative cascade. Also, in mice, rats and rabbits, there are still in tact notochordal cells, which are lost during adolescence in humans. The loss of these cells has also been speculated to be involved with the onset of degeneration[2]. Additionally, smaller animal models are cheaper and easier to work with. A variety of methods have been used to induce degeneration, including axial loading, injection of proteolytic enzymes, incisions and annular puncture[99]. Our lab has documented

the use of 18g percutaneous needle puncture in a caudal rat disc to induce disc degeneration within 4 weeks[105]. One drawback of all animal models has been the upright posture of the human spine; however, one group also investigated this, by amputating the forelimbs of rats and inducing an upright posture[106].

While the direct mechanisms that allow these methods to trigger the degenerative cascade is still yet unclear, these models result in a definite breakdown in the extracellular matrix of the disc, specifically a loss of hydrating ability. While the mechanism for proteolytic enzymes such as chondroitinase ABC, the goal is clear, to cleave the GAG chains on the proteoglycans and reduce swelling capacity. Other efforts have been made to discover more detailed steps in this degenerate cascade, such as monitoring microscale shear in an annular puncture using confocal microscopy[107]. Other theories that induce breakdown suggest that the annular puncture or tear reaches a critical size, in which the nucleus is unable to pressurize, and also disrupt annular fiber properties[99, 108]. Direct mechanisms of degeneration are still being understood, however, it is clear that the breakdown results in a lowered swelling capability caused by loss of proteoglycans, resulting an inability to pressurize, thus our focus is on the intradiscal pressure.

In this study, we use our previously reported methods to induce degeneration in caudal rat discs. Using this, along with a previously developed custom miniature fiber optic pressure sensors, we will investigate intradiscal generation during loading[95, 97]. We hypothesize that the degenerate group will have a reduced ability to generate an intradiscal pressure, while the control, normal group will have a greater ability than the diseased group. Additionally, we also hope to establish a relationship

with the intradiscal pressure and an applied external pressure. This will help future understanding of the behavior of the disc.

3.2 Materials and Methods

3.2.1 Animal Surgeries

Skeletally mature Sprague-Dawley retired male breeder rats (6-9 month old) (Harlan Laboratories, Indianapolis, IN) were anesthetized using vaporized isoflurane and punctured in the caudal 4-5 IVD using an 18g hypodermic needle, into the center of the disc. Prior to puncture, the disc was fluoroscopically visualized using a Fluoroscan III mini C-arm (Hologic, Northbrook, IL). The diameter of the disc was measured and the needle was inserted into the center of the disc, verified via x-ray. The rats were allowed normal food and water and cared for by the Central Animal Research Facility at the University of Maryland, College Park, for an additional 8 weeks. Following our previous work on a degenerative puncture model in caudal rat discs[105], the rats were euthanized after 8 weeks, and harvested for the c3-4 and c5-6 motion segments, healthy control and adjacent degenerate discs respectively. All procedures were approved by the Institutional Animal Care and Use Committee at the University of Maryland, College Park.

3.2.2 Pressure Measurement

Soft tissues were carefully removed from around the vertebrae and potted into custom fixtures using polymethyl methacrylate (PMMA) dental cement (Bosworth

Company, Skokie, IL). This fixture was then mounted onto a Bose-Electroforce materials testing system (LM-1, Bose Corp, Eden Prairie, MN). Again, using fluoroscopic verification, we inserted a custom fiber optic Fabry-Perot pressure sensor through a 22g hypodermic needle guide into the midpoint of the disc. In brief, the Fabry-Perot interferometry based fiber optic pressure sensor has a diameter of 363µm and was calibrated in a custom pressure chamber using a semiconductor pressure transducer (Kulite Semiconductors, Leonia, NJ) [95, 97].

3.2.3 Loading Conditions

Both healthy and degenerate disc groups (n=5) were subjected to the same mechanical testing. The specimens were first preloaded with 0.05 MPa to establish a reference configuration similar to that of the caudal disc *in vivo*. The disc under the tare load is then considered the zero stress point. Each motion segment was subject to 30 second step loads of 0.05, 0.25 and 0.45 MPa with 30 seconds of rest (0 MPa) in between. Figure 3.1 illustrates the loading scenario experienced by each disc. Following the last rest period, the disc is then loaded again to 0.45 MPa for 300 seconds to observe the creep response after step loading. Intradiscal pressure (USB4000/SpectraSuite, Dunedin, FL), displacement and applied load (WinTest, Bose Electroforce, Eden Prairie, MN) were all recorded at 1 Hz during the experiment.

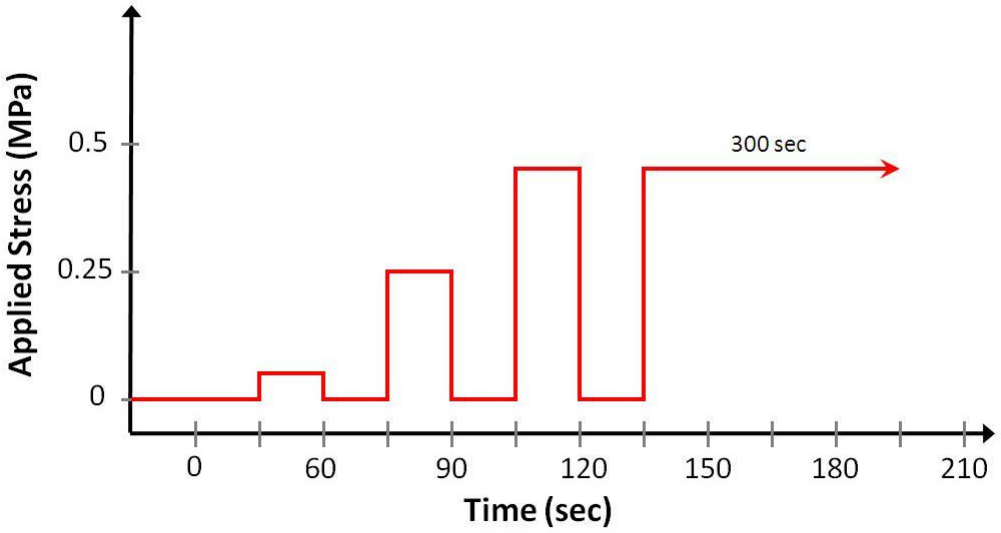

Figure 3.1 Shows the loading scenario for all of the motion segments. Discs were initially loaded with 0.05 MPa applied as ambient normalizing stress. This was then considered zero stress point. The discs were then loaded with 30 second increments of 0.05, 0.25 and 0.45 MPa with 30 seconds of rest in between. After the last rest period, an additional 0.45 MPa was loaded for 300 seconds to observe the creep response following the step loading.

3.3.3 Statistics

IDP measurements at each loading step, as well as the slope of the trend lines were analyzed using an independent-sample T test (SPSS 14.0, IBM, Somers, NY). A P-value of less than 0.05 was used to represent statistically significant differences.

3.4 Results

Each step load applied to the motion segment generated an immediate increased response within the NP to increase hydrostatic pressure and react to the imposed external stress. Figure 3.2 shows a representative pressure curve during the loading regimen. At the beginning of each step load the pressure takes a slight ramping approach to achieve the desired pressure. A similar lagging effect is seen

during the relaxation period as it takes a few seconds to reach the resting pressure. These rounded responses are likely due to the property of the tissue, as it takes time for the biological environment to react to the applied stress. Additionally, there is a relaxing of the intradiscal pressure when the applied stress was held for 5 minutes. This healthy disc creep response was later analyzed using viscoelastic models against the degenerate counterpart. We also established that the ambient intradiscal pressure for a healthy disc at simulated rest was 93±4 kPa. This value was obtained under the application of 0.05MPa axial stress on the disc, an accepted pressure used as a tare load to represent stress imposed by the body under physiologic conditions.

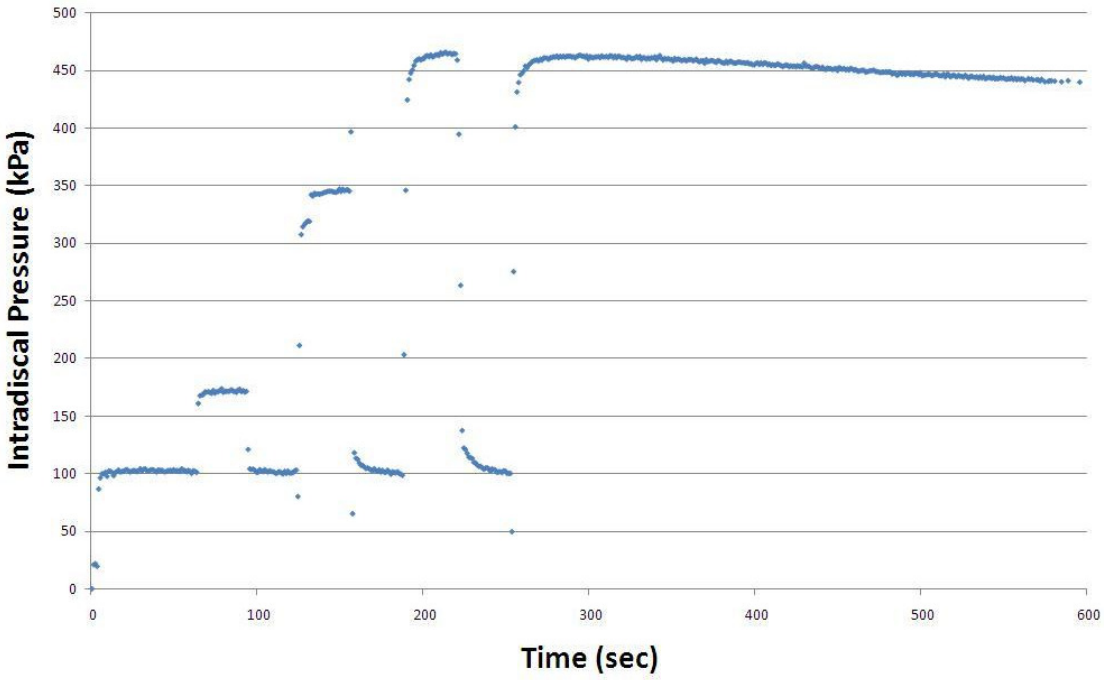

Figure 3.2 Intradiscal pressure was measured using a custom fiber-optic pressure sensor at 1 Hz. This is one sample degenerate rat disc, loaded under the loading conditions. Note the steps in intradiscal pressure while the tissue itself is experiencing the same step loads.

Figure 3.3 shows the each step load in bar graph format to better illustrate the significance changes in response between the healthy and the degenerate groups. At 0.25 and 0.45 MPa, the healthy group generated a significantly higher intradiscal pressure than the degenerative counterpart ($p > 0.05$). These represent a lowered ability to pressurize under loading, a critical job of the disc when absorbing and dispersing load. All values are represented in Table 3.1.

Table 3.1 Summary of the measured intradiscal pressures and the corresponding applied stress.

Applied Stress (MPa)	Degenerate IDP (MPa)	Healthy IDP (MPa)	p-value
0.05	**0.0696 (±0.0129)**	**0.0834 (±0.0082)**	**0.374**
0.25	**0.2314 (±0.0401)**	**0.3674 (±0.0342)**	**0.049**
0.45	**0.3541 (±0.0272)**	**0.6165 (±0.0879)**	**0.041**
Slope	**0.8225 (±0.1723)**	**1.3968 (±0.3904)**	**0.034**

Standard deviation is expressed in parentheses following the measured pressure.

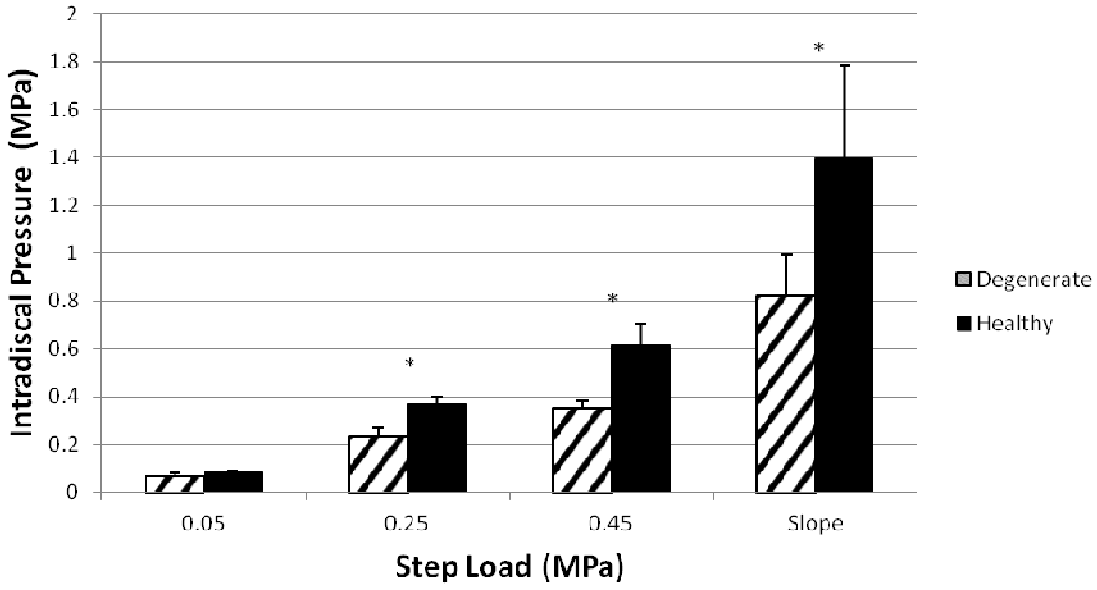

Figure 3.3 Each of the step loads shown is represented in bar format to show the difference between healthy and degenerate groups. Paired t-tests were performed to compare IDP generated between degenerate (punctured) discs and the adjacent control (non-punctured) discs. There are significant differences between IDP at 0.25 and 0.45MPa. Additionally, the difference in dimensionless slope was also determined to be statistically significant. * Shows significance ($p < 0.05$).

The relationship between applied force and generated intradiscal pressure was characterized using a linear approximation defined by a slope, as shown in Figure 3.4. Intradiscal pressure was observed to be linearly related to the applied stress, for both the healthy as well as the degenerate groups. However, the degenerate group had a diminished capability to generate pressure compared with the healthy group. A linear fit applied to define the relationship between applied and generated pressure yielded good results for both healthy and degenerate groups. The inability to pressurize becomes more and more drastic as the applied stress increases.

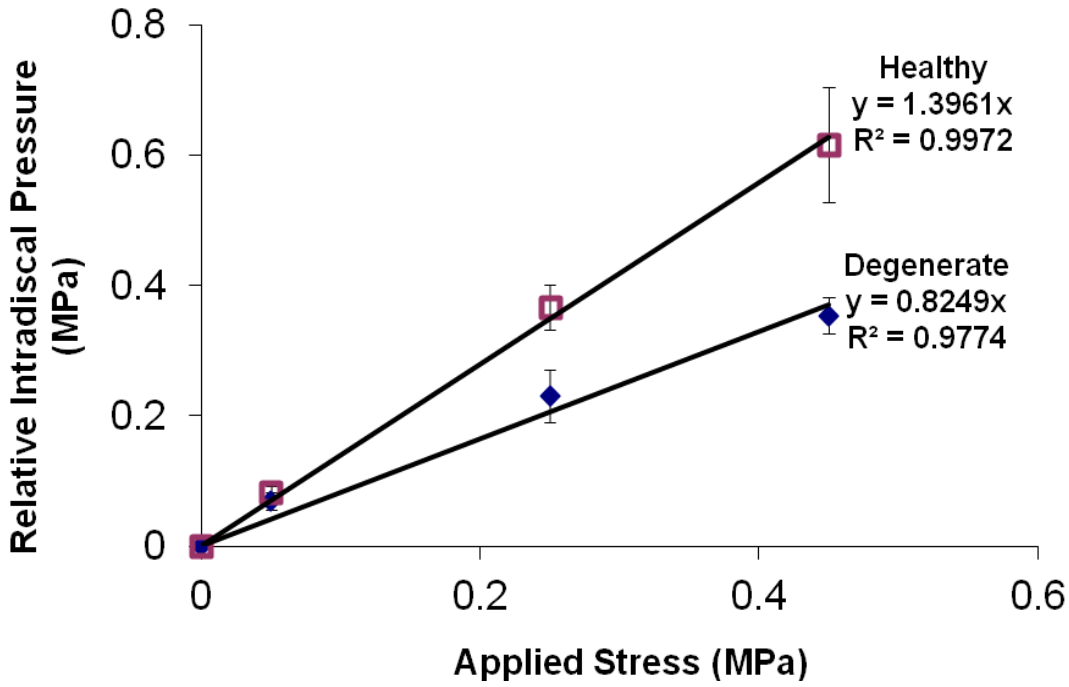

Figure 3.4 This figure shoes the relationship between the intradiscal pressure in the NP and the applied pressure on the disc. IDP generated was plotted against the stress applied for both healthy and degenerate discs. These relationships were approximated by linear functions. It shows that the healthy disc is much more responsive to external loads, and is able to generate a higher intradiscal pressure as a response, given the same loading conditions. The change in the slope exhibited by degenerate discs indicates a compromised ability to pressurize.

When compared, this slope also yields a statistically significant difference between healthy and degenerate groups. The difference in the linear slope relationship between IDP and applied stress was 1.40 in healthy discs and 0.82 in the degenerate discs. All linear approximations obtained yielded R^2 values greater than 0.95. To compare the healthy and the degenerate groups, we created a ratio of the healthy:degenerate intradiscal pressure generated at the 0.45 MPa step was 1.71. This value will allow us to compare our results with other similar studies, and better define the difference between our experimental and control groups.

Compressive displacements of the discs were examined at each step load as well as the five minute hold at the end. The time-dependent creep at each step was fitted to Cassidy's fluid transport of the disc model to determine a pattern at each step[109]. This is a viscoelastic model created for the disc that is based on the fluid flow properties in and out of the disc, dividing the disc into contributions of the NP, AF, and the endplates, represented by D, G and k respectively. We have previously used this model to discover changes in the viscoelastic properties of the disc as a result of changing load histories, and has proven to be more sensitive and more physically relevant than the stretched exponential model and the standard linear viscoelastic solid model[97]. The healthy group for each step was examined using the viscoelastic model and compared with the degenerate pair, and no significance was found. Results were reported in Table 3.2. There was too much variation and no separation between the healthy and degenerate groups for any of the coefficients. Absolute displacements were slightly higher for degenerate discs (Figure 3.5); however, these

were also not statistically significant. While initial disc heights were not taken, the degenerative discs have shown consistency in presenting a decreased disc height. If this displacement may be presented as strain, the smaller initial disc height may translate to a larger change in strain, which may result in a more statistically significant change in strain between healthy and degenerate discs.

Table 3.2 The coefficients fitted from the Cassidy fluid transport viscoelastic disc model.

		Step Loads			
		0.05 MPa (10 sec)	0.25 MPa (10 sec)	0.50 MPa (10 sec)	0.50 MPa (5 min)
D	Degen	3.050 ± 0.99	1.208 ± 0.23	1.556 ± 0.45	2.208 ± 0.77
	Normal	2.740 ± 0.94	1.025 ± 0.22	1.436 ± 0.59	2.602 ± 0.92
G	Degen	0.00645 ± 0.0003	0.00429 ± 0.0012	0.00420 ± 0.0006	0.00113 ± 0.0002
	Normal	0.00502 ± 0.0022	0.00289 ± 0.0004	0.00365 ± 0.0014	0.00169 ± 0.0005
k	Degen	0.1028 ± 0.0511	0.2372 ± 0.0523	0.1242 ± 0.0229	0.0054 ± 0.0014
	Normal	0.1478 ± 0.1162	0.3074 ± 0.1112	0.1663 ± 0.0710	0.0055 ± 0.0014

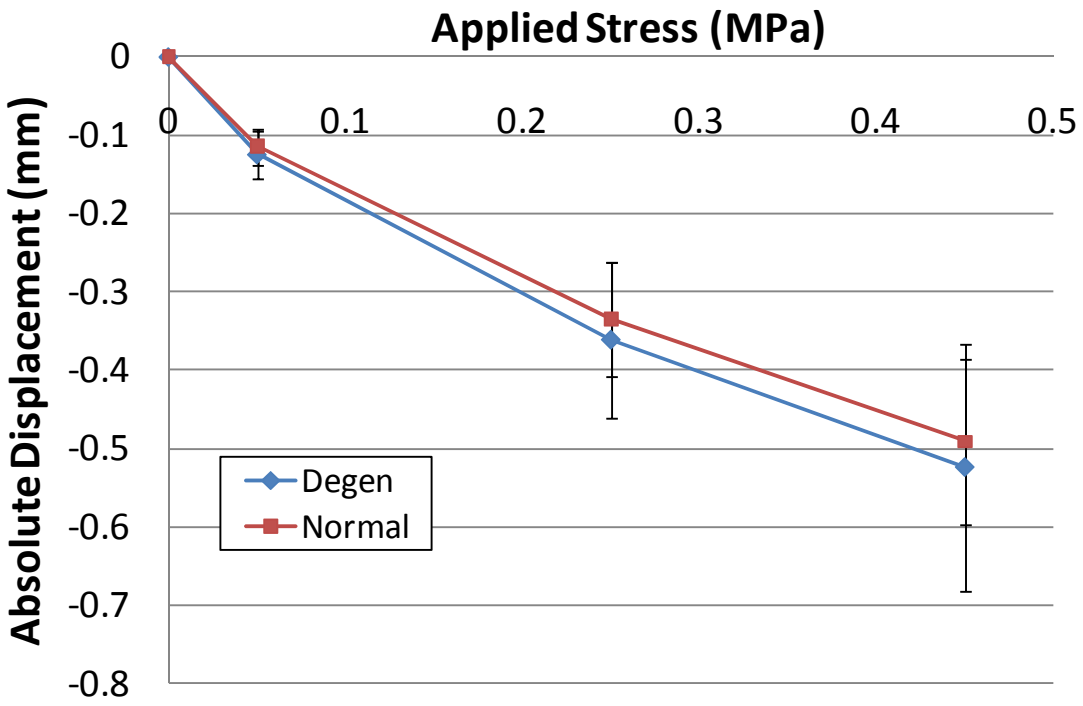

Figure 3.5 Plot of displacements achieved at each loading step. The normal group shows slightly less displacement under compression than the degenerate group, but differences were not statistically significant

3.4 Discussion

The ability to resist load is dependent on the generation of hydrostatic pressure within the NP. This experiment has shown a direct relationship with the intradiscal pressure and the load placed on the motion segment itself. There have been few examples of direct intradiscal measurements in rat discs, and this experiment allows direct comparison with other animal models, as well as human findings. The direct measurement of intradiscal pressure allowed for observation of the immediate response of the disc and the hydrostatic pressure generated. The small lag in response showed that the response is not immediate after a load is place, and it takes time for the pressure to build. A small creep or relaxation was seen in the pressure as well after the applied pressure was held for 5 minutes. This would be consistent with the water collected initially in the extracellular matrix being released back into the rest of the body.

We discovered the ambient, or intrinsic resting pressure for the caudal disc to be 0.093 MPa. This value is an important finding, as it can be compared to and used as a baseline for other animal models. This value is relatively similar to the healthy resting pressure of a porcine lumbar disc, which was seen to be 0.081 MPa[32]. A healthy disc in a human sample is much more difficult to come by, and a ambient pressure value has not been obtained. Given the porcine intrinsic intradiscal pressure, it is good to see a similar value present. Although it does not validate our value, it allows similar comparison to be made between animal models.

As shown in our previous experiments, an 18g needle puncture into the center of the disc induces degeneration in a rat tail model. Using this degeneration rat

model, we are able monitor the behavior of the degenerate model compared to a healthy one. In this experiment, the degenerate model allowed us to track the intradiscal pressure of a healthy hydrated disc and compare it to a diseased one. As seen in Figure 3.4, the healthy disc responds to the applied load, however, the degenerate disc shows a decreased ability to pressurize. The compromised ability to pressurize in the rat caudal disc puncture model is likely due to the breakdown of the extracellular matrix in both the NP and the AF. This breakdown of function is in large part due to a decrease in tissue hydration, as a result from the degeneration. In each step load, the healthy disc showed greater pressurization than the degenerate group. The larger the applied load, the greater the separation between the groups.

The relationship between pressure generated and pressure applied is an interesting one. This experiment establishes a linear relationship for both a healthy rat disc as well as a degenerate rat disc. We can use this linear approximation and slope to predict the pressure generation within the disc, given an applied axial load. It is again seen that the degenerate model shows a lack of pressurization when compared to the healthy disc. The slope representing the degenerate group is significantly shallower than the healthy group, indicating a lesser response. This lack of response is likely due to the breakdown of the extracellular matrix and therefore an overall loss of ability to fully hydrate. The disarray experienced in the matrix incorporates a major loss of proteoglycans, which is the main hydrophilic molecule that attracts and helps the disc maintain water and swell. This inability to swell parallels the inability to generate pressure, and therefore cushion loads.

Another way to compare the healthy and degenerate groups is to establish a ratio of intradiscal pressure generation at a given step load. At the 0.45MPa step load, we have a healthy:degenerate pressure ratio of 1.71. This is the same order of magnitude found in the porcine disc, using an lumbar endplate injury model, which had a healthy:degenerate intradiscal pressure ratio of 3.65[32]. Any variation between the two values, can be due to a variety of factors, two of which are most likely. The deviation can firstly be due to the difference between species, spinal location (lumbar vs caudal), and pure size. Additionally, the degree of degeneration induced by the endplate injury versus an annular puncture can also produce varying results. What is more encouraging is the comparison to human samples. Adams and colleagues discovered a healthy: degenerate pressure ratio in human discs to be 1.45, with Thompson grading of I:IV[10]. This is remarkably similar to our ratio of 1.71. Although not conclusive alone, when combined with our histological images[105], these observed intradiscal pressures make a strong case in being an incredibly viable animal model for degenerate discs. It suggests that our rat caudal annular puncture model can be compared directly with grade IV degenerate human discs. Our results suggest that there may be important parallels in the biochemical and structural changes in the NP and AF between human disc degeneration and injury-induced degeneration in rats.

It is surprising that the overall creep response in each step of the loading regime did not yield any discernable difference between healthy and degenerate. The stretched exponential model and the standard linear viscoelastic solid models are both standard models used to describe viscoelastic behavior in biological tissue, including

in IVDs. In our previous work, we have used both of these, as well as the Cassidy fluid transport model to identify small changes in the creep response of isolated motion segments[97]. While the stretched exponential model had a hard time identifying small changes in creep response, the standard linear solid and the fluid transport model, made specifically to describe disc behavior, have both been effective finding small behavioral differences. All three models were unable to identify a trend in each of the three step loads as well as the final held load in terms of displacement, creep curve. The overall displacement showed by the motion segment in Figure 3.5, did accumulate a modest change in absolute displacement. Since this displacement measurement was taken by the material testing machine, some of the overall strain may be due to compression of the vertebrae; however, the majority of the displacement can be attributed to the compression of the disc. The degenerate discs showed a slightly larger willingness to deform as compared to the healthy discs. Consistent with the pressure generation, the healthy discs were able to pressurize and better resist the load, while the degenerate group absorbed less of the load and transferred that applied stress into a greater absolute displacement. Although the healthy control group did not yield a significantly different displacement from the degenerate group, it indicates a trend that the mechanism of load support has changed with degeneration.

Our previous experiments have shown through histological examination and biomechanical analysis, that we are able to induce degeneration in a rat caudal disc using a trans-annular radiographically guided 18g needle puncture. This experiment monitored the intradiscal pressure generation of a degenerate group induced using

this method, and compared it with an adjacent normal control group. Results conclusively show that the degenerate group shows a compromised ability to pressurize during loading, and this lack of pressure response increases as the applied load increases. We identified a linear relationship between generated intradiscal pressure and applied stress, which also shows the deficiency of the degenerated discs. Additionally, the ratio comparing healthy to degenerate pressures closely resembles that observed in human discs, comparing grade I:IV discs. And although the displacement changes were not significant, they support the idea of a broken down extracellular matrix and compromised mechanics of the degenerate discs. Overall, these results show that our degeneration model can be accurately used as a successful animal model to represent human disc degeneration. Caution must still be taken; while histological and biomechanical evaluation suggests similarities with human degeneration, it remains unclear if mechanisms leading to changes are the same.

Chapter 4 Role of Load History in Intervertebral Disc Mechanics and Intradiscal Pressure Generation[2]

Thus far, efforts have slowly begun to hint at the omnipresent hydration factor that influences all aspects of disc function, particularly in the NP. Other studies have hinted at the impact of load history as an unknown influencing factor in their experiments, so this study is meant to simplify the idea of prior loading and discovery the real impact of this history. Hydration in the disc is changed after loading, thus changing the loading response of the disc in future compression. This idea is explored through the viscoelastic creep response, and then subsequently direct measurement of the intradiscal pressure. This investigation is aimed to show that this minor change in past loading makes a tangible difference in future behavior of the disc.

4.1 Introduction

The multiphasic nature of the intervertebral disc (IVD) plays a key role in its time-dependent and spatially heterogeneous mechanical behavior. Although tissue hydration is broadly accepted as a mechanism that governs soft tissue mechanics, its contribution to the IVD has not been fully explored. Grossly, it has been shown in various tissues, that changes in hydration affect viscoelastic behavior [75, 96, 110-115]. While no comprehensive set of tests has been performed in any individual system, these studies show that effects are strongly dependent on loading parameters and

[2] As published in D Hwang, AS Gabai, M Yu, AG Yew, and AH Hsieh. Role of load history in intervertebral disc mechanics and intradiscal pressure generation. Biomechanics and modeling in mechanobiology (2011). [Epub ahead of print].

tissue type. On the microstructural level, tissues exhibit decreased permeability with dehydration [116, 117] due to consolidation of the extracellular matrix (ECM) [118, 119]. Crosslinking and degradation of the ECM has also been shown to play a role in modulating the disc's viscoelastic behavior [120]. Biologically, altering tissue hydration may also initiate osmoregulatory functions of cells *in situ*, independently of changes in tissue microstructure [121-123]. Thus, hydration plays a significant role in IVD mechanobiology by generating responses by changing both osmolarity and cell shape. Since decreased water content and altered disc mechanics are mutually associated with degenerative disc disease (DDD), understanding their relationship may also provide insight into disease etiology.

For the IVD, the intradiscal pressure (IDP) is a parameter that represents the aggregate function of the three subregions: nucleus pulposus (NP), annulus fibrosus (AF), and cartilaginous endplate (EP). Subtly distinct from the overall stress-strain behavior of the disc, IDP is a direct quantitative indicator of the internal pressurization of the NP. Consequently, IDP is sensitive to changes in swelling of NP tissue, tension from bulging annular lamellae, and EP permeability. These mechanisms are supported, in part, by the observed water loss of the disc under compression is mostly due to decreased hydration in the NP rather than the AF [124]. The role of loading on IDP has been well documented by Adams and colleagues through stress profilometry studies using strain gauge-based pressure transducers. These studies have shown that the ability for IDP to be generated is strongly dependent on posture and load distribution among subregions in the disc [10, 125, 126].

With higher loads and greater water loss, load is transferred from the NP to the AF, and stress peaks are created in throughout the AF.

During compressive creep loading, commonly used to represent the time-averaged effect of spinal loading, interstitial fluid is expressed from the disc in a spatially- and temporally-varying manner. The re-distribution of water is complicated by multiple flow paths, the structural interactions among disc subregions, shifts between intra- and inter-fibrillar compartments, and consolidation of ECM molecules. For human discs, it has been previously shown that in the neutral position intradiscal pressures decrease up to 15% after several hours of static creep compression at physiologic levels of force [10]. However, spinal loads are seldom steady, considering the different activities that an individual might undertake. Because of these complexities, we hypothesize that the IDP cannot be predicted based solely on applied stress, but also governed by prior loading.

In this study, we characterize the extent to which load history contributes to disc mechanics overall, and particularly to the IDP. We chose to utilize rat caudal discs because of their relevance as animal models in mechanobiology research, and because of our ability to measure IDP in these discs with a previously developed fiber optic pressure sensor [95]. In order to establish an effect of load history, we chose first to employ a static load to simulate a time-averaged stress and circumvent potentially confounding factors associated with frequency-dependence of disc mechanics. Using three different analytical models, we characterized how different load histories influence aggregate creep behavior, physical elastic and viscous parameters, as well as zonal mechanics of the disc, and separately measured IDP directly using analogous

patterns of load history profiles. Results show that IDP generation is greatly affected by prior loads. Even relatively short durations of static loading resulted in dramatic alterations in subsequent IDPs generated. In contrast, changes in the gross mechanics of the disc were detectable only after long durations of creep compression. Therefore, while the disc provides consistent mechanical function, the internal stresses distributed through the disc are strongly dependent on load history. This may have significant consequences on IVD cell mechanobiology.

4.2 Materials and Methods

4.2.1 Specimen preparation

Skeletally mature (6-9 month old) Sprague-Dawley rats were euthanized using CO_2 asphyxiation according to protocols approved by the Institutional Animal Care and Use Committee at the University of Maryland, College Park. Caudal motion segments (c4-5 and c6-7) were isolated, and surrounding tissue carefully removed. Specimens for Experiment 1 were placed in frozen storage (-20ºC) until use, at which time samples were thawed in a protease inhibitor cocktail (PBS containing 1mM EDTA-disodium salt, 1mM EDTA-tetrasodium salt, 5mM of Benzamadine, 10mM N-Ethylmaleimide, 1mM Phenylmethylsulfonyl fluoride) at room temperature for approximately 2 hours. All chemicals were obtained from Thermo-Fisher Scientific Inc. (Waltham, MA). This protease inhibitor solution was used to minimize enzymatic degradation of the ECM during thawing and testing, as well as saturate the disc so that discs uniformly start in a fully swelled configuration prior to testing. Specimens for Experiment 2 were isolated and used fresh for testing. Radiographs

were obtained using an X-ray cabinet system (Faxitron Corp, Buffalo Grove, IL). Images were scanned from the radiographic film and analyzed using ImageJ to measure disc height and diameter, within a standard error of ±3.2% and ±1.2%, respectively. The motion segments harvested from the rat tail were carefully cleaned of tissue (muscle, tendons and ligaments) from the vertebral portion of the motion segments. Surrounding tissues were removed to minimize confounding effects on applied stress and to facilitate mounting in fixtures. Some soft tissue surrounding the disc itself was left in place, to minimize tissue dehydration. The motion segment was then potted into custom fixtures using poly(methyl methacrylate) dental cement (Bosworth Company, Skokie, IL) and mounted onto a Bose-Electroforce materials testing system (LM-1, Bose Corp, Eden Prairie, MN). Two sets of mechanical tests, designated as Experiments 1 and 2, were performed as described below.

4.2.2 Experiment 1 – Load history effects on compressive creep behavior

The purpose of Experiment 1 was to determine the effects of load history on the gross mechanical behavior of motion segments. For these tests, a reference configuration was set by applying a ramp compressive stress to 0.05 MPa over 2 seconds, and holding the displacement fixed for 500 seconds. Pilot studies had shown that this duration allows stress relaxation to reach equilibrium in all specimens. Since samples were previously frozen and fully saturated in protease inhibitor solution for Experiment 1, we used a low value of 0.05 MPa as a resting stress to generate a consistent degree of hydration across samples. For each specimen, stress relaxation to an equilibrium value was confirmed, and the force

tared. Tissues were then subjected to sequential static creep compressive stresses, consisting of a Prestress Phase followed by an Exertion Phase (Figure 4.1). The Prestress Phase varied from group to group in terms of compressive stress values and durations. Seven groups were studied (n=6), defined by combinations of three different compressive stresses (0.1, 0.3, 0.5 MPa) and two different durations (2,000 and 10,000 seconds) and including a no Prestress control (held without additional load for 10,000 seconds). Based on our pilot studies, it was determined that creep strain approximately reached equilibrium after 10,000 seconds, and 2,000 seconds was approximately the duration to reach one-half of the 'steady-state' strain. All calculations for applied stress were performed using the undeformed cross-sectional area of caudal discs, computed using radiographic measures of disc diameters and assuming circular cross-sections.

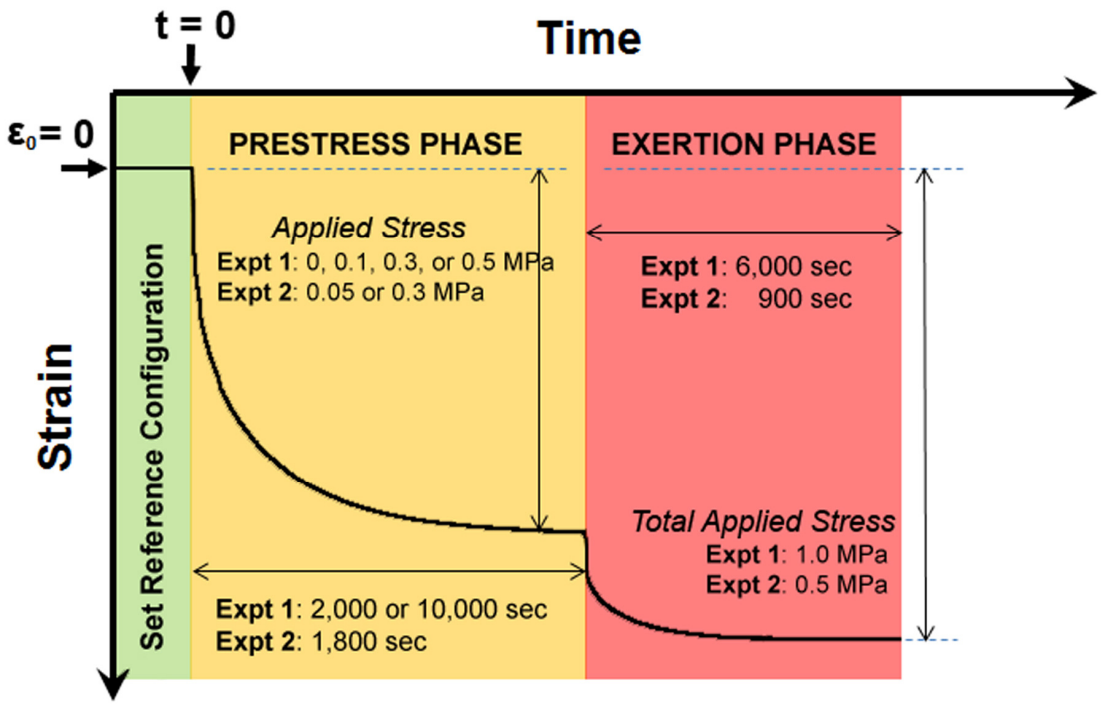

Figure 4.1 Schematic of the loading regimens used to explore the effect of load history on disc mechanics. A reference configuration was set after equilibrium was reached using stress relaxation at 0.04 MPa, at which point the strain was tared and time set to zero. Various combinations of applied compressive stress and duration were used during the Prestress Phase. The Exertion Phase consisted of a single total stress-duration condition that was identical for all groups regardless of load history. Results presented in this study represent the response of motion segments for the Exertion Phase only.

During the Exertion Phase displacements (recorded at 1Hz) were used for subsequent creep analyses and for comparison among the groups with distinct load histories (i.e. different Prestress Phases). This phase was identical for all groups, including the no Prestress control, and consisted of a final total applied compressive stress of 1.0 MPa held for 6,000 seconds. Due to the long duration of the test, motion segments were fully submerged in protease inhibitor solution for the entire experiment. Since the forces applied to discs were low, introducing saline-soaked gauze would likely generate load artifact, and spraying with saline would provide an

unsteady hydration environment. Moreover, Pflaster et al. suggests that the disc is "exposed to a fluid bath" during *in vivo* conditions, and further results indicate that a wrap or spray technique would not provide sufficient external fluid "available" for the disc to fully swell, thus the submersion technique was used [127].

4.2.3 Analysis of motion segment mechanics

As a way to quantify the effect of load history on compressive creep behavior, we used three analytical models to compare motion segments during the Exertion Phase, after having been subjected to different load histories in the Prestress Phase. It is important to note that these models are 1-D representations of creep, and do not consider complex geometries, material properties, or phenomena that are present in 3-D. The first is the stretched exponential equation, which has previously been used to describe changes in disc mechanics arising from mechanical or surgical manipulations that alter transport characteristics across the disc.[80, 81, 105] Strain is given by

$$\varepsilon(t) = \varepsilon_\infty + (\varepsilon_0 - \varepsilon_\infty) \times \exp\left[-\left(\frac{t}{\tau}\right)^\beta\right] \qquad (1)$$

where two parameters, β (stretched parameter) and τ (time constant), are used to describe the shape of the exponential increase in compressive strain over time, which at equilibrium is predicted to be ε_∞.

The second is a lumped parameter rheological model, variations of which have also been used with good results for describing creep behavior of IVDs. Viscous and elastic coefficients are quantified separately to provide physical

interpretation of the response, but these are averaged over the entire disc and possess little mechanistic basis. The specific formulation we selected is the standard linear viscoelastic solid composed of a Maxwell fluid (spring in series with dashpot) in parallel with a Hookean spring. For a constant stress, the strain is expressed by

$$\varepsilon(t) = \sigma_0 \left[\frac{1}{E_2} + \left(\frac{1}{E_1 + E_2} - \frac{1}{E_2} \right) \times \exp\left(- \frac{E_1 E_2}{\mu E_1 + \mu E_2} t \right) \right] \qquad (2)$$

where E_1 and μ represent the elastic and viscous parameters, respectively, in the Maxwell element, while E_2 denotes the spring in parallel and represents the long-term effective modulus.

The third is a model that was developed to describe fluid transport across the permeable EP due to applied loads modified by a linear dependence on consolidation of the NP and elongation of the annular lamellae.[82] In this formulation, strain is

$$\varepsilon(t) = \varepsilon_0 + \left(\frac{\sigma_0 - P_0}{D} - \frac{h_i G}{2kD^2} \right) \times \left[1 - \exp\left(- \frac{2kDt}{h_i} \right) \right] + \frac{G}{D} t \qquad (3)$$

where the parameters D, G, and k can be considered to arise from physical effects due to changes in osmotic pressure with NP consolidation, time-dependent changes in AF tension, and the permeability of the EP. Experimental input parameters include the initial disc height, h_i, applied creep load, σ_0, and estimated resting nucleus osmotic pressure $P_0 = 0.1$ MPa.

In all cases, the strain used in these analyses was defined as engineering strain. Values for unknown parameters were obtained for each specimen by curve fitting the Exertion Phase of the experimental data with each equation (1-3) using the Curve Fitting Toolbox, part of the MATLAB software package(The Mathworks, Natick, MA). A unique best fit was found using the nonlinear least squares method.

While the solution was dependent on starting conditions, this was the only fit that resulted in an R^2 >0.95.

4.2.4 Experiment 2 – Load history effects on intradiscal pressure

Experiment 2 was performed expressly for measuring the effects of load history on IDP generation. The general mechanical testing scheme is the same as that of Experiment 1, but because of the presence of a fiber optic pressure sensor, applied compressive stresses and durations were adjusted to ensure that displacements were small enough not to be influenced by or incur damage to the sensor during testing. After loads were tared, the Prestress Phase consisted of two different compressive stresses (0.05 and 0.3 MPa) held for 1800 seconds, followed by an Exertion Phase of 0.5 MPa for 900 seconds. During the loading scenario, the inserted pressure sensor would measure the intradiscal pressure, which arises from both fluid and solid phase stresses acting on the diaphragm of the sensor tip.

4.2.5 Intradiscal pressure measurements

Miniature Fabry-Perot fiber optic pressure sensors were fabricated as previously described (Figure 4.2) [95]. Briefly, two polymer layers (NOA 68, Norland Products, Cranbury, NJ) were placed over the cross-section of a capillary tube that had been cleaved flat. The polymer layers were cured and then sputtered with an approximate 800µm layer of 50:50 Ni-Ti (verified using topography mapping system, Polytec TMS-1200). Two more protective layers of polymer were added and cured. This tube was then mounted on bare fiber optic core with an approximate cavity

length of 30 µm and glued in place; and a thin protective sleeve was added to strengthen this interface. Each pressure sensor was then calibrated using a custom pressure chamber and a semiconductor pressure transducer (Kulite Semiconductors, Leonia, NJ). We have previously shown using a custom-made calibration chamber that the repeatability and linearity of the sensor are excellent [95], and the sensors we used in this study exhibited precisions within 3.7%.

After the motion segment was mounted in the testing system, a micrometer stage was used to insert a modified 22 gauge needle trans-annularly to one-half the diameter of the IVD. The fiber optic pressure sensor was then inserted into the NP through the needle. After insertion, the pressure sensor was held fixed while the needle was retracted, leaving only the pressure sensor in the NP. During the experimental loading regimen, IDPs were measured using a spectrometer (USB4000, Ocean Optics, Dunedin, FL) and data sampled using SpectraSuite software (Ocean Optics, Dunedin, FL) at 1 Hz, along with the displacement and force values from the Bose-Electroforce materials testing system.

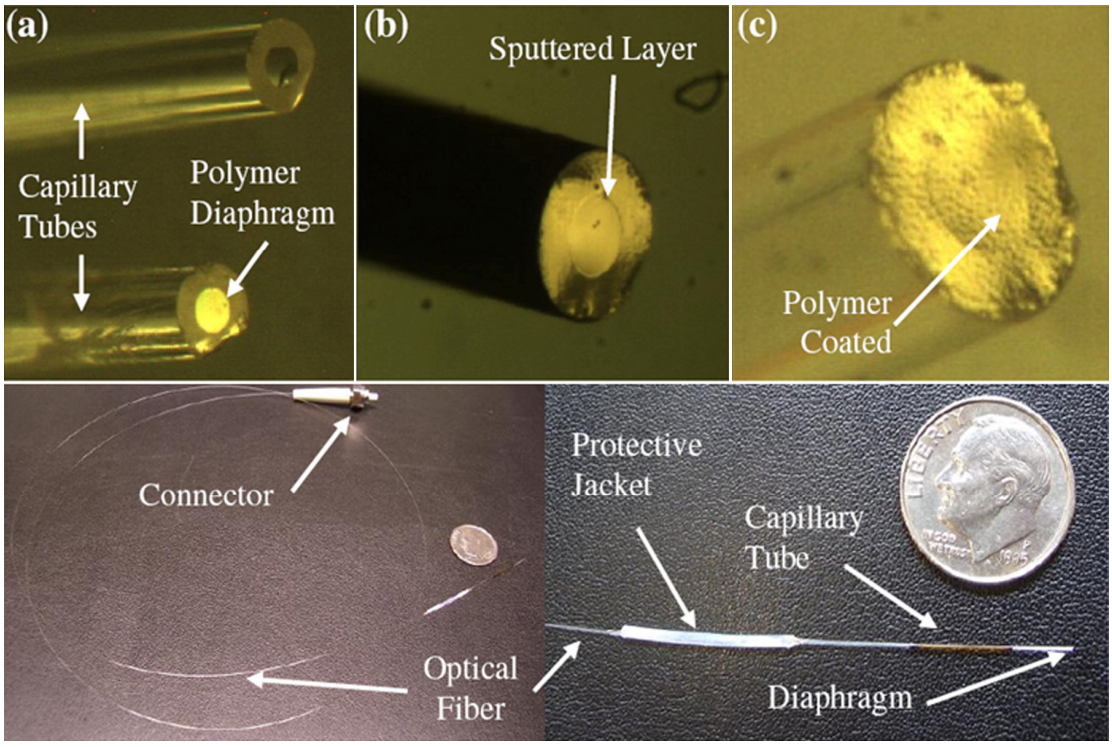

Figure 4.2 Micrographs of the diaphragm-based Fabry-Perot micro optical sensor used for measuring IDP in rat caudal discs. The optical fiber is sputtered with a reflective layer (b) and polymer coated (c), before being inserted into capillary tubes capped with a polymer diaphragm (a). The finished pressure sensor can be inserted through a 22g hypodermic needle. The coin (Ø = 17.91mm) is shown for size reference.

The investigation of the effects needle size on degeneration has been well documented, showing a general trend of larger needle to disc height ratio as being detrimental toward disc health [128]. Our lab has previously explored the effects of needle size on biomechanical function and subsequent occurrence of degeneration (Hsieh, Hwang et al. 2009). Results conclusively demonstrated that trans-annular punctures into the a rat caudal disc by a 22g needle neither compromised mechanical behavior during creep loading, nor caused any degenerative changes. Our pressure sensor has a diameter of 363µm as compared to approximate disc diameter of 5mm and disc height of 1.2mm. This is roughly a 30% ratio of intrusion to disc height,

which is believed to be within a safe range [128]. Based on these data, the use of a 22g needle to guide the insertion of our pressure sensor was expected to have minimal impact on disc mechanics.

4.2.6 Statistical analysis

All data were confirmed to be normally distributed. For Experiment 1, parameters obtained from curve fitting Equations 1-3 to the data were compared using one-way ANOVA among groups with different load histories. For Experiment 2, measured and computed stresses were compared using one-way ANOVA, as well. Pairwise comparisons were all performed using Tukey's HSD post hoc tests. Analyses were performed using SPSS 14.0 (SPSS, Chicago, IL) with critical significance levels set to $\alpha = 0.05$.

4.3 Results

4.3.1 Load history effects on compressive creep behavior

Analyses of Exertion Phases after varying Prestress treatments revealed that the mechanical behavior of the motion segment was not markedly affected by load history, but that there were subtle changes in elastic and viscous properties arising from alterations in function of the disc's subregions. Specifically, compressive strains could be described by similar exponential relations, essentially independent of Prestress treatment. However, specimens with a greater starting hydration at Exertion possessed significantly stiffer and more viscous coefficients. These appeared to be

related to changes in contributions from the NP, AF, and EP to fluid transport. Table 4.1 lists measured endpoint strains following Exertion load in Experiment 1; all strains were comparable, particularly after 10,000 seconds. Values obtained from curve fits in Experiment 1 are listed in Table 4.2.

Table 4.1 Measured strain values at the end of the Exertion Phase of Experiment 1

		measured strain, ε	
		2,000s	*10,000s*
PRESTRESS	**0 MPa**		0.40 ± 0.05
	0.1 MPa	0.36 ± 0.01	0.40 ± 0.07
	0.3 MPa	0.37 ± 0.03	0.37 ± 0.06
	0.5 MPa	0.43 ± 0.02	0.43 ± 0.03

Compressive creep strain of motion segments was well-described by the stretched exponential equation (Equation 1, Figure 4.3), yielding $r^2 > 0.99$. Curve fits to the data yielded values for β and ε_∞ that were not statistically different among the various combinations of preload magnitude and duration ($p > 0.05$). Most pairwise comparisons for τ were not statistically significant ($p > 0.2$), with the lone exception being a significant difference between 10,000 sec, 0.5 and 0.3 MPa Prestress groups ($p < 0.05$).

Table 4.2 Parameters obtained from curve fits of Equations 1-3 to Exertion Phase data of Experiment 1

		Equation 1					
		β		ε_{inf} (mm)		τ (s)	
		2,000s	10,000s	2,000s	10,000s	2,000s	10,000s
PRESTRESS	0 MPa		0.76 ± 0.07		0.41 ± 0.05		1316 ± 299
	0.1 MPa	0.87 ± 0.05	0.84 ± 0.05	0.37 ± 0.01	0.41 ± 0.07	1308 ± 97	1454 ± 335
	0.3 MPa	0.88 ± 0.03	0.73 ± 0.10	0.37 ± 0.03	0.42 ± 0.07	1392 ± 209	1054 ± 110
	0.5 MPa	0.82 ± 0.21	0.75 ± 0.03	0.43 ± 0.02	0.40 ± 0.03	1260 ± 564	1671 ± 83

		Equation 2					
		E_2 (MPa)		E_1+E_2 (MPa)		μ (MPa.s)	
		2,000s	10,000s	2,000s	10,000s	2,000s	10,000s
PRESTRESS	0 MPa		2.48 ± 0.31		4.16 ± 0.71		1758 ± 539
	0.1 MPa	2.46 ± 0.06	2.28 ± 0.38	3.74 ± 0.20	2.94 ± 0.50	1284 ± 232	834 ± 235
	0.3 MPa	1.91 ± 0.14	1.73 ± 0.33	2.62 ± 0.21	1.92 ± 0.41	788 ± 106	239 ± 83
	0.5 MPa	1.18 ± 0.04	1.26 ± 0.10	1.50 ± 0.07	1.36 ± 0.10	385 ± 83	173 ± 25

		Equation 3					
		D (N/mm)		G (mm^2/s)		k(mm^3/N.s)	
		2,000s	10,000s	2,000s	10,000s	2,000s	10,000s
PRESTRESS	0 MPa		6.01 ± 0.62		1.16 ± 0.42		6.98 ± 1.14
	0.1 MPa	7.22 ± 0.36	10.69 ± 2.03	0.57 ± 0.28	1.36 ± 0.52	4.98 ± 0.44	3.03 ± 0.43
	0.3 MPa	7.25 ± 0.94	18.42 ± 2.18	0.72 ± 0.30	1.88 ± 1.09	4.70 ± 0.54	2.30 ± 0.34
	0.5 MPa	6.26 ± 1.49	19.25 ± 2.45	0.74 ± 0.57	2.09 ± 0.24	4.71 ± 0.64	1.55 ± 0.21

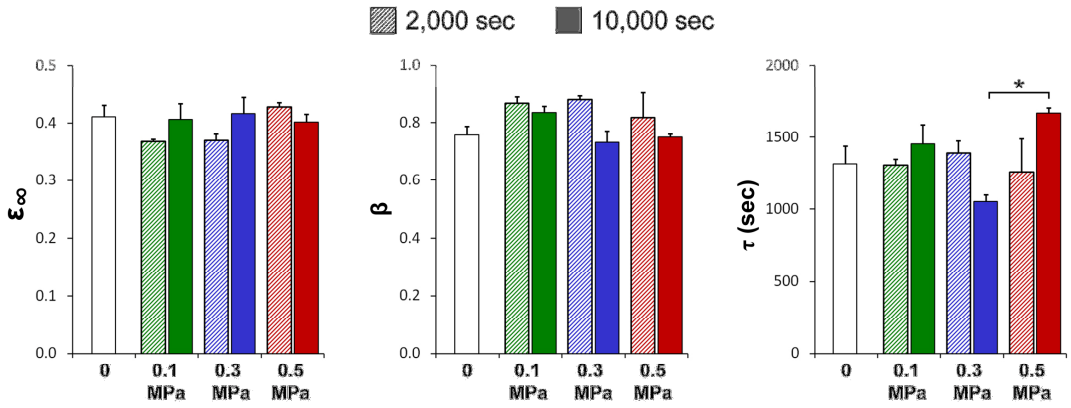

Figure 4.3 Analyses of Exertion Phase compressive creep behavior using the stretched exponential relation (Eqn 1). Three parameters (ε_∞, β, and τ) were obtained from curve fits with $r^2 > 0.99$. Cross-hatched and solid bars (including zero) represent Prestress Phase durations of 2,000 and 10,000 seconds, respectively. * represents a statistically significant difference ($p < 0.02$). No other significant differences were observed ($p > 0.2$). Data are presented as $\mu \pm$ SEM.

Although a simple exponential description of creep strain was not markedly influenced by load history, subtle differences in creep behavior were detected by the lumped parameter model (Equation 2, Figure 4.4), which also yielded excellent fits ($r^2 > 0.99$). Viscosities as well as short-term (as $t \rightarrow 0$) and long-term (as $t \rightarrow \infty$) effective moduli demonstrated significant differences among Prestress treatment groups. Each of the three parameters exhibited different patterns in group-wise differences. Long-term effective moduli (E_2) were grouped predominantly by Prestress magnitude. Short-term effective moduli (E_1+E_2) appeared to fall into three categories according to the combination of load magnitude and duration, suggesting that this parameter may be linked to the hydration level of the tissue. Viscosity exhibited similar group-wise differences as the short-term modulus.

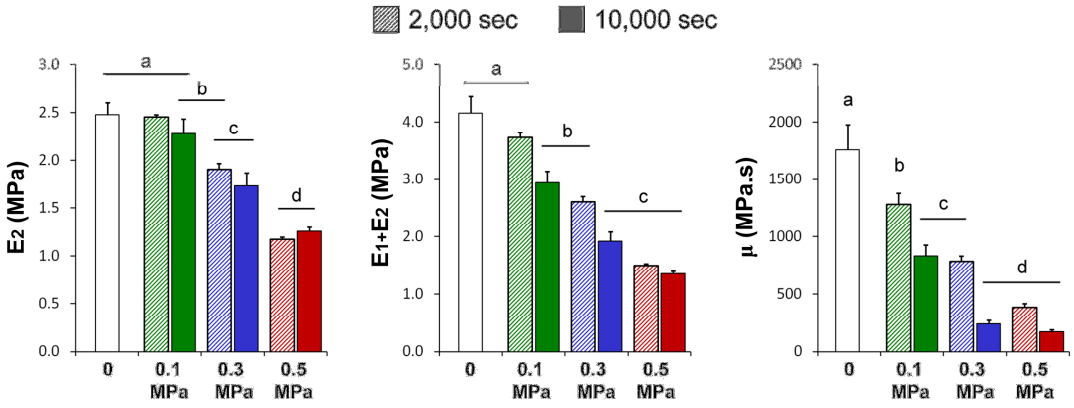

Figure 4.4 Analyses of Exertion Phase compressive creep behavior using the standard viscoelastic lumped parameter model (Eqn 2). Three parameters (E_1, E_2, and μ) were obtained from curve fits with $r^2 > 0.99$. Long-term (E_2) and computed short-term ($E_1 + E_2$) effective moduli are presented here. Cross-hatched and solid bars (including zero) represent Prestress Phase durations of 2,000 and 10,000 seconds, respectively. Letter categories encompass groups whose differences were not statistically significant between each other ($p > 0.15$), but are significantly different from groups in other letter categories ($p < 0.05$). Data are presented as μ ± SEM.

Results from analyses using the fluid transport model (Equation 3, Figure 4.5) – which also yielded excellent fits ($r^2 > 0.99$) – suggest a mechanistic basis for changes in moduli and viscosity. Trends in the dependence of *D*, *G*, and *k* on load history were dramatic. Parameter *D,* effects of NP consolidation*,* was essentially unchanged for shorter load histories, but exhibited a significant load-dependent increase with longer Prestress. Parameter *G*, contributions of AF tension, possessed statistically significant contrasting effects between short and long Prestress durations. Permeability, *k*, was load-independent for shorter Prestress, but load-dependent for longer Prestress. One can parametrically assess how increases and decreases in *D*, *G*, and *k* impact creep behavior of the motion segment. It can be shown that resistance to creep due to consolidation of the NP accompanies increases in *D*, due to viscoelastic stretching of the AF with decreases in *G*, and due to strain dependent EP

permeability with decreases in *k*. Importantly, the data suggest that with higher magnitudes and longer durations of Prestress, load bearing during exertion relies more on NP consolidation and less on AF tension.

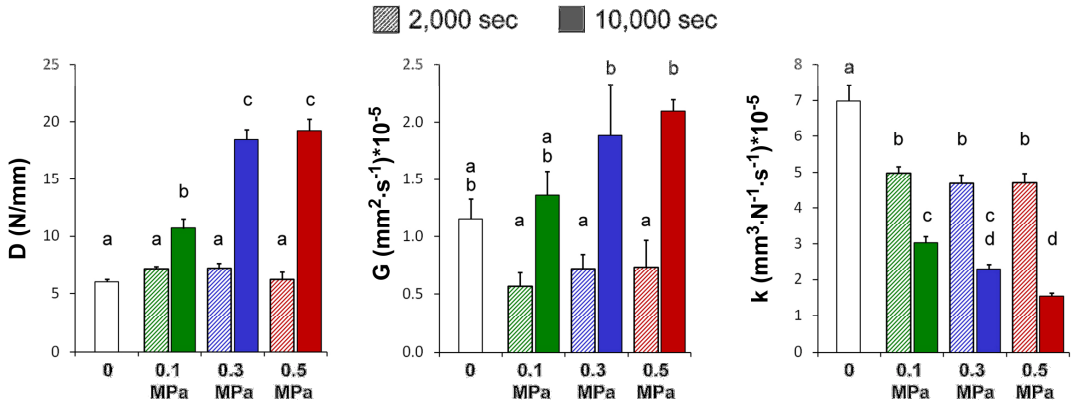

Figure 4.5 Analyses of Exertion Phase compressive creep behavior using the fluid transport model (Eqn 3). Three parameters (D, G, and k) were obtained from curve fits with $r^2 > 0.99$. Cross-hatched and solid bars (including zero) represent Prestress Phase durations of 2,000 and 10,000 seconds, respectively. Letter categories encompass groups whose differences were not statistically significant between each other ($p > 0.2$), but are significantly different from groups in other letter categories ($p < 0.02$). Data are presented as μ ± SEM.

4.3.2 Load history effects on intradiscal pressure

Because results from the fluid transport model suggested that subregions of the IVD were differentially involved in mediating creep strain according to load history, we investigated the model interpretations directly using an IDP sensor. In particular, we expected that since parameter *D* and *G* both increase with a higher Prestress, measured IDP should be smaller when greater Prestress magnitudes are applied. During the Prestress Phase, application of 0.05 and 0.30 MPa compression induced IDPs (mean ± SD) of 97.5 ± 44.3 and 289.6 ± 116.8 kPa above resting

pressures, respectively. In both cases, decreases in IDP over time accompanied creep during the Prestress Phase. The Exertion Phase exhibited a striking difference between the two load histories. Increasing applied stresses to a final magnitude of 0.5 MPa led to final IDPs of 537.2 ± 51.2 kPa for the 0.05 MPa Prestress group, but only 373.7 ± 99.1 kPa for 0.30 MPa group (Figure 4.6).

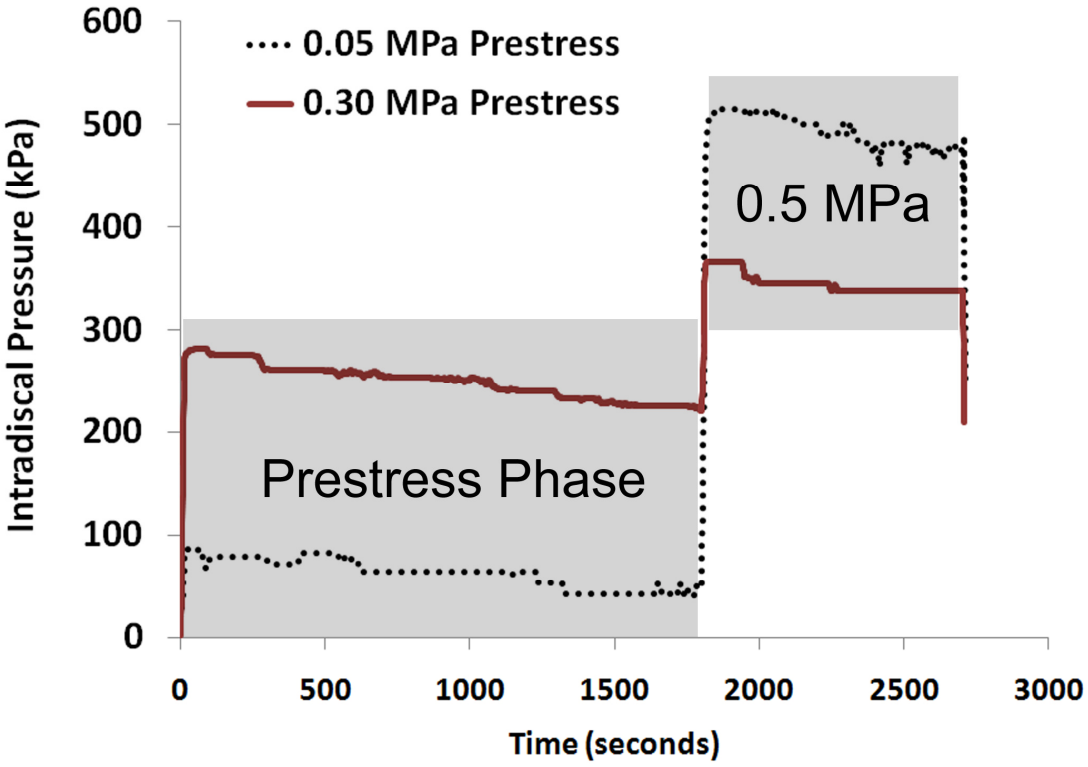

Figure 4.6 Average IDP measurements for Prestress Phases of either 0.05 or 0.3 MPa compressive stress applied for 1,800 seconds, followed by an Exertion Phase of 0.5 MPa applied for 900 seconds.

To determine whether sensor insertion resulted in altered disc mechanics, we compared 0.3MPa Prestress creep curves with (Experiment 2) and without (Experiment 1) sensor insertion. Inspection of the master plots for the two curves

demonstrate that there were no overt changes in creep behavior with the pressure sensor inserted (Figure 4.7).

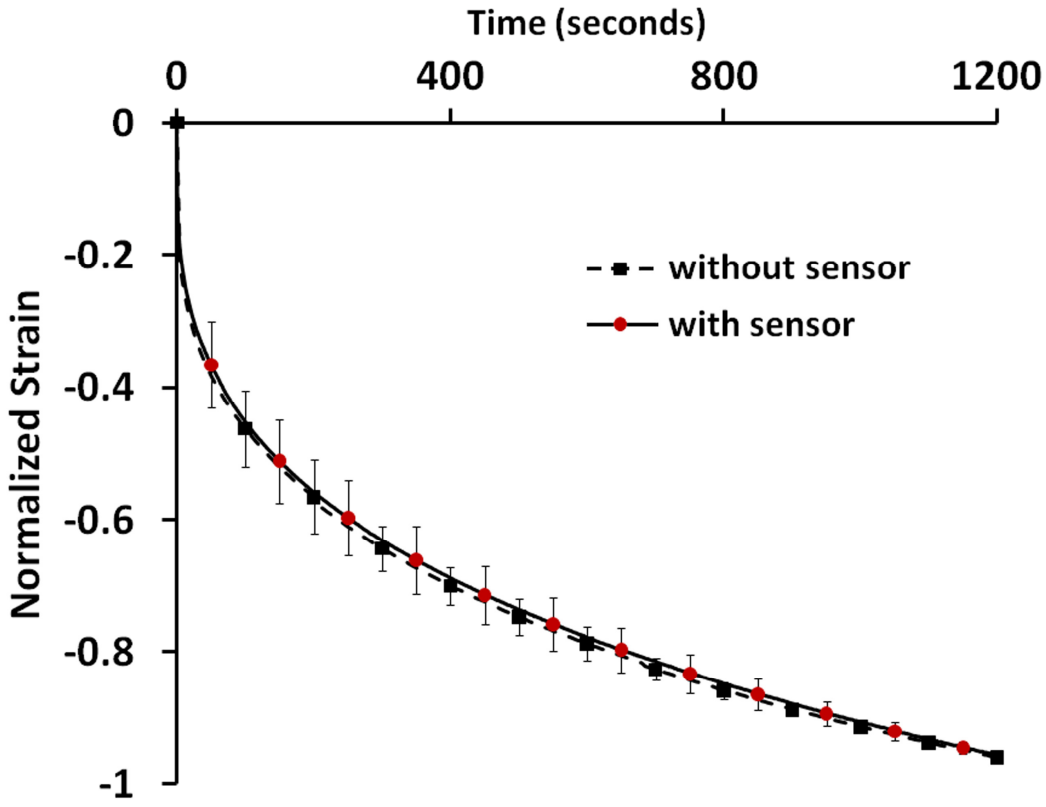

Figure 4.7 Master plot of the compressive creep behavior of intact motion segments and motion segments in which pressure sensors were inserted during Prestress loading at 0.3 MPa. Graphs were generated by normalizing curves to the strain attained at 1400 seconds (the duration of Experiment 2 using fiber optic sensors). The transient response of the disc with and without the presence of the sensor were nearly identical. Data are presented as μ ± SD. For clarity, error bars are shown only at set intervals and alternating between the two curves.

Since the sensor tip measures only transverse stress in the NP, it does not provide any indication as to the general stress state of the tissue. In order to capture the inequality between the axial and transverse stresses, we developed a quantity analogous to the octahedral shear stress (*OSS*). The analysis is illustrated in Figure 4.8 and is based on using the difference between IDP and a computed axial NP stress

(σ_{NP}) to represent the difference in principal stresses in the matrix (σ_{ECM}). Using the following equations, the *OSS* can be computed from this simplified model.

$$OSS = \sqrt{\frac{1}{9}\left[(\sigma_{ECM,x} - \sigma_{ECM,y})^2 + (\sigma_{ECM,y} - \sigma_{ECM,z})^2 + (\sigma_{ECM,z} - \sigma_{ECM,x})^2\right]}$$

Substituting in for σ_{ECM} using measured IDP and computed σ_{NP}, we get

$$OSS = \sqrt{\frac{1}{9}\left[(IDP_x - IDP_y)^2 + (IDP_y - \sigma_{NP})^2 + (\sigma_{NP} - IDP_x)^2\right]}$$

For axisymmetric discs, such as caudal discs, the radial stresses in the x- and y-directions are assumed to be equal. Thus, $IDP_x = IDP_y = IDP$, and we can simplify to

$$OSS = \frac{\sqrt{2}}{3}(IDP - \sigma_{NP})$$

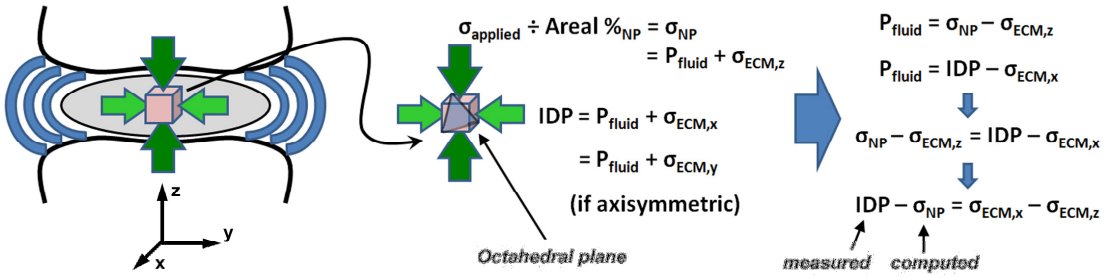

Figure 4.8 Schematic illustrating the computation of octahedral shear strain based on knowledge of applied stress and measured intradiscal pressures.

Although the assumptions of quasi-static conditions and idealized uniformity in stress distributions, cross-sectional areas, boundary conditions, and material properties are clearly simplifications, the measure offers a quick method to estimate the shear stress environment generated after load application, using only the known applied stress and measured IDP. From our data, we find that the magnitude of shear is significantly higher, and the IDP dramatically lower, during the Exertion Phase

when a higher Preload stress was applied (Figure 4.9). Whereas IDP exceeded *OSS* for both, the 0 to 0.05 and the 0 to 0.3 MPa Prestress steps, as well as the 0.05 to 0.5 MPa Exertion step conditions, *OSS* was only comparable to IDP for 0.3 to 0.5 MPa Exertion step.

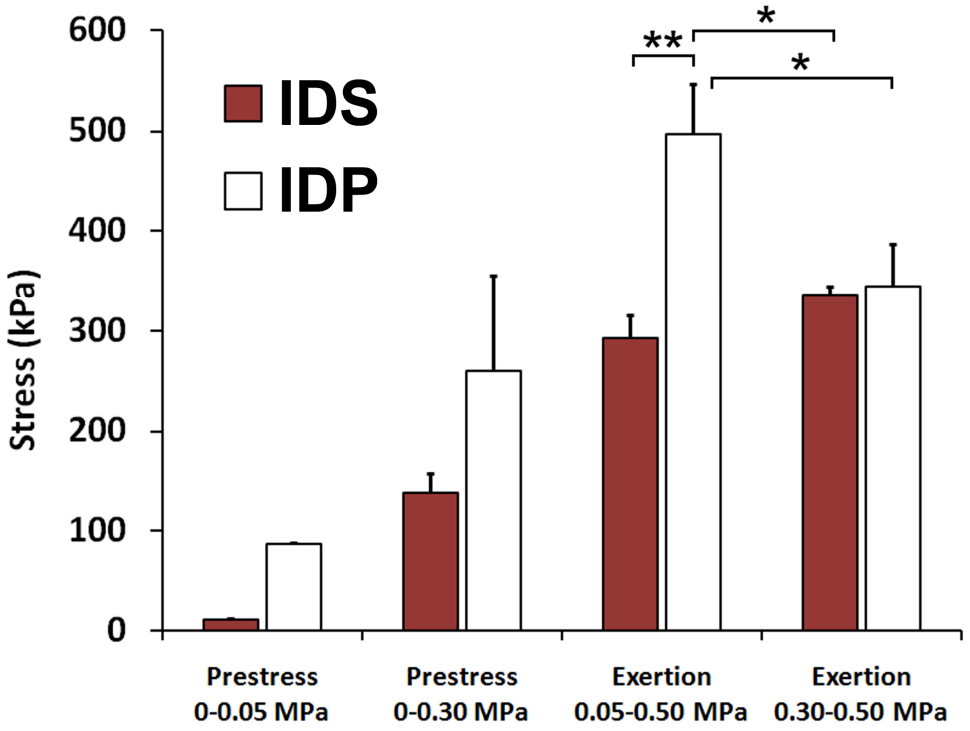

Figure 4.9 Calculated values of octahedral shear strain (OSS) and measured intradiscal pressure (IDP) values in the nucleus pulposus at the end of the Prestress/Exertion Phases of compressive creep loading. IDPs under Exertion loading were significantly larger than OSS after low 0.05 MPa Prestress ($p < 0.01$), and also significantly larger than IDP and OSS after high 0.30 MPa Prestress ($p < 0.05$). Data are presented as $\mu \pm$ SEM.

4.4 Discussion

Since biological tissues exhibit viscoelastic material properties, mechanical behavior is dependent on the sequence of prior loads. In particular, sustained loading over time results in interstitial fluid exchange both within and across tissue

boundaries. While altering water content by pre-loading tissues has been studied in terms of the aggregate mechanical behavior of motion segments, its implications on zonal mechanics and mechanobiology have not been explored. In this study, we applied carefully selected levels and durations of compressive stress within the physiologic range, generally thought to have little impact for disc function, and demonstrated that subsequent mechanical behavior is influenced by load history. Though a simple exponential relation was unable to detect change in creep behavior during Exertion, models that possess a rheological component to describe viscous flow found subtle differences that were statistically significant. Importantly, models predicted marked changes in zonal functions that we were able to verify through direct measurements of IDP. In fact, sensitivity to load history was much more pronounced than was predicted by analytical models. Using a simple computation, we interpret the measured IDP values according to load history, and suggest a mechanism by which certain spinal load histories might contribute to the aging process, even in the absence of excessive applied stresses.

There are few studies with which our results can be discussed in the same context, and comparisons are difficult to make because of distinctions among experimental systems (sample species and locations), procedures for varying hydration, and analyses. In terms of aggregate disc behavior, Race et al. found that adjusting hydration through compressive load application (as we had done) results in an increase in tangent moduli after 30 minutes, but a decrease after 2 hours, during monotonic loading.[75] Although we observed similar decreases in both measures of compressive moduli, E_2 and E_1+E_2, we did not find the same biphasic time-dependent

response that they had. It should be noted, however, that our values were obtained by analyses of creep behavior, rather than direct stress-strain measurements. Costi et al. found contrasting results.[96] Using ovine lumbar segments, specimens tested in a bath exhibited lower stiffnesses in compression, torsion, and bending compared with specimens dehydrated for several hours and then tested in ambient air. Because water content and testing environment were simultaneously varied, it is difficult to determine whether the difference in observed effects was due to one or both factors.

With respect to IDP, our results are consistent with load history effects observed by Adams et al.,[10] who examined stress profiles before and after creep loading. In this study, IDP progressively decreased during constant force application during both Preload and Exertion Phases. We found greater decreases in IDP during Prestress than Exertion (30% vs 7%), and different magnitudes of pressure drops for each loading condition. These changes, while comparable in magnitude to those reported by Adams et al., were observed in a much shorter timeframe. This may be due to differences in disc maturity and/or species. During the Prestress Phase applied stress and IDP were initially similar, but the decrease in IDP under a constant load necessarily results in an imbalance between the transverse and axial stress components. Adams et al. also observed this phenomenon, finding that the ratio of vertical to horizontal stress measurements increased after creep loading.

To estimate the shear associated with the difference between transversely- and axially-directed stresses, we utilized IDP measurements and an adjusted applied stress, respectively. This adjusted stress assumed that the AF functions in tension only to resist lateral expansion of the NP tissue, and not as a compression-resisting

strut between vertebrae. While this is clearly a simplification of the AF's load-bearing role, we have previously observed that rodent caudal discs exhibit significant outward buckling when sustained compression is applied (unpublished data). This is similar to what others have reported in the anterior AF of intact human [129] and ovine discs.[130, 131] Based on computational predictions[132] and direct pressure sensor measurements,[10] the axial loads in the anterior AF are fairly low. Although discs that undergo degenerative changes after puncture [105] or static loading[133] likely sustain more axial compression, much like the posterior AF of human discs,[10, 132] our assumption for this current study is at least reasonable for comparison among the experimental groups.

Magnitudes of OSS notwithstanding, it is interesting to note the trends of IDP and OSS observed with the different load histories. It has been postulated that the age-associated degradation of proteoglycans leads to loss in osmotic pressure, decreased disc pressurization and increased shear stress in the NP. The altered mechanobiologic environment then causes deregulation of gene expression, resulting in NP remodeling into more fibrous tissue morphologies. Findings from this study suggest that additional contribution may come directly from load histories that compromise IDP generation and further stimulate mechanobiology-induced biochemical changes. When discs were loaded from the reference configuration or after minimal compressive stresses, IDP remained well above OSS. However, after moderate levels of compressive stress, OSS increased to comparable levels of IDP. Theories in mechanobiology posed by Carter and colleagues as well as Prendergast and colleagues are based on competing influences of pressure and shear,[134, 135] with

OSS often used as a quantitative measure of the shear environment. When considering the competing parameters of OSS and IDP, as seen in Figure 4.9, the Prestress loads and the 0.05MPa to Exertion Prestress group all show significantly higher IDP generation, as compared with OSS. In the Prestress group, for 0.3MPa to Exertion, IDP decreases and OSS increases to comparable values. Our interpretation of these trends is that higher Prestress generates greater annular stress relaxation and radial consolidation of the NP, both of which contribute to a lower IDP. In turn, the load-bearing role of the annulus fibrosus may shift from predominantly tensional to axial compression. Although we cannot measure this directly, it is consistent with what others have also hypothesized [133, 136]. The decrease of annular contribution (i.e. increase in G) seen in the fluid transport model also supports this notion. Based on these theories, we have developed a conceptual model (Figure 4.10) to explain how certain load histories may influence the relative magnitudes of OSS and IDP to stimulate remodeling from cartilaginous to fibrous tissue. In the NP, it has been shown that OSS corresponds with a threshold effect with NP cell apoptosis,[137] while hydrostatic pressures stimulate NP maintenance.[138-141] Thus, load histories that tend to generate greater shear and lower pressure in the NP may accelerate age-related changes in the IVD.

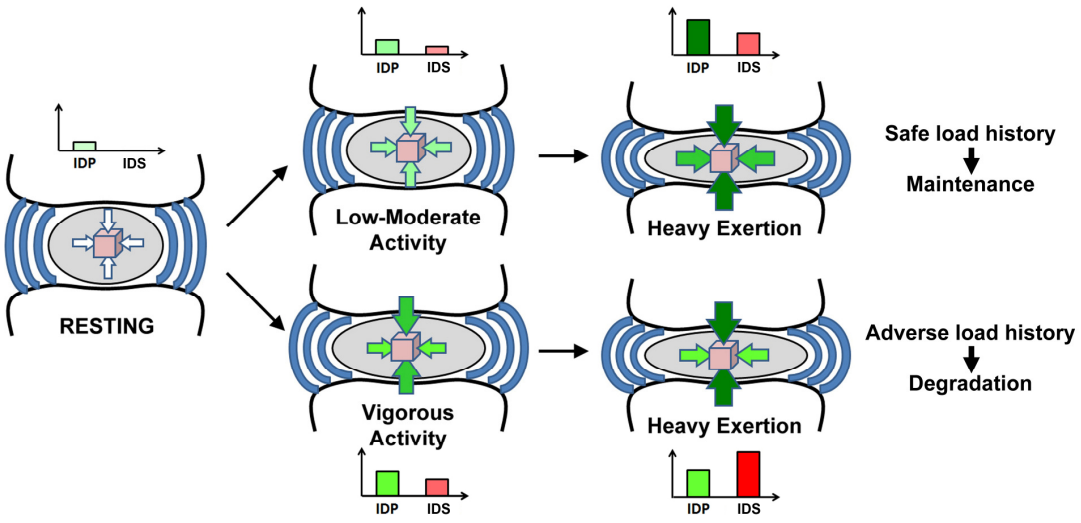

Figure 4.10 Our working model for the role of load history on OSS and IDP in the NP. Illustration shows how two load paths to the same high exertion load may lead to distinct OSS-to-IDP ratios. Based on hypothesized mechanobiology principles, the "safe load history" would promote maintenance of NP cell phenotype, while "adverse load history" would stimulate a degradative response. Bars for IDP and OSS are meant to illustrate relative changes, not actual magnitudes.

Although mathematical analysis of compressive creep behavior was a straightforward approach for guiding the experimental aspect of this study, the models we used were either incapable of or inadequate for fully resolving the effects of load history on internal disc mechanics. One important factor to consider is the nature of the models, which cannot capture three-dimensional phenomena that may be important in disc creep. Even though creep behaviors are similar, there may be distinct events occurring in other dimensions. The exponential description of creep demonstrates that the overall mechanical behavior of the motion segment is essentially unchanged, suggesting that changes in stress within the IVD would not adversely affect mechanics of the spine. While the standard viscoelastic solid showed differences in stiffness and viscous behaviors, it could not discriminate effects on individual disc subregions. For this purpose, the fluid transport model was useful, but

still was only able to detect changes for long duration Prestress conditions. Our experiments demonstrated that, even below 2,000 seconds of Prestress, there were significant changes in IDP, despite model predictions that D, G, and k do not differ among stress magnitudes at these durations. It should be noted that a number of simplifying assumptions were made by Cassidy et al.[82] in developing Equation 3, but it is unclear how significantly these assumptions contribute to model sensitivity. Also, it is possible that leaching of GAGs from the IVD during extended durations of testing in a fluid bath could have contributed to a reduced sensitivity of the mathematical analyses, but this was not explicitly investigated in this current study.

Rat caudal discs markedly differ in size and composition from adult human discs, but the biological function and regional structures are similar. Past studies have shown that there are many biomechanical similarities among certain species and between spinal and caudal discs [99, 120]. However, one key difference in biomechanical function between adult human discs and rat caudal discs is the roughly 43% shorter time constant for rat discs during creep compression [142]. Because our model outcomes showed that Exertion response was strongly dependent on Prestress duration, our observations are very likely to exhibit an exaggerated response compared with that which would be found in adult human discs. It remains to be determined how juvenile human discs might compare with these two tissues. Nevertheless, we believe the observed principles likely remain applicable.

One of our reasons for using rat caudal discs is the prevalence of rodent tail loading models in disc mechanobiology research. Such studies have demonstrated that magnitude and frequency of dynamic loading can be important in regulating disc

health.[13, 143-145] A second and equally important motivation is our particular interest in the changes that occur in human IVDs during early adulthood. Like immature human discs, rat caudal discs possess a predominantly notochord-derived cell population in the NP. While age-related changes in NP mechanics are not well-characterized, it is likely that the unique protein composition, cellularity, and consistency of notochordal NP tissue impart specialized material properties that affect IDP generation. Thus, we expect our results to have the most relevance to human IVD mechanobiology during growth. Although the loads that were selected for study span the range of what are believed to be from prone to low and moderate exercise to heavy labor, these are estimated for adult discs and may overestimate those experienced by immature discs.

An additional point of concern lies in the insertion of a sensor to measure IDP. As of yet, there are no validated means to measure IDP non-invasively, and many groups have utilized the same invasive approach as we have [10, 32, 146]. In agreement with these reports and our own previous work, our current study demonstrated that the transient mechanics on the level of the motion segment were not affected by the insertion of the fiber optic sensor (Figure 4.7). The fact that pressure measurements did not rapidly dissipate after loading also suggests negligible pressure venting or leakage after the insertion of the sensor into disc. Taken together, these various studies suggest that for small enough diameter sensors the effect on IDP generation may be minimal. Although Michalek *et al.* found that even 30g needles altered disc mechanics under compression, their needles were blunted and likely produced more damage to the annulus than traditional tapered hypodermic needles [147]. While

specific implications of these limitations require further investigation, we believe that our findings on the role of load history in the internal mechanics of the disc remain broadly applicable in IVD mechanobiology.

Chapter 5 Effects of Load History on Nucleus Pulposus Gene Expression in Caudal Rat Discs

The previous experiment determined the hydrostatic pressurization in the NP, thus identifying the cellular environment for NP cells. Through calculation we found greater and lesser pressurized environment as well as a condition that yielded greater shear stress. Given *in vitro* experiments, hydrostatic pressure has yielded a biological response towards maintenance and remodeling of the NP ECM, while increased shear may result in increased breakdown. This experiment uses further simplified load histories to determine if the predicted higher pressurized environments would result in increased gene expression for anabolic ECM genes.

5.1 Introduction

The incidence of low back pain is widespread across populations all over the world. Low back pain is often attributed to deregulated biological function and compromised mechanics of the intervertebral disc (IVD)[148]. These biological and mechanical changes are related to degenerative disc disease and aging. This breakdown and disease is characterized by a loss of load resistant properties, centered around the swelling of the disc. As this ability to retain water is lost, the IVD becomes more and more compromised. The continual breakdown of the disc severely hinders the function of the disc, which is to provide flexibility for the spine as well as absorb loads. During degeneration, the extracellular matrix begins to breakdown, limiting hydration and disc health[1]. It is still uncertain what causes these extracellular

changes, but experiments have showed that they are linked to many different and not fully understood biological processes.

The nucleus pulposus (NP) is the inner gelatinous core of the IVD, and plays a critical role in the load bearing function of the disc. In a healthy disc, the NP maintains fully hydrated, however, in a diseased disc, the matrix that makes up the core becomes more and more broken down, losing its ability to retain water. This hydrated state allows the NP to pressurize as a response to applied loads. The ability to generate a hydrostatic load to disperse the applied forces is the main reason why the fluid content in the disc is such a subject of emphasis. Hydration has also been shown to influence both the instantaneous stiffness as well as viscoelastic behavior[75, 96]. The hydration level in the disc changes and responds to applied loads, however, as a viscoelastic material, there is a recovery time associated with these physical parameters.

Exploring the mechanics of is a critical first step in understanding how the disc functions, which will provide insight to biochemical reactions and changes in the disc as well. Disc hydration is directly linked with the health of the extracellular matrix, however, other factors have also been shown to contribute. We have previously shown in our lab that load history also influences current and future behavior of the disc, particularly in terms of hydration. Using an analytical model we previously showed that load history has a profound effect on the mechanical function of different subregions, end plates, annulus fibrosus and the NP[97]. Furthermore, we showed directly measured and showed the dependence of the intradiscal pressure on prior loading. Load history influences disc hydration and other factors, impacting the

disc's behavior for subsequent loads[10, 16]. These changing conditions offer an equally changing environment for the cellular activity within the discs. Chemical and physical factors such as changing hydrostatic pressure or osmolarity have been shown to influence the metabolic behavior of the cells[149]. While disc cells have been extensively studied *in vitro*, or in organ culture, few groups have monitored the cellular change influenced by *in vivo* loading[150].

In this study, we demonstrate the influence of the cellular environment due to altered load history. At any moment, the hydration of the disc is linked with its biomechanical function. We have shown that this hydration and intradiscal pressure to be influenced by different load histories. We apply relatively known environments on the cells by using loading scenarios we have explored in the past, and study their effect on the cellular behavior given this environment. This shows that load history is important when describing the response of the disc, in terms of mechanical and biological response.

5.2 Materials and Methods

5.2.1 Short History Group

Skeletally mature Sprague-Dawley male retired breeders (9-18 month old) were anesthetized via inhalation using isoflurorane gas and prepared for surgery. Using radiographic confirmation (Fluoroscan III, Hologic Inc., Bedford, MA), two sets of holes were drilled into the vertebrae of the caudal c5-6 motion segments. Pins were inserted into the holes and used to attach a custom set of rings used to mount onto a Bose Electroforce benchtop materials testing system (LM-1 Bose Corp, Eden

Prairie, MN). For the short history loading group, there were 3 control groups and one experimental load history group, shown in Figure 5.1. The experimental group (n=5) consisted of an hour of axial loading at 0.5 MPa followed by an hour at 1.0 MPa. Control group one (n=5) was held unloaded for an hour, followed by a 1.0 MPa load. Control group two (n=3) was loaded at 0.5 MPa for one hour followed by a held 0 MPa load. The last control group (n=3) was subject to 0.75 MPa loading for 2 full hours.

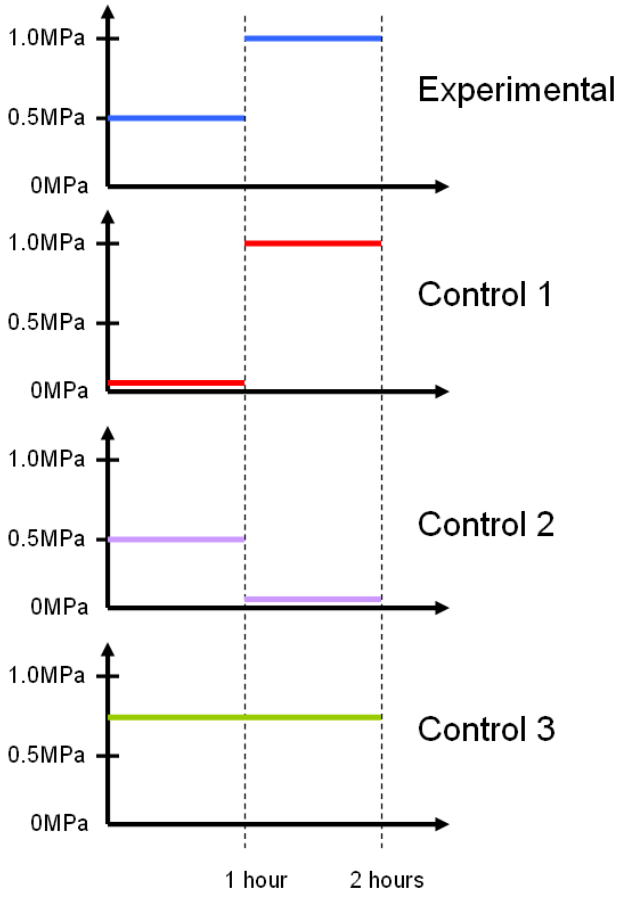

Figure 5.1 Loading regime for the 4 short history loading group.

Force applied was estimated using the desired stress and approximate circular cross section of disc from radiographs. After each group was loaded for two hours, the rat was euthanized and the NP was harvested for gene expression analysis. The experimental c5-6 disc was harvested along with the adjacent c4-5 disc, to be used as an internal control. Loading regime was recorded for displacement and load at a rate of 1 Hz. Radiographic images were also taken throughout the loading regime and used to monitor disc height. Rats remained anesthetized during the entire surgical procedure as well as loading period. All protocols and procedures were approved by the Institutional Animal Care and Use Committee at the University of Maryland, College Park.

5.2.2 Long History Group

As described above, skeletally mature Sprague-Dawley rats were used. The same preparation for surgery and ring mounting procedures mentioned above were used. In the long history loading group there was one experimental group and one control group, shown in Figure 5.2. The experimental group (n=5) was loaded at 0.5 MPa for one hour, followed by three hours of loading at 1.0 MPa. The control group (n=5) was controlled and unloaded for one hour, followed by three hours of loading at 1.0 MPa. Following four hours of loading, each rat was again, euthanized and the experimental c5-6 and the internal control c4-5 discs were harvested for gene analysis. Loading regime was recorded for displacement and load at a rate of 1 Hz. Radiographic images were also taken throughout the loading regime and used to monitor disc height.

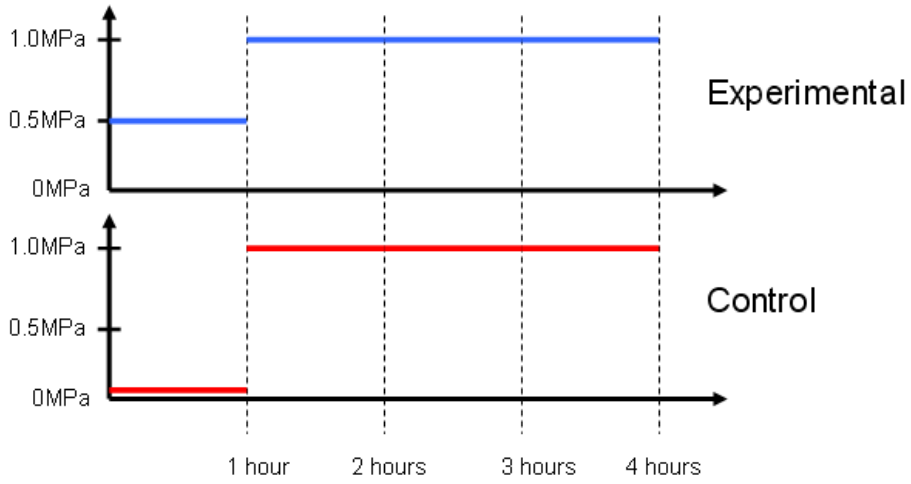

Figure 5.2 Loading regime for the long history loading group.

5.2.3 Gene Expression Analysis

NP tissue was harvested from the experimental samples and placed in 350µl of lysis buffer and flash frozen using liquid nitrogen. RNA was isolated from the tissue sample using an RNEasy Micro isolation kit (Qiagen, Valencia, CA). Samples were transcribed and real time RT-PCR was performed with SsoFast EvaGreen supermix in triplicate using iCycler (Bio-Rad Laboratories, Hercules, CA) to quantify expression of the following genes: collagen II, aggrecan, sox9, ADAMTS-4, collagen I and TonEBP with 18s as a housekeeping gene.

Table 5.1. Primer sequences used in the real time RT-PCR reactions.

Gene Name	Primer Forward Sequence Primer Reverse Sequence	GenBank Ascension #
Rat 18s	5' CGC GGT TCT ATT TTG TTG GT 3' 5' AGT CGG CAT CGT TTA TGG TC 3'	X01117
Rat Type II Collagen A+B	 5' GTG AGC CAT GAT CCG C 3' 5' GAC CAG GAT TTC CAG G 3'	NM_012929
Rat Aggrecan	5' GGA CTG GGA AGA GCC TCG A 3' 5' CGT CCG CTT CTG TAG CCT GT 3'	NM_022190
Rat Sox-9	5' AAT CTC CTG GAC CCC TTC AT 3' 5' TTC CTC GCT CTC CTT CTT CA 3'	XM_343981
Rat ADAMTS-4	5' AGG CCG GAA ATA ACC TCA CT 3' 5' TGG GGT ACT GTC AGG TAG GC 3'	NM_023959
Rat Type I Collagen	5' GCC CAG AAG AAT ATG TAT CAC CAG A 3' 5' GGC CAA CAG GTC CCC TTG 3'	NM_053304
Rat TonEBP	5' TCA CGA GGA AAG ATG GCT CTA CT 3' 5' GGA ACT CCT GCT GGC TGA GT 3'	NM_0011074 25.1

5.2.4 Disc Height

Radiographs were taken at one minute intervals for 10 minutes after every step load, and every 10 minutes at all other times. These images were recorded and processed using a custom MatLab (MathWorks, Natick, MA) program. Briefly, this program measured the distance between three parallel segments across the disc, at the left, right and middle. These distances were measured and averaged to yield the disc height at each time point. These distances were converted into strain by dividing by the disc height measured at time zero, before loading began. The standard solid viscoelastic model was applied to the displacement curves after each step load. Also the final strain was recorded at the end of the loading regime.

5.2.5 Data Analysis and Statistics

Relative quantification of real-time RT-PCR data was performed using the $\Delta\Delta C_t$ method (Livak and Schmittgen, 2001). Briefly, the C_t values for each triplicate

were averaged and used for subsequent calculations. ΔC_t was computed by subtracting the averaged C_t values of the internal control gene 18s from those of the gene of interest. $\Delta\Delta C_t$ for each gene of interest was computed by subtracting the ΔC_t of the baseline control (adjacent unloaded c4-5 disc) from the ΔC_t for the loaded disc. These $\Delta\Delta C_t$ values for each gene of interest of each group were then expressed as relative changes in mRNA levels (fold difference) through the exponential relation: $2^{-\Delta\Delta Ct}$. Data are reported as the average value of the range of calculated fold difference, which incorporates the standard deviation of the $\Delta\Delta C_t$ value in the fold difference calculation as $\Delta\Delta C_t$+SD and $\Delta\Delta C_t$-SD. Statistical analyses (JMP 7.0, Cary, NC) were performed using am independent T-test, comparing the experimental gene expression with each individual control group (α=0.05). One way ANOVA with Tukey's HSD post hoc analysis was performed on the final displacement strains of the disc heights.

5.3 Results

The biological response of NP cells are examined here using the relative change of gene expression after different loading scenarios. Figure 5.3 represents the quantitative results of real time RT-PCR shown in units of fold difference on a logarithmic scale for genes examined for the short history loading group. The preloaded experimental group showed consistently higher gene expression than all of the controls. While this experimental group was not statistically significant from the nonpreloaded group, it did show change from the other two control groups. All of the genes explored showed a decreased gene expression in the preloaded, no exertion group as compared to the experimental group, however, only collagen II was

statistically significant. More statistical relevance can be observed when the experimental group is compared to the 0.75 MPa hold group, as collagen II, collagen I and ADAMTS-4 all show statistical significance, while other genes continue to support this difference, despite lack of significance. The trends presented here are able to suggest or explain disc behavior. The short history 2 hour loading groups are meant to show immediate response to the loads given known environment the cells are experiencing.

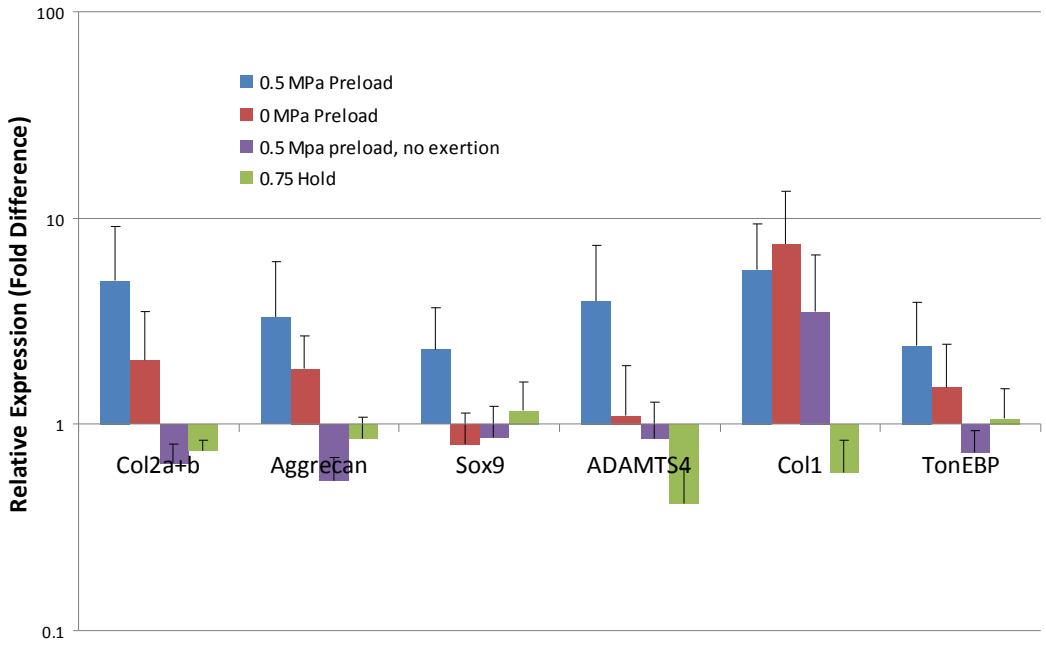

Figure 5.3 Real time RT-PCR was performed on each of the short history loading scenarios. The experimental group was compared to each control group individually using an independent T-test ($t<0.05$) as there was no need to compare the control groups with each other. While there were no differences found between the preloaded experimental group and the nonpreloaded control group, a number of statistical differences were found with the other two control groups.

The long history group was examined to determine if there was a change after an additional 2 hours of loading. The total of 4 hours did not help capture the biological response of the cells, as the separation between experimental and control groups lessened, instead of widening. The experimental preloading group showed no statistical difference from the no preloading group (Figure 5.4). Not only was there no significance, all but the collagen I gene expression was almost identical, and close to the relative expression of the unloaded adjacent internal control. The relative expression for these genes was close to 1.

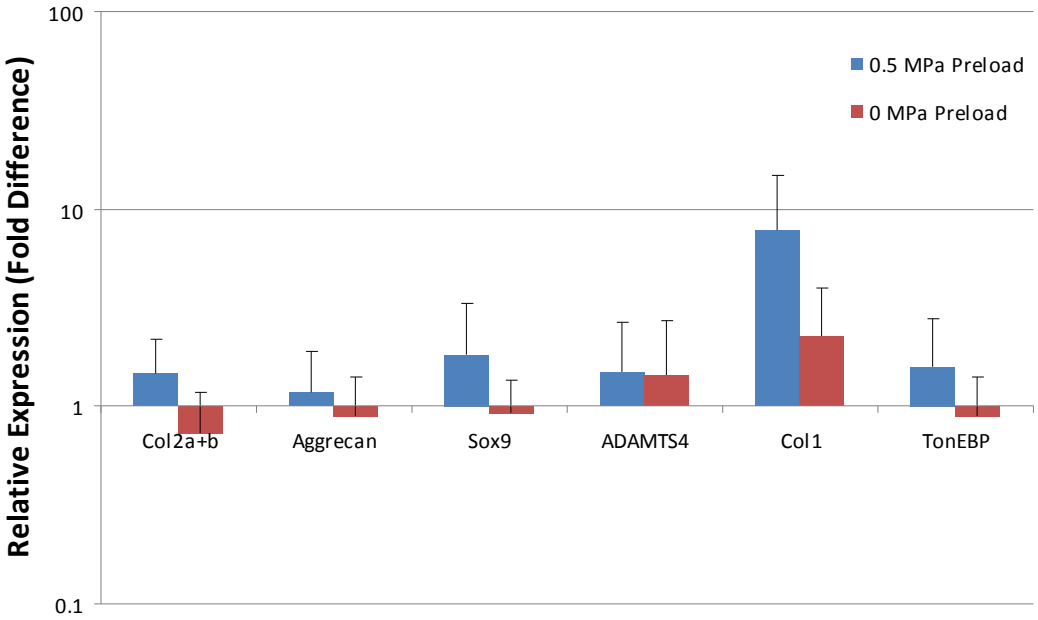

Figure 5.4 The long history loading regimes were compared over a variety of relevant genes, however, none of the gene expression changes were statistically significant, using an independent T-test ($t<0.05$). The gene expression between the preloaded and non preloaded groups are markedly more similar, suggesting that the extra time under loading was beginning to allow the biological response reach equilibrium.

The disc height was recorded to garner evidence of changing viscoelastic properties between the loading groups. The resolution of the images taken proved to be inadequate to observe any viscoelastic change in the creep response, using the standard viscoelastic solid model. The strain observed, however, provided a final displacement change at the end of the loading program, shown in Figure 5.5. In the short history group, this end strain was compared and showed no difference among the preloaded experimental group and the no preload control 1 group and the 0.75 MPa held control 3 group. There was a statically difference with the preloaded no exertion control 2 group. In the long history group, however, there was a change between the experimental and the control group.

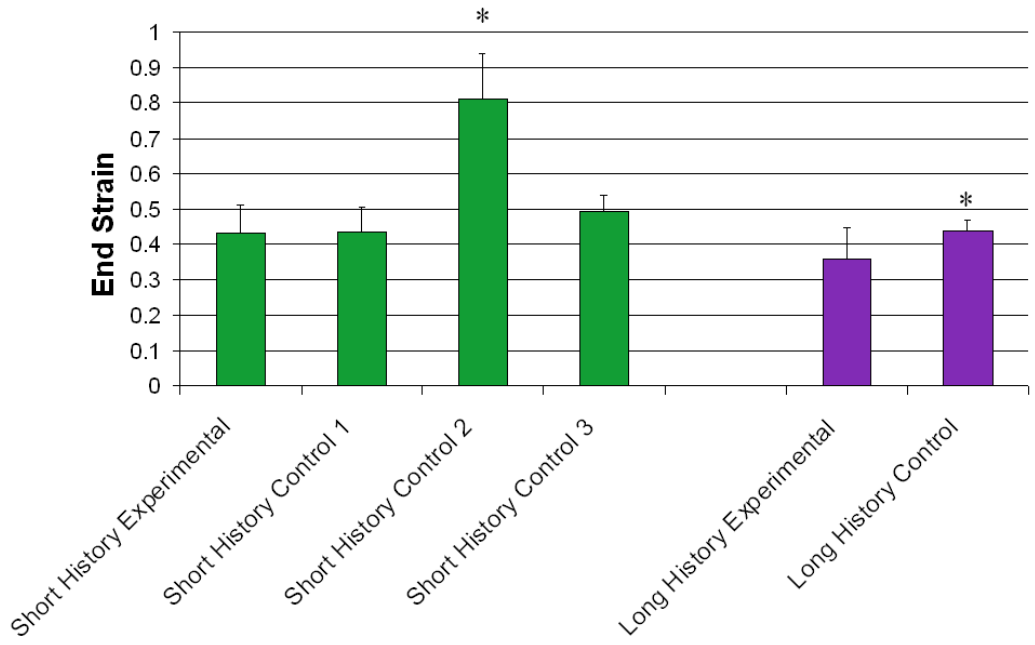

Figure 5.5 Disc height measurements did not yield conclusive data in terms of creep response. The final disc heights were recorded and showed no significant difference between the 0.5 MPa preloaded group and the no preload and the 0.75 MPa hold groups. These three groups showed a difference with the no exertion 0.5 MPa preload group. In the long history group, the two groups also had statistical significance in disc heights using a one-way ANOVA with Tukey's post hoc HSD analysis ($\alpha<0.05$).

5.4 Discussion

Our past work has shown that load history influences hydration and mechanical behavior of the IVD, particularly the intradiscal pressure. More specifically, given a low initial preload, followed by a higher exertion load, the intradiscal pressure generation is lower than if the exertion load was applied alone[97]. Given this simple example of the effects of prior loading, we understand the state of the NP during this exertion state. We can compare the preloaded to the nonpreloaded group and predict relatively, that the hydrostatic pressure within the disc is higher in

the nonpreloaded group. Using this behavior, this experiment then examines the biological response of the cells in terms of gene expression of relevant proteins.

The gene expression of the preloaded experimental group shows greater, albeit not significant, expression of catabolic extracellular matrix proteins including collagen II, aggrecan and sox9, as compared to the control 1, nonpreloaded group. This is contrary to what we originally predicted, as it has been shown that increased hydrostatic pressure causes both, increased collagen and proteogylcan synthesis as well as increased gene expression of collagen I, collagen II and aggrecan with NP cells in alginate beads[151, 152]. Instead we saw that there is a decrease in aggrecan and collagen II for the higher pressure environment of the nonpreloaded group. It is believed that hydrostatic pressure should stimulate build up of extracellular matrix proteins such as collagen II and aggrecan, however neither collagen II, aggrecan, nor sox9, an collagen II promoter showed increased levels. ADAMTS-4 showed upregulation in the preloaded, low pressure group, which leads to a breakdown of aggrecan, the main proteoglycan that is responsible for hydrating the disc. This may not be a destructive path however, as it is shown to be combined with an increase of aggrecan, which may indicate a remodeling or restructuring and rebuilding of the extracellular matrix. This could suggest that instead, the inadequate pressure buildup signaled the cells to regenerate and reorganize matrix. Both the preloaded and nonpreloaded group both showed comparable increased gene expression for collagen I, the more fibrous structural element in the disc, which is expected under any loading scenario.

A different approach was taken to explore the influences of the disc on cellular productivity. A number of other groups have explored the influence of osmotic pressure, rather than applying hydrostatic pressure using mechanical means They suggested that mechanical stimulus of static stress or cyclic strain were not as influential as osmolarity, also showing that rising osmolarity could induce expression of aggrecan and collagen II[149]. To additionally investigate the effects of osmolarity, the exploration of TonEBP, a tonicity enhanced binding protein, in this study was to test the response of TonEBP in this *in vivo* setting given known pressure changes. It was expected that the changing pressures would stimulate the expression of TonEBP due to its tonicity sensitive elements. TonEBP, which also functions as an aggrecan promoter, has been linked to helping regulate and encouraging proteoglycan remodeling to compensate for hyperosmotic environment[153]. Encouraging a build up of aggrecan under a hyperosmotic environment would encourage a greater capacity to sequester water, and therefore prevent future hyperosmotic events. Comparing the preloaded and nonpreloaded groups, the preloaded group with less pressure would indicate a smaller volume and less hydration, therefore a higher osmotic environment as compared to the better hydrated nonpreloaded higher pressure group. Using this definition of osmotic environments, we can reason the increased expression of collagen II, sox9, aggrecan and TonEBP, as they were more responsive to the increased osmotic environment in the preloaded group.

While papers have shown that 20 seconds of mechanical stimulation is enough stress to induce an increase in proteoglycan synthesis within 2 hours[154], other groups have shown that the peak gene expression response occurs at 24 hours, and does not

return to normal levels until 72 hours after loading[155]. Since our loading scenario requires the gene expression analyzed to correspond to the precise instant of pressurization by the disc, we chose a short 2 hour loading regime. However, as the response was not adequate to induce a significant gene response, an additional 2 hours was added after the initial preloading state. In this long history group, we again compared the preloaded group with a nonpreloaded group, following 3 hours of exertion load instead of the one hour experienced in the short history group. Not only did the expression levels all fall to close to natural levels, the separation between the two groups also lessened. The gene expression shows that collagen II, sox9, aggrecan, ADAMTS-4 and TonEBP all show relative expressions close to one, which is normalized to the natural unloaded disc. While the relaxation of the intradiscal pressure is well beyond 3 hours, this may also be explained by the influence of the tonic, and therefore osmolarity within the disc, which may have been initially hypertonic, however, after additional time, may have reached equilibrium, as cells pull small molecules and ions to reach a resting state. This osmotic environment may have returned to a normal environment, while the pressure from the mechanical exertion still remained, which would account for the lowered expression of all of the genes examined.

The use of the preloaded, no exertion group, control 2, was to offer data to ensure no residual response from the preload on the measured gene expression after the exertion load. This no exertion group provided evidence that the preload had no immediate impact on the measured expression of the experimental group by yielding results that were below the natural adjacent unloaded control disc. While collagen II

was the only statistically significant group, aggrecan, sox9, ADAMTS-4 and TonEBP all were close to achieving significance, adding to this trend. In combination with the no preload group, the no exertion group proved that it required the successive loads of both the preload and the exertion load to cause the increased biological response experienced by the experimental group.

The 0.75 MPa hold control group was introduced to expose the disc to an equal amount of stress averaged over the time period, as the experimental group to reinforce the idea of load history. One hour of 0.5 MPa preload and 1.0 MPa exertion load was equated to 1.5 MPa experienced over the two hours of loading. This was normalized to 0.75 MPa for both hours, to total the same average stress experienced by the disc over 2 hours. Again, this control 3 group showed a drastic difference from the gene expression displayed after the preloaded experimental group. Collagen II, collagen I and ADAMTS-4 all showed a statistically significant change between the preloaded experimental group and the 0.75 MPa hold group. Not only was it different, it did not even show the same expression pattern. Instead of a lesser degree of gene expression, this control group showed little change from the natural unloaded adjacent disc.

To further emphasize this point, Figure 5.6 was created to illustrate the influence of the sequential loading experienced by the preloaded experimental group. The short history experimental group experienced two hours of loading. The 0.75 MPa hold group also experienced two hours of loading, while the long history no preload control group received three hours of loading. Both of the compared control groups experienced either the same average stress or a greater amount of stress than

the short history experimental group, yet the gene expression results show almost no response for both the 0.75 MPa hold group as well as the long history nonpreloaded group, while the preloaded short history experimental group had significantly larger response. These loading scenarios have similar attributes, with the only difference being the addition of the preload, which was then increased to an exertion load. This sequential step load caused this more drastic gene response, signifying that prior loading is important when predicting the biological response as well.

Lastly, the end strain observed by the radiographs of the disc heights in the short history group, only managed to show significant change between the no exertion control group from the other two control groups and the experimental group. A significant difference between the experimental group and the control group was able to be detected in the long history group. This helped verify that although the loading mechanics of the long history groups were different, the gene expression for that group remained surprisingly similar. Unfortunately, the resolution of the radiographs taken was unable to provide a clear enough analysis to show the changing creep response between the preloaded and nonpreloaded groups.

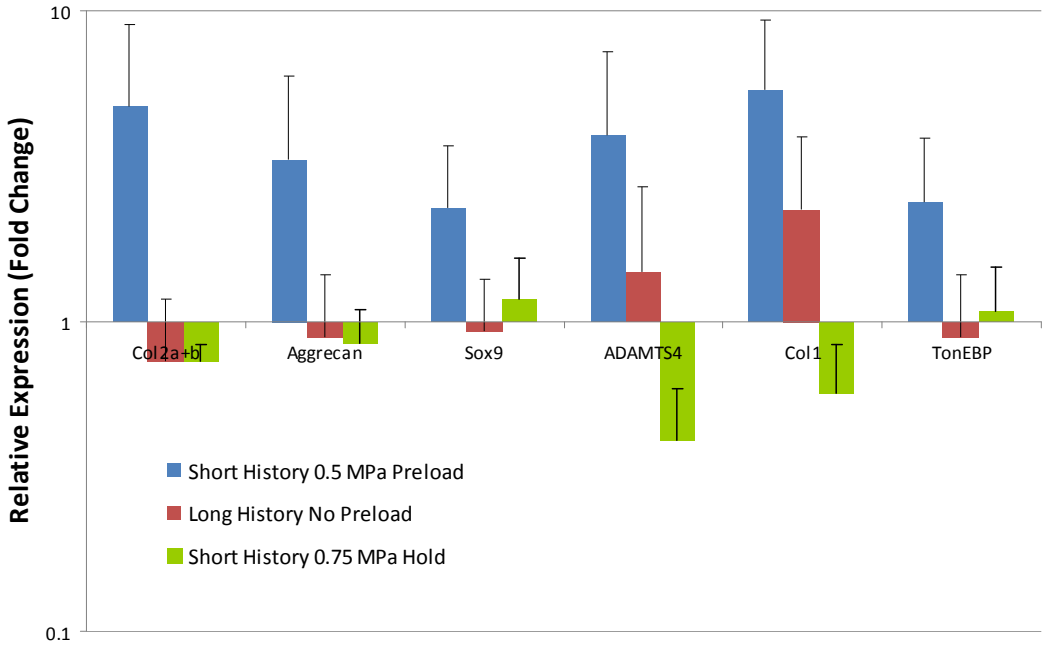

Figure 5.6 These testing groups were selected due to their similar loading nature. The short history preloaded group was loaded for two hours, first with low, then a higher exertion load. The long history no preload was loaded at the high exertion load for 3 hours total, while the short history loading 0.75 hold group was loaded for 2 hours. While the long history non preloaded group and the 0.75 hold group were both loaded for 2 or more hours, they show remarkably different results than the preloaded group. This may be due to the changed environment in the disc due to the differing load histories, notably a gradual 2 step load instead of only one large load. Statistical significance is noted, however a number of other gene comparisons between the long history control and the short history experimental group were close to reaching significance (sox9, collagen I and TonEBP).

Many things were learned about the biological response of NP cells after known load histories. While the anticipated high intradiscal pressure did not yield expected changes in catabolic gene expression, there was a noticeable difference between the low and high preloaded groups, as well as the control groups, showing that the unique sequence of preload and exertion load changes the behavior of the

disc. Control groups 2 and 3 confirmed that the unique response garnered from the experimental group did not result from the preload alone, or from the total stress placed on the disc, respectively. What can be concluded is the ability for differing load histories to elicit a response. While the no preload group generated a smaller gene response, the high stress preload experimental group yielded a definite response, causing increased gene expression for the anabolic genes as well as the catabolic ADAMTS-4 gene. This study has also eliminated hydrostatic pressure as the primary driving force behind dictating gene expression of NP cells under loading. It is likely due to a combination of the other physical environmental factors suggested, tonicity and shear stress, or an unknown chemical stimulus. What was learned was that NP cells are indeed sensitive to the subtle changes in environment imposed by differing load histories, and that these changes are not alone dictated by intradiscal pressure. The hydration and osmolarity need to be further examined in order to determine a dominant factor that triggers our observed response. Additionally, we see through the long history group that there is likely a biological equilibrium that is reached between 2 and 3 hours of loading at one stress. While it takes over 3 hours for the intradiscal pressure to reach equilibrium, we saw a loss of response by all groups, as the nonpreloaded and high preloaded groups both showed gene expression close to that of the unloaded adjacent control disc during the long history experiment. The physical pressure parameter is again shown as not the lone dictating factor for the biological response of NP cells.

The effects of load history have been captured in terms of intradiscal pressure and general viscoelastic behavior. This study effectively begins to translate some of

these physical changes experienced by the discs with given loading histories, into biological changes experienced by the cells, as shown through gene expression. While we initially predicted the generated hydrostatic pressure dictating gene response, it then became clear that another driving factor was in play, which we now believe to be osmolarity. There are many contributing factors when it comes to cellular behavior, with many triggers and conflicting signals. More study is necessary to fully understand what is dictating the response; however, it is clear that prior loading does change and further complicate the behavior of the disc, mechanically and biologically.

Chapter 6 Optimizing Miniature PAMs for an *in vivo* Rat Disc Loading Device

Our experiments have shown short term immediate effects of load history, however, the more interesting story involves influences of load histories as they are applied over a longer period of time. While past devices have been made for long term dynamic loading for a caudal rat disc, the PAMs offer a number of benefits including a lighter weight that improve upon the existing designs. Miniature PAMs are a relatively new concept and thus need to be characterized and optimized for our need due to customizable nature and number of combinations available.

6.1 Introduction

Intervertebral disc mechanics has been widely researched in the past in an effort to understand the cause of low back pain, experienced by greater than 70% of people in their lives[156]. The intervertebral disc is also a complex fibrocartilaginous tissue unlike the more commonly studied articular cartilage. Instead of varying in depth, the intervertebral disc is made of a gelatinous core called the nucleus pulposus, which is surrounded by a fibrous lamellar ring structure, the annulus fibrosus and capped by cartilaginous endplates. The complexity of the disc's structure has made its behavior more difficult to understand and predict. To understand the biological changes experienced by the disc during loading, many approaches have been taken to load the disc cells including *in vivo*, organ culture and in scaffolds. Common research models have included cadaver spines, various large animals (bovine, ovine) and small animals (rat, rabbit)[12, 13, 15, 98, 144, 154, 157]. The most obvious disadvantage

towards cadaver spines is the difficulty to harvest living tissue and therefore inability to resultant biological response after applied loads. Our lab has focused on the development of using a caudal rat disc model, in which we've developed a trans-annular puncture induced generation protocol[105], and have a good understanding of *in vitro* cell behavior in monolayer on tissue culture polystyrene, and collagen thin films, as well as in alginate 3D culture[158].. This study aims to take advantage of the commonly used rat model to create an *in vivo* loading device capable of long term loading to study biological changes over time.

There have been many devices that apply long term loading regimes in vivo, however, these systems are designed for larger animal models[98, 159, 160]. In the rat model, a number of groups have studied gene expression and protein synthesis after loading, however, these are mainly short term experiments lasting only up to a few hours under anesthesia attached to a bench top loading device[16], but few devices have been used to examine dynamic long term loading on the disc[13, 150]. While a controlled dynamic loading scenario is our goal, another creative method that must be mentioned is a model that applies stress on the spine through the amputation of the forelimbs and forced hind leg ambulation in rats[106]. While innovative, the ability to control loading using this method is limited and only shows the degenerative process of upright posturing in rats. Most notably, Wuertz et al. used a piston based pin and ring device for rat tail disc loading for up to 8 weeks[150]. This is a robust device that is easily controlled and used for a variety of loading scenarios, so it was the basis or model for our own design. With our device, we hope to reduce weight and size, as well as cost. We plan to achieve this through the use of Pneumatic Artificial Muscles

(PAMs) attached to a similar ring device utilizing cross-pins that are drilled through the vertebrae of the motion segment to be loaded. Cost of construction and spare parts for repair are low for the PAM device, while achieving the same goal of a customizable loading regime.

Pneumatic Artificial Muscles (PAMs), also known as McKibben actuators, are soft smooth actuators made using an elastomeric bladder enclosed within a braided sleeve. Briefly, as pressure is applied to the bladder, the PAM expands in girth, while decreases in length. This contraction is the desired "stroke" as compared to a conventional piston actuator. While not new to the medical or biological setting, as it was originally used in orthotic devices in polio patients[161], more recently this type of actuator has been used in manipulation and joint control in robotic systems, extension of wing flaps in aircrafts, as well as a variety of other applications[162-164]. The relatively simple design, and minimal material is composed of the elastic bladder, mesh braided tubing and the small aluminum end-fittings. Not only does this make the design lightweight, but also relatively inexpensive to produce. Also, these simple parts may be swapped for a change in material, braid angle, or size for an unlimited combination of properties[165]. Other noted advantages of the PAM actuator include durability, reliability and a high power to weight ratio as compared to electrical or hydraulic actuators[166, 167]. To our knowledge, this is the first attempt to develop PAMs at the small length scale (<inches). Another big advantage the PAM provides is the smooth actuation motion, which is particularly important when dealing with biological samples; there isn't a sudden impact between loading commands, as the

bladder provides a smooth transition between loads. Unlike a pneumatic piston, which has to overcome the friction on the stroke shaft, the PAM is able to flow smoothly between loads. This is relevant when loading a biological sample such as a disc because a sudden application of load may exert trauma upon the tissue instead of the desired load, which would provide very different mechanical results, as well as possibly cause damage on a cellular or structural level. An additional benefit from the frictionless stroke motion is the retraction of an unloaded PAM. In a piston, there is inherent friction stemming from the shaft of the piston itself. If this friction is in place, a loaded tissue that is suddenly unloaded must battle this friction in order to relax, however, with the PAM, this frictionless stroke would allow immediate relaxation. One disadvantage is that stroke length that is limited by the elasticity and girth of the bladder. However, in our applications, displacements are relatively small, and stroke length would not be a relevant factor. Lastly, the flexibility of the PAM allows a number of additional benefits towards loading the disc. Most obviously, the tail is itself, a flexible joint system that may bend or flex due to loading or because of rat motion. The PAM system would allow the flexibility for this to occur. Additionally, the flexibility allows for future application of bending studies, to overload the disc on one side and open a whole new type of loading regime to investigate.

6.2 Methods

6.2.1 Mini-PAM Assembly

A mini-PAM is composed of a latex bladder surrounded by a braided sleeve. These two materials are held together with swaged end fittings. Each end fitting is made of a 0.5-in length, 6-32 threaded rod and a 3/16-in diameter outer swage tube. The threads on a 1/8-in section of the threaded rod length are removed. One of the end fittings is given a thru-hole so the mini-PAM can be inflated and deflated.

In order to assemble the actuator, the latex bladder is placed inside the braided sleeve, and centered. The non-threaded sections of each end fitting are placed inside the ends of the latex bladder and held in place by the elasticity of the bladder. Epoxy is added over a small section of the braid where the end fittings meet the bladder, which aids in holding the assembly together after curing. The swage tubes are then positioned over the braided sleeve so that half of the swage tube covers a portion of the threaded rod and half covers a portion of the rubber tube.

The assembly is then placed into a 3/16-in collet until one swage tube is fully within the collet. The collet is tightened in a milling machine, permanently deforming the tube and clamping the ends. The process is repeated on the other end. The assembly is removed from the collet. Excess braid is trimmed from the outsides of the clamped swage tubes, and the mini-PAM is left until the epoxy cures. After the swaging process, the mini-PAM should be able to withstand an axial force of about 50 lb without slippage in the end fitting.

In order to assess the effectiveness of the mini-PAMs and adequately compare the different materials and options available, we constructed two sample PAMs for

each varying specifications shown in Table 6.1 and Figure 6.1. We explored variations in bladder material, braid material as well as length. Two samples were created and tested for each combination of material and length. These samples will be tested to find the optimal combination for this application.

Table 6.1 Combinations of lengths and materials to be tested.

Length	Braid Material	Bladder Material
1 inch	Kevlar	Latex
0.75 inch	Kevlar	Latex
0.5 inch	Kevlar	Latex
1 inch	Nylon	Latex
0.75 inch	Nylon	Latex
1 inch	Kevlar	Silicon

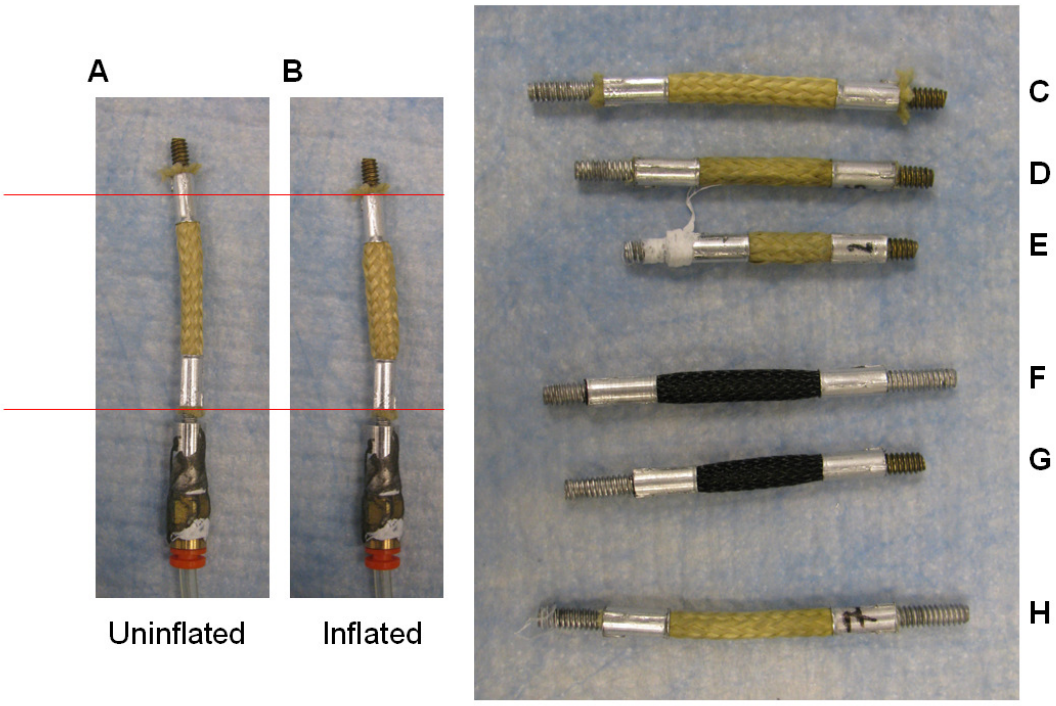

Figure 6.1 An uninflated PAM (A) is lined up with an inflated PAM (B) to show the compression and stroke length of a Kevlar PAM. A 1 inch, 0.75 inch, and 0.5 inch Kevlar, latex bladder PAM is represented by (C), (D) and (E), respectively. 1 inch and 0.75 inch Nylon, latex bladder PAM is shown as (F) and (G), while (H), represents a 1 inch Kevlar PAM with a silicon bladder.

6.2.2 Fixed Pressure Characterization

The characterization of PAMs is accomplished by charting a force vs displacement cycles for each individual PAM at different fixed pressures[166]. This is used to track the behavior of the PAM while pressurized and obtain a maximum force output at each given isobar. The mini-PAMs were each loaded onto a Bose Electroforce materials testing system (LM-1 Bose Corp Eden Prairie, MN) To characterize the PAMs, first a relationship was determined between force exerted, pressure applied and change in length was determined. Each range of experiments

started with a displacement of 0mm, and applied with a pressure to obtain 0.50N. Pressure applied below this threshold does not fully inflate the PAM and therefore does not induce force generation by the PAM. At each 5 psi pressure increment, this maximum starting force was recorded, and the crosshead was lowered until the force exerted by the PAM was zero. This maximum displacement, representing the stroke length of the PAM at a given pressure, was then programmed into the loading module. At each fixed pressure increment, the PAM was cycled between zero displacement and the appropriate maximum displacement for 30 second intervals with a constant strain rate of 0.05mm/sec, forming a sawtooth waveform shown in Figure 6.2. The force exerted during the three cycles was recorded. This process was repeated in increments of 5psi until a maximum starting force reached 12N, which corresponds to approximately 1 MPa of stress for a rat tail disc. A force-displacement relationship was established for each pressure increment. Since we will be using two PAMs per tail loading device, this would be double the maximum force needed during long term loading regimes. In addition to obtaining the maximum force exertion at each pressure increment, as well as a maximum stroke length, this test also tracks the force displacement relationship for each given PAM that will allow further comparison.

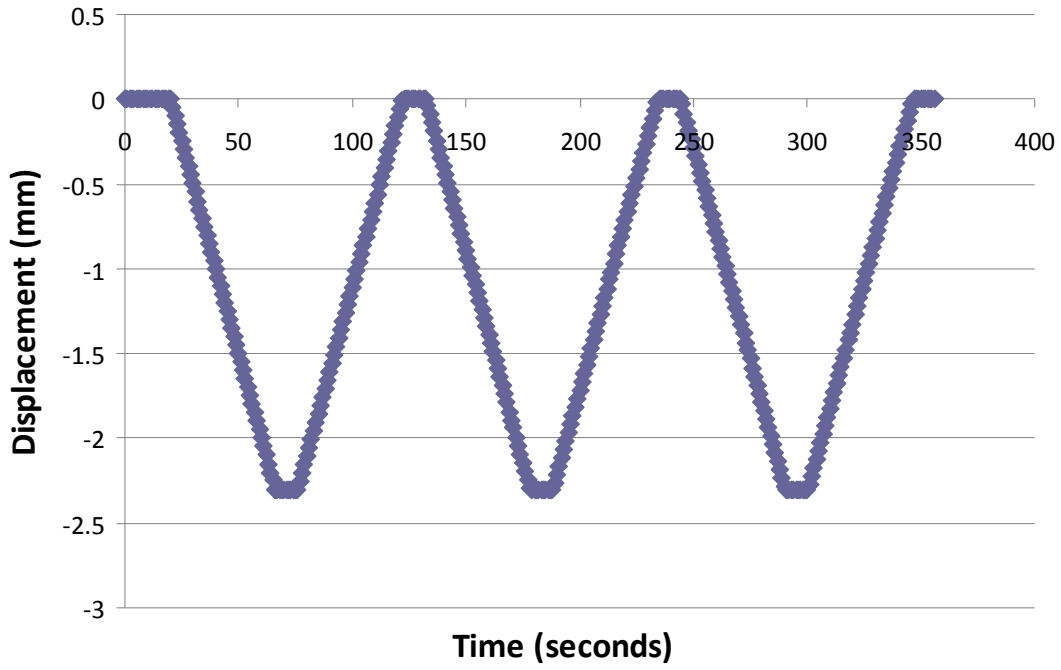

Figure 6.2 Displacement controlled loading during fixed pressure characterization. This is a sample output of the displacement control of a 1inch Kevlar, latex bladder PAM applied with 50psi.

6.2.3 Fixed Displacement Characterization

The use of our long term loading system is dependant on the PAM adjusting pressure to keep up with a changing displacement. This means the displacement and pressure will change simultaneously; therefore characterization now, with a fixed displacement will show the behavior of the PAM given changes in the other parameter. This part of the study explores the behavior of the mini-PAMs while fixing the displacement and varying the applied pressure. The relationship found with this characterization method will also be compared to results found with the fixed pressure characterization to ensure a similar relationship regardless of what variable is changed. This is important to investigate, as our final loading device will

be subject to changing displacement due to the viscoelastic properties of the tissue as well as changing pressure to allow us to dictate an applied force. Five minutes of rest was given for each PAM after each test to allow ample time to recover. Preliminary tests showed that PAMs recovered well within the first minute. Each PAM is then held at fixed displacements and increased pressure to use a second method to verify the relationship between displacement, applied pressure and exerted force. With the PAM still mounted in the materials testing bench, the displacement was held constant, starting at 0mm. The pressure was increased in increments of 5psi while the force exerted by the PAM was recorded, exemplified in Figure 6.3. The pressure was increased until the recorded force reached 20N. Five minutes of rest was allowed, and this time, the pressure was raised to the previous maximum and decreased at 5psi increments, again with the exerted force recorded. Given data found in the previous experiment, minimal pressure was applied while the displacement was decreased by 0.1mm. The procedures of increasing and decreasing pressures were repeated and recorded for each 0.1mm displacement increment ending with a maximum displacement of 0.5mm. The inflation and deflation measurements are fairly similar and account for any hysteresis in the system, and are averaged for further comparison.

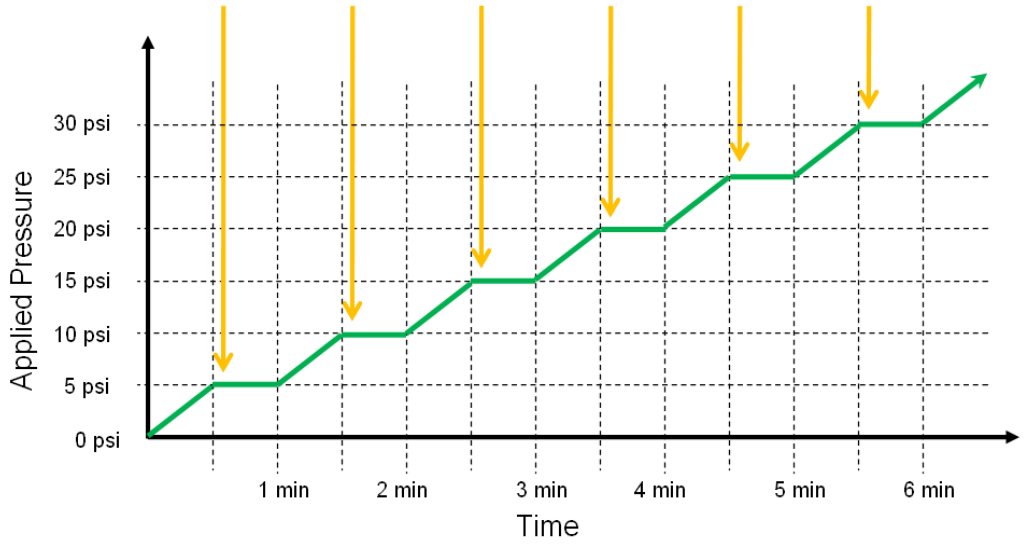

Figure 6.3 Example of incremental increase of pressure while the displacement held constant during the fixed displacement characterization.

6.2.4 Ex Vivo Viscoelastic Feedback Testing

After characterizing the relationship of the PAM, calibration is made with an equation to dictate input pressure given a measured strain or displacement. Since live tissue has viscoelastic properties, this system needs to be tested to ensure a stable force can be maintained with only displacement feedback. A frozen rat caudal 4-5 disc was thawed at room temperature for 4 hours and mounted onto a custom loading device that includes two PAMs as the driving force. In this experiment two 1in Kevlar braided, latex bladder PAMs were used. Cross pins are drilled into the vertebrae of the motion segment and mounted onto rings that are attached to our testing device. A load cell is fixed in series with the tail, while a strain gauge is attached in parallel as a feedback for the loading device (Figure 6.4). We developed an interface in LabView (National Instruments, Austin, TX) to apply and maintain a constant 18N compressive force (roughly 1.5MPa) on the disc as calculated for a

circular cross section of the caudal disc diameter measured using a radiograph. The feedback coming from the strain gauge is fed back into the equations gathered during the characterization step and results in an increase in pressure to compensate for the viscoelastic creep experienced by the disc. This test is to ensure that we are able to maintain a constant force, despite the creep of soft tissue while using only displacement feedback.

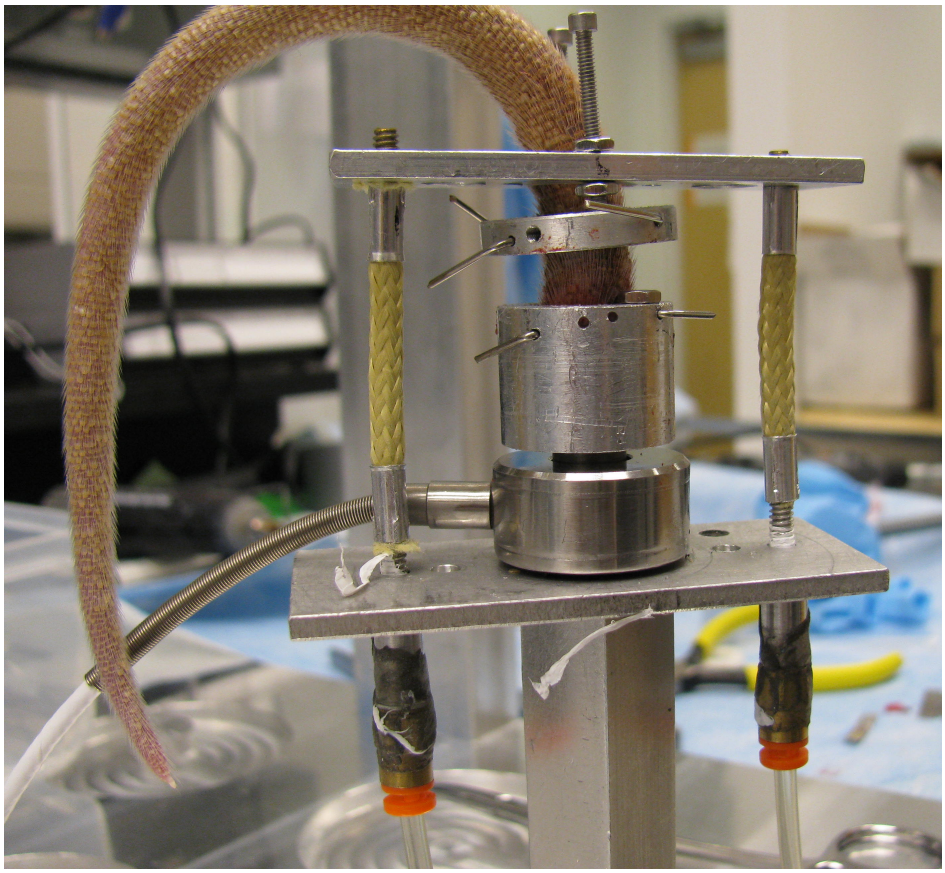

Figure 6.4 Picture of the *ex vivo* test setup.

6.3 Results

6.3.1 Fixed Pressure Characterization

By applying a constant pressure and varying the displacement, we were able to obtain the limits of each set of PAM devices. First we are able to determine the operating range of the PAM by finding the minimum inflating pressure. Then with each step, we are able to monitor the maximum force generation at each given pressure. Given enough pressure, all samples tested provided enough force to apply a minimum of 12N at maximum extension. It is observed that the more pressure applied to the PAM, the greater the stroke length as well as the force generated. The maximum force generation is found at each pressure, as well as stroke length. The pressure range necessary to generate our desired force will also be critical in choosing the correct PAM. These will be important in comparing the properties with a changing pressure. Additionally, this knowledge will help decide which PAM is optimal for our purpose. As seen in Figure 6.5, there is a slight hysteresis in the PAM, as the stretching and relaxing takes different paths. The behavior of the PAMs was observed given a range of static pressures applied. This allowed a relationship to be determined between the applied pressure, the displacement and the pressure generated for each given PAM. This characterization was necessary to compare the different materials available to us, as well as the variability among PAMs with the same materials.

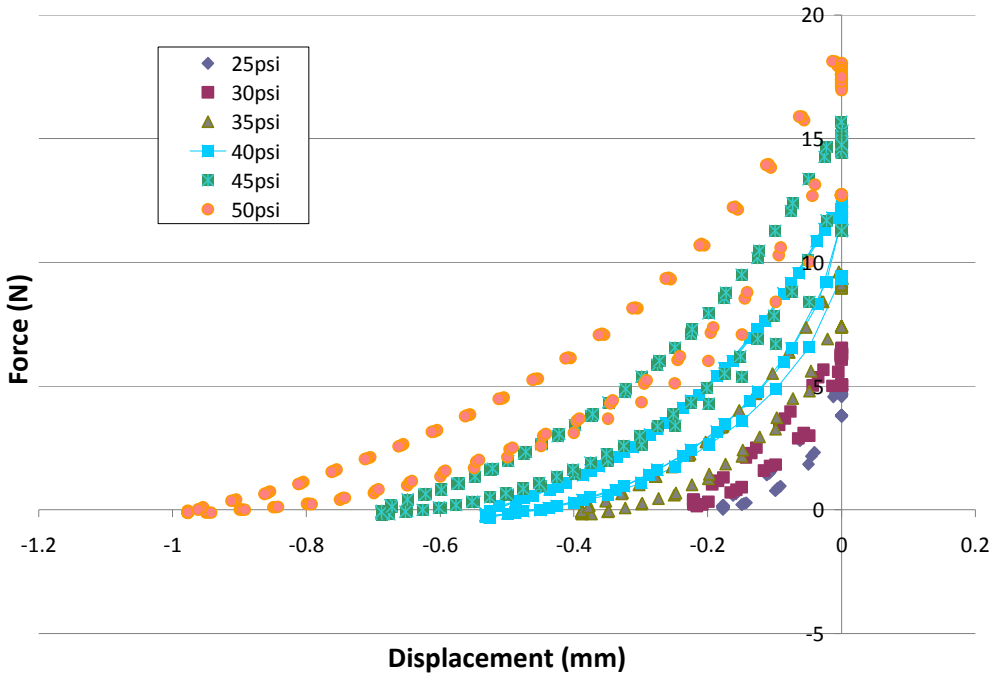

Figure 6.5 Example of a force-displacement graph cycles for a 1in Kevlar, latex bladder PAM. Each pressure isobar is included and shows the increased force generated with each increment. The hysteresis can also be observed between the compression and tension experienced by the PAM under displacement control.

All of the PAMs created were able to reach exertion of 12N, requiring at most 65psi to reach that force at full extension. When comparing the lengths, the longer the PAM, the lower the pressure needed to obtain the same amount of force. For example, when comparing the Kevlar braided, latex bladder PAMs, we see that the 1in is able to reach over 12.67N given just 50psi of pressure, while the 0.75 and 0.5 in PAMs are only able to generate 10.08 and 9.06N, respectively as shown in Figure 6.6. The range of motion or stroke length is also equally correlated, as the longer PAMs have a longer stroke length. The 1in PAM at 50psi had a stroke length of 0.673mm compared to 0.342 and 0.291mm of the 0.75 and 0.5in PAMs. Considering length

only, the same trend is also seen with the Nylon braided, latex bladder PAMs as well. The longer 1in Nylon latex PAM generates a larger force of 17.77N and a longer stroke length of .275mm at 50psi, compared to the 10.25N and .207mm stroke of the 0.75in Nylon latex PAM.

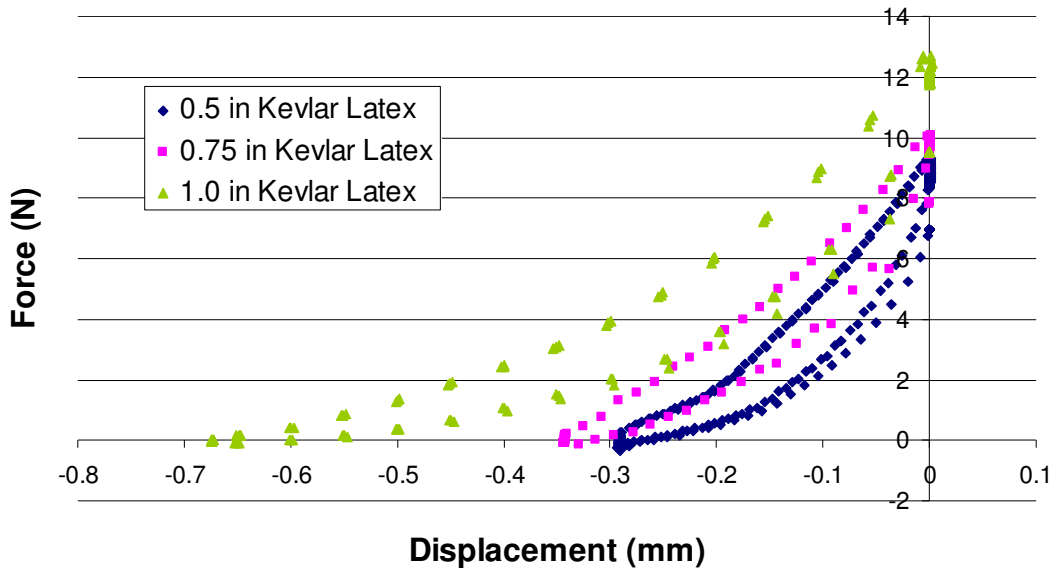

Figure 6.6 he effects of PAM length is explored in this study. The force-displacement graph for three PAMs (0.5, 0.75 and 1.0 inch Kevlar, latex bladder) are plotted together at 50psi fixed pressure to compare the behavior between varying lengths of the same material PAMs. The maximum force and stroke length can both be observed to increase with an increase in length.

Comparison amongst the materials was another point to be considered. It was learned early on during the fabrication stage that the silicon bladder would be more difficult to work with, which lead us to suspect it to be hard to create consistent PAMs. This was true with the two Kevlar braided silicon bladder 1in PAMs we tested, as one sample yielded 17.6N and 0.49mm of displacement given a pressure of

65psi, while the other yielded 22.7N and 0.67mm of displacement with only 40psi. The discrepancy between the two was surprising, despite difficulty with the material, since the two samples were chosen as the two most similar pair created. This showed that the silicon bladder was too sensitive given our assembly methods and we are unable to consistently create PAMs of the similar properties.

When comparing the two braiding elements, the Kevlar material provides a loose fitting almost fabric-like weave of material, whereas the Nylon material provides a more rigid mesh, netting that surrounds the internal bladder. Both the Kevlar and the Nylon materials offer consistent results, however given similar sizing, the Nylon mesh provides a larger range of force generation as compared to the Kevlar counterpart. At 50psi, the 1in Nylon PAMs generates almost 18N of force, while the 1in Kevlar PAM only produces about 13N. This trend is consistent with the 0.75in PAM as well. This loss in force generation is made up for in increased stroke length. While the Nylon PAMs produce higher forces, the Kevlar PAMs have a larger range of motion. Even the 0.5in Kevlar PAM had a larger stroke length, 0.291mm, as compared to the 0.275mm stroke length of the 1in Nylon PAM.

Another interesting point we observed was when the PAM was inflated to pressure, this initial maximum pressure was different from the one generated when the displacement was cycled. In Figure 6.7, we can see that initially, when the 40psi was applied, the force generated was around 9.34N, but after a full stroke length, the PAM was returned to the original length, full extension, however, the force was raised to 12.02N which slowly relaxed over time. After each cycle of the stroke length, the maximum force was returned to around 12N and displayed the same

behavior. All of the PAMs tested, with all of the braid and bladder materials, all showed this behavior. This represented approximately a 25, up to 50% increase in force generation for the Nylon braided PAMs at high pressures. Each PAM also exhibited excellent repeatability, as each of the 3 runs for each PAM overlapped with the other two runs perfectly as seen in Figure 6.7. This is another important factor, as the ability for the PAM to function repeatedly after loading and yield the same response. This ensures that the PAM will produce consistent results over numerous experiments as well as consistent results during cyclic loading.

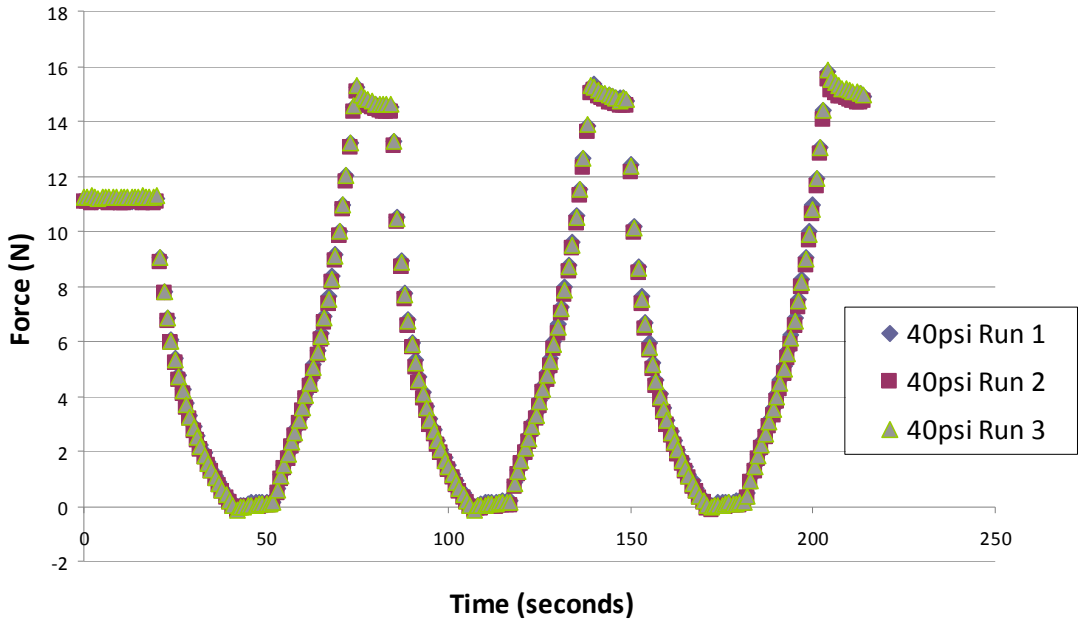

Figure 6.7 A sample force vs time graph is shown here to emphasize the repeatability of the PAM during the three cycles of displacement controlled loading. Shown here is three separate runs of a 1inch Kevlar, latex bladder PAM held a pressure of 40psi. Note that the readings overlap exactly, showing that the properties between runs do not change.

6.3.2 Fixed Displacement Characterization

Further characterization of the PAMs was done by holding the displacement at certain levels and changing the input pressure at 5psi increments, while measuring the force generated. This provided a different view at the behavior of the PAM. These observed forces were plotted against the applied pressure and graphed for each sample PAM, exemplified in Figure 6.8. A relationship was plotted and a linear best fit line was found for each displacement. The slope of each displacement line was compared to each other to determine how similar or otherwise predictable the behavior of the PAM would be. Each of the linear fits yielded R^2 values greater than 0.99. This linear behavior is beneficial towards defining and characterizing each PAM, creating a simple relationship between pressure, displacement and force.

For each PAM, the maximum change in slope between all of the displacement lines was 0.117. This shows that all of the lines were relatively parallel and showed even response regardless of what displacement the PAM was stretched to. While the slopes all fell between 0.05 and 0.12, the only group that was outside of that range was the 1in Nylon PAMs. The 1in Nylon PAM had a large variability between the displacements. This was possibly due to the larger range of forces that it could produce, but the difference between smallest and the largest slope amongst all of the displacement was 0.54. This variability was much larger than all of the other samples.

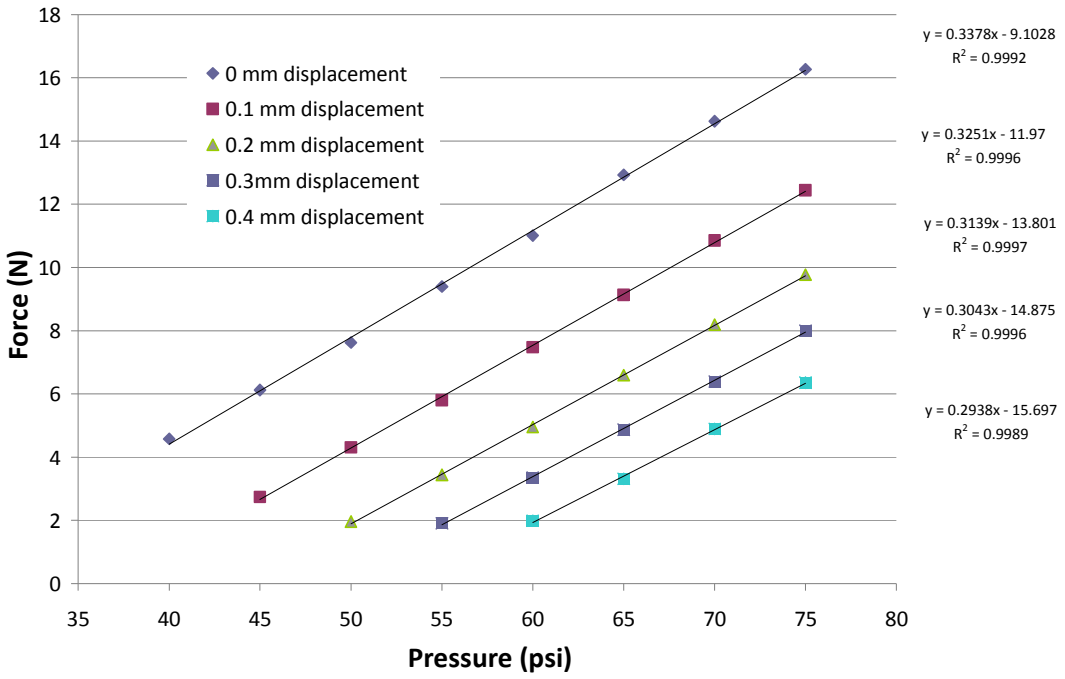

Figure 6.8 A sample force-pressure graph of a 0.75 inch Kevlar, latex bladder PAM from the fixed displacement characterization experiment is shown here. Linear best fit approximations were applied to each fixed displacement increment. All increments show relatively consistent slope exhibited, meaning the relationship between force and pressure doesn't change with changing displacement.

6.3.3 Comparison of Fixed Pressure and Fixed Displacement Results

The fixed pressure and the fixed displacement tests observed the behavior of the PAM from two perspectives. It showed the function of the PAMs given either a static pressure or displacement scenario, to ensure that it would function as expected. A comparison was then made between the two methods to ensure that the PAM behaved similarly when the two methods intersected. In the case shown in Figure 6.9, at the maximum unstretched displacement of 0mm, the force reading was found given different applied pressures in both sets of tests. They are graphed here to show that indeed we observed the behavior from both tests. This is important because it

shows that regardless of a changing displacement or a changing pressure, we may expect the PAM to behave similarly, and any relationship mathematically defined one way, would be translatable the given a change in the other counterpart.

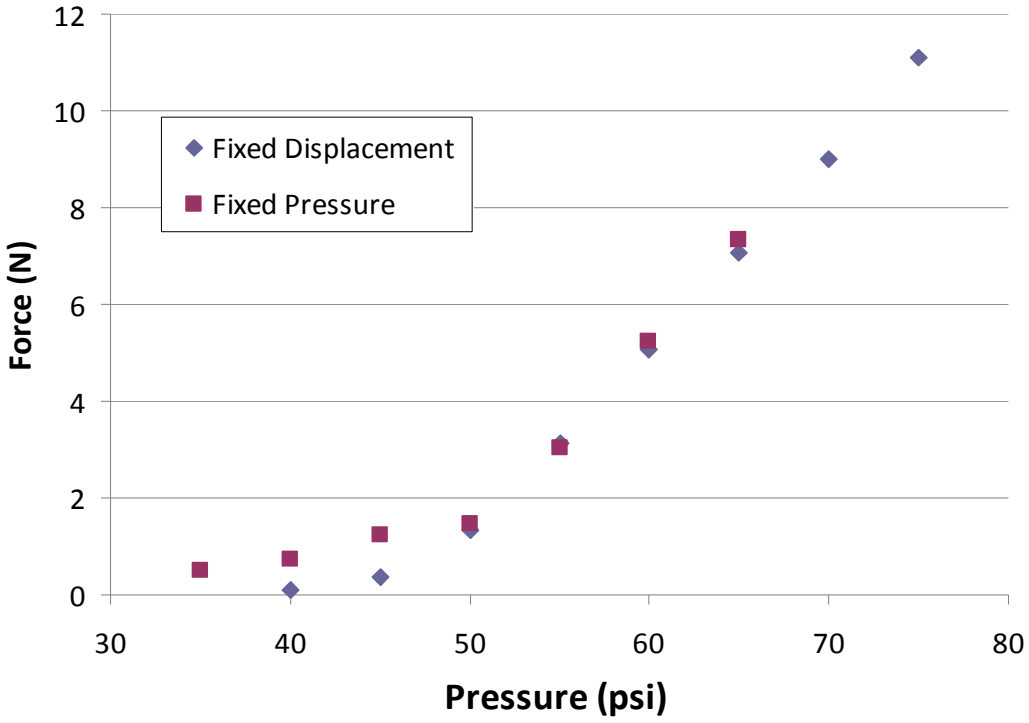

Figure 6.9 A comparison of the force-pressure graphs between the fixed pressure and the fixed displacement characterizations show an overlapping linear region that should be the target area for the PAMs to be used. The maximum pressures obtained at each pressure increment were taken and plotted against the measurements found at 0mm displacement. In addition to the stable linear region seen, a toe region is observed below 2N. This toe region represents instability and unpredictability on the low end for the PAMs, and should be avoided during usage to prevent unreliable function. This sample graph is taken from a 0.75inch Kevlar, latex bladder PAM, with data take at 0mm displacement in both the fixed displacement and fixed pressure experiments.

One additional point we found when it was graphed this method, was a toe region when the low force was generated. This has been observed for some other

larger PAMs before, as this toe region shows instability in the lower ranges of both pressure and force. Every PAM tested showed this toe region, the smaller PAMs with a smaller toe region, while longer PAMs with a larger toe region. In this case, the toe region extends until around 2N and then straightens to a linear relationship. This linear portion as well as the toe region was illustrated by both the fixed pressure and the fixed displacement experiments. It can be concluded that, as long as the toe region is defined, and the PAM is used to function outside of this region, and remain in the linear region, the behavior will remain both stable and predictable.

6.3.4 Rat tail disc loading in vitro

The PAM system is dependent on feedback of one of the displacement parameter and the desired force output to determine the amount of pressure to input into the device. After a relationship was found between these three parameters, it was input into a Labview program to allow automatic feedback during a long testing scenario. In this experiment, the goal was to use the displacement feedback to maintain a desired force, despite the constant change due to the viscoelastic creep from the animal tissue.

Using this configuration, we were able to maintain a relatively stable force applied to the tail (Figure 6.10). The target 18 N was not achieved, as the calibration was slightly off, and therefore did not quite reach the desired 18 N. The pressure was increased over the 30 minutes to compensate for the viscoelastic creep; however, it never reached the 18 N. The initial jump in force was only 13.88 N, which is only 77.1% of the intended 18 N force. The force exertion eventually reached 16.88 N,

which was 92.5% of the intended exertion. These results show that the initial calibration, or intercept value was not high enough to account for the required force. The initial intercept showing the need for pressure needs to be increased, so the target force is reached immediately in the beginning. The force then continued to increase, while the displacement was increased, which showed that the slope was too steep. The slope needs to be adjusted lower to result in no force change with the changing displacement. This can be adjusted in the future, and tested *in vitro* before for every set of PAMs before each *in vivo* experiment.

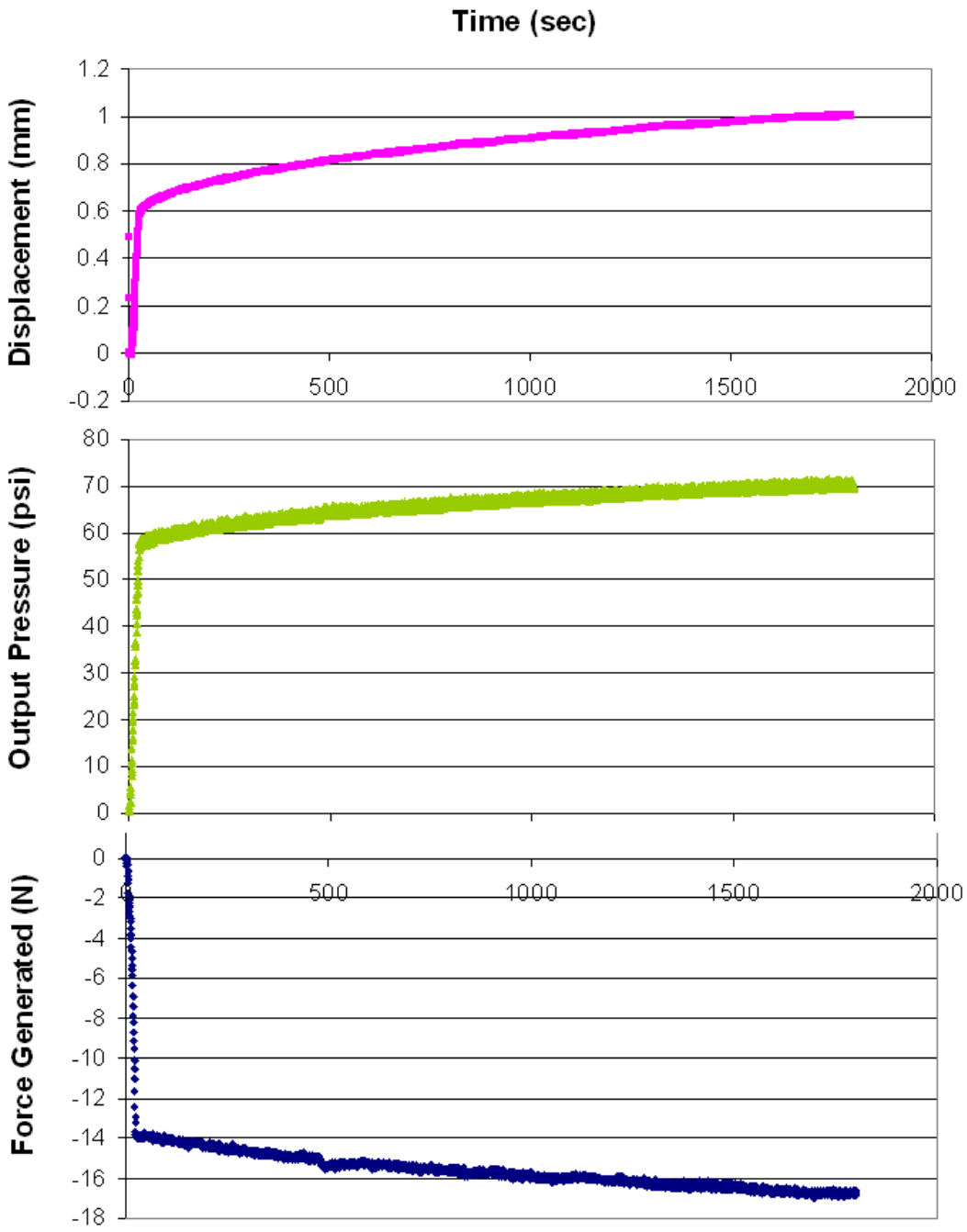

Figure 6.10 The in vitro test showed an inability to fully reach the target 18N, but was able to maintain a relatively stable force, as the system tried to keep pace with the viscoelastic creep of the tissue. Further calibration is necessary, as well as possible the addition of another pneumatic control, to allow independent calibration for each PAM, instead of an averaged response to control both PAMs.

6.4 Discussion

In this study, we demonstrated the feasibility of implementing a lightweight, flexible, frictionless actuator for applying compressive loads, and characterized its use in an animal model of intervertebral disc loading. Through miniaturization, we were able to adapt designs typically used in large robotics applications toward a small animal model. Because of the nonlinear behavior of PAMs, substantial mechanical characterization must be performed in order to apply loads with precision[163, 165]. As such, the relationships between inflation pressure, applied force, and PAM length must be explicitly determined. This was achieved by measuring force during incremental changes in length at constant pressures, and during incremental changes in pressure at fixed lengths. Using parameters obtained from our characterization experiments, we were successful in applying well-controlled loads to rat caudal discs.

Initial findings from the fixed pressure characterization showed that all PAMs fabricated were able to generate at least 12N of force. Since 12N corresponds to a stress of approximately 1MPa on a typical rat caudal disc (based on disc dimensions measured from radiographs and the assumption of circular cross section), this force is adequate for our applications. The anticipated usage will employ two PAMs mounted on the *in vivo* loading device, which will provide a 0-2MPa operating range for compressive stress application. It has been estimated that compressive stresses of 1MPa (roughly 300% body weight) and above represent a harsh exertion loads, and this value has been widely used as the basis of many biomechanics and mechanobiology experiments[75, 168]. Our in vivo experiments will apply dynamic compressive forces with variations in load history under load control.

6.4.1 Selecting the Optimal PAM Specifications

Outcomes of our mechanical characterization were used to assess PAM dependence on material and length as well as their uniformity and consistency. As a result of the characterization experiments, we were able to make choices about material and length specifications to use in our loading device. The most obvious choice made was the selection of the bladder material. The silicon bladder proved to be unreliable in terms of uniformity. Fabrication with the silicon bladder was less precise, which led to greater variation, and ultimately unreliable product. The force profiles showed that the silicon bladder PAMs were unreliable; the variation between the PAMs would provide very uneven properties when loaded in parallel. The choice between the braided mesh materials was more difficult. While both the the Nylon and Kevlar mesh provided adequate properties, when combined with the latex bladder, there were subtle differences that distinguished each. The Nylon mesh provided a more dynamic range of force generation, while Kevlar mesh provided a larger stroke length. This trend was observed for both the 1 in as well as the 0.75 in PAMs, showing consistency between PAM lengths. While the expanded force range offered by the Nylon PAMs is an attractive property, given our known or anticipated usage, the force yielded by the Kevlar PAMs are more than adequate. We tested both types of PAM, and both materials were able to provide double the desired force. Additionally, stroke length becomes important, as there is a significant amount of viscoelastic creep during axial loading of an intervertebral disc. The 0.5 in Kevlar PAM, the shortest PAM we tested, had a longer stroke length than the longest, 1 in Nylon PAM. This showed that the shortest Kevlar PAM was able to provide

adequate force, while providing a longer stroke than the Nylon PAMs. Since force generation was adequate for both materials, the most favorable combination of materials were the Kevlar mesh with a latex bladder. With this we provide sufficient force, maximum stroke length and reliable and repeatable construction.

We relied heavily on the characterization tests to select appropriate dimensions for the PAMs used. Consistent with other larger and previously used PAMs[166, 169], we found that the longer the PAM, the greater the force and stroke it can produce. The 1in PAM required less pressure to reach 12N, while the 0.75 and 0.5in PAMs required progressively more pressure to reach the same exertion. Although it would initially seem that the higher force capability of a long PAM is an advantage, size and precision must also be considered. Weight differences among different sized PAMs are negligible. Considering motion segment lengths in the rat tail, smaller more compact devices would be easier to handle and less obtrusive for the rat. In terms of force generation, we found that smaller PAMs require greater inlet pressures, and this broader range of pressure permits finer control over applied loads. However, in contrast with the force needed during testing, the stroke length of PAMs must accommodate the range of creep displacement anticipated for tails discs subjected to compression. Experiments have shown over 1mm during creep compression [97]. Given the limits of pressure in our testing setup, we were not able to measure absolute stroke length for each PAM, but it is understood longer PAM have a higher stroke length. In order to ensure that sufficient force could be generated for a PAM shortened by 1mm, a longer PAM would be necessary. Based on the competing

factors of precision and magnitude of force generation, the 0.75 in PAM was deemed the most appropriate of the three lengths tested.

6.4.2 PAMs as Actuators for in vivo Rat Tail Loading Device

Ultimately the PAM-based rat tail loading apparatus will be subject to time-varying displacements and time-varying forces due to not only the dynamic nature of the loading regimen, but also the viscoelastic behavior of the intervertebral disc. A load-controlled mechanism, therefore, requires monitoring displacements, while adjusting the inlet pressure. The characterization of the PAMs using both static pressure and static displacement was necessary to verify that the PAMs behaved similarly as each parameter is adjusted. The linear relationship established between pressure and applied load during the fixed displacement characterization yielded good fits, meaning that the equations found would be reliable when calculating needed applied pressure. When this set of slope was compared, the variation amongst them differed by less than 0.117 (N/psi) for all PAMs tested except for the 1 in Nylon PAMs. The variation within that group had a range of 0.54, which is more than four and a half times larger than all of the other groups. This showed that the 1 in PAM was much harder to predict and therefore less reliable and should not be used. We believe that this is due to the dynamics of the Nylon mesh after reaching a certain size. The calculated slope would change too drastically for a simple relationship to be defined. This provided additional information to exclude the Nylon 1 in PAM as a possibility in the *in vivo* loading device.

Comparison between changing pressure and displacement was conducted by plotting the results from the fixed pressure and fixed displacement experiments on the

same graph to compare the slopes generated. When compared, we found that the two experiments yielded results that were in line with the other seen in Figure 6.9. This was encouraging, as it meant that we could reliably predict force regardless if the displacement or the pressure was changing. It showed from both perspectives, regardless of displacement change due to creep, or our pressure adjustments, we could accurately account for and produce the force we desire. With these, we determined a relationship between the displacement, pressure and force, and we can accurately predict how the PAM will respond. This shows promise as we will be able precisely control and regulate the loads we apply using the PAM in the loading device.

6.4.3 Limitations of PAMs in this Application

While we have listed the many benefits of using PAMs for our application, the results have revealed a few spots of caution. In the fixed pressure characterization, the trials were all identical, but they all exhibited a large hysteresis when the displacement is allowed to reach zero force. Unequal path taken by the PAM results in an increased force output after the first cycle, this higher force will never be reached during our testing scenario. While it is intended that our loading device will provide cyclic loading, it will be force control, not strain, and will never have the force dictated by strain, as the pressure will constantly be calibrated to supply more or less pressure into the PAM. The initial force yielded during the testing scenario will be the highest force generated by the PAM, and will not enter the higher force range. The PAM will not be forcibly stretched longer, rather only be relaxed by a passive

rehydration. The extra tier of force achieved will not be present during our loading experiments, and should not interfere, as long as care is not taken to actively pull apart an already loaded PAM.

Another point of caution is the identification of a toe region when the force generated is plotted against the pressure applied. This is shown in the fixed displacement characterization plots, and when both characterizations were compared. The toe region found on these graphs, shown in Figure 6.9, show that there is a region that does not behave as reliably or predictably. This toe region shows that below 2 N of force, where we can not accurately calculate or generate force; meaning the PAMs should only be used above the 2 N range. The linear range shown from the held displacement graph, is also the portion that is in line with the results from the held pressure graphs. Similar toe regions occur in the low force, low pressure areas on other larger PAMs tested for other applications. Unpublished data suggests that this region is static, and limited to around the 2 N range. In the larger PAMs, however, this 2 N becomes insignificant, or even undetectable, as the force ranges to over 1000 N, so 2 N then occurs within normal fluctuations. Due to this reason, this toe region has gone unnoticed until recently, as these PAMs and these small applications are the first of this magnitude. Fortunately, this still means that the PAM can be used predictably when outside of the toe region, and within the linearly defined region.

6.4.4 Ex vivo Loading Using PAMs

There was limited success in applying a constant force towards biological tissue, in this case a rat tail disc. We showed that our system of displacement

feedback was active and was able to track the viscoelastic creep. The initial intended force was not reached, however, and should be adjusted to apply increased pressure in the initial stages. After the initial jump, we showed that we could maintain our initial force; however, it also continued to increase, in response to the change in displacement. This showed that our slope calibration was slightly off, as the increased pressure more than overwhelmed the displacement increase. Instead the slope needs to only balance the changing displacement to result in a static exertion force. When considering the initial force that was reached, the system was held semi-stably, as there was only a 21% increase in force while the system was trying to remain static. The PAMs can be recalibrated as a set, on a *in vitro* system before each *in vivo* run, to ensure the accurate functionality of the PAM system. This would allow changes in equations and calibrations to the 2 PAMs as a unit in the device, rather than individually.

Some of these inaccuracies could be due to the use of only one pressure regulator. At the time of testing, we tested the two PAM system using one set of tubing connected and controlled using one pressure regulator. Although the two 0.75 in PAMs were similar, they were not the same, and therefore had different equations, with different slope and intercept values, which could have made a difference in the overall output. To account for two sets of equations, they were averaged and used in the Labview code, however, future work has already begun to use two sets of pressure regulators, so that the PAMs can be controlled independently and offer more precise control.

6.5 Conclusion

Small miniature PAMs were successfully created for use as a force actuator in an axial caudal rat disc loading device. Upon testing many materials and configurations, a 0.75 in PAM, with a latex bladder and Kevlar braided mesh was selected as the most appropriate combination of variables for this application. There was reliable and repeatable data recorded for force and displacement measurements, given a static pressure input, as well as equally dependable data for force and pressure, given a static displacement. When compared, both sets of data agreed with each other, and provided a linear relationship between pressure and force. A toe region was discovered when the forces generated are below 2 N, however, outside of that, the PAM behaves linearly and can be used freely outside that toe region. In the in vitro loading system, the PAMs need to be further calibrated in the future, to better reach the desired applied force. The force, pressure and displacement relationship must also be slightly adjusted to allow for better control of a stable desired force. This objective may be reached easier with the help of an additional pressure regulator, so that each PAM may be treated independently rather than as a unit.

Chapter 7 Conclusions and Future Work

The overarching goal for this project was to investigate the IVD, as it pertains to behavior, both mechanical and biological. The hydration within the NP became a factor that influenced these changing responses and motivated further exploration. Much is still unknown about the disc, needs to be discovered, before we fully understand the cause and effects of degeneration. The complex environment that comprises the disc still has many undefined parts that contribute to how the disc behaves. The work presented in this dissertation only begins to uncover some of the simple properties of the disc, beginning with pressurization. It also leads the way in revealing the effects of load history on the disc's mechanical behavior as well as biological response.

A degenerative model was first successfully developed in a rat disc in order to provide a case study for future experiments in our lab. This model used a trans-annular puncture, guided radiographically to induce the degeneration. We explored several size needles, but found that an 18g needle was the only size that could reliably trigger the desired effects. The creep was monitored and fitted using viscoelastic models, and verified change in response. Histological changes were also monitored up to four weeks and confirmed breakdown of the AF. Our results were consistent with other explored puncture or stab models. This study additionally provided a key point that helped us pursue further studies. It showed that using a 22g needle puncture would disrupt neither the mechanics, nor the biological health of the disc. This meant that we would be able to insert a small sized pressure sensor using a 22g

needle as a guide, and not affect the disc; a critical detail that would allow us to make pressure measurements in the NP.

Utilizing the collaborative efforts of Dr. Yu's lab, we were able to develop a miniature fiber optic pressure sensor based on Fabry-Perot interferometry. It was the smallest pressure sensor at the time, measuring 360µm, able to fit into a 22g needle and inserted into a caudal disc. Along with the degenerative rat tail model, we used the pressure sensor to observe intradiscal pressure during intervals of block loading. We compared healthy and degenerate discs and showed a decreased capacity by the degenerate discs to generate a hydrostatic pressure. This is consistent with what was seen in a porcine model, and more importantly human cadaver discs. Our observed healthy to degenerate ratio was surprisingly similar to that of the human discs, demonstrating that our degenerate model behavior drew comparison with a grade IV degenerate human disc.

To begin research on the effects of load history, frozen caudal rat motion segments were loaded with varying preloads and immediately applied a following larger exertion load. The creep response was fitted using three different viscoelastic models: the stretched exponential model, the standard solid viscoelastic model and a fluid transport of the disc model. The latter two showed that indeed the disc behaved differently given changing prior stress. More specifically, the fluid transport model suggested that the intradiscal pressure was a key element in this change. To further capitalize on the miniature pressure sensor, we measured the pressure generation of the NP given similar loading conditions. We found that the load history directly changed the pressurization of the disc, as an applied preload significantly lowered the

pressure generation during the exertion load. In this experiment, we verified experimental finding with mathematical modeling, and then observed the change directly.

After exploring the mechanistic behavioral changes, our investigative efforts turned to the biological impact of load history. Similar to our previous experiment, we applied preloads followed by exertion loads and harvested NP cells to measure gene expression. A panel of associated genes were investigated, most notably type II collagen and aggrecan. Given the known pressurized environment of the NP, the nonpreloaded group was predicted to produce elevated response for a number of catabolic genes, which would parallel other *in vitro* experiments with applied hydrostatic pressure. Instead the preloaded, lower pressure environment yielded a greater response, which we now believe to be due to a higher tonic environment with a higher osmolarity. A longer loading regime was also applied in attempt to capture the gene expression with a higher response to gain additional statistical significance; however, the expression was instead lower, suggesting the disc reached a biologic equilibrium. Two additional control groups were also investigated to compare and ensure that the resultant gene expression was indeed due to the combination of the preload and exertion load and not due to the preload alone, or a higher average applied stress.

Until this time, the prior loading regimes have been limited to a short duration due to anesthetic constraints on live animal experiments. To combat this, we began designing a long term loading device using a novel device created by Dr. Wereley's lab, the PAM. A number of uniquely small PAMs with a variety of materials and

specifications were created and tested to use as the actuating component of our loading device. It was determined that a 0.75 inch PAM with a latex bladder and a Kevlar mesh braiding would be the optimal materials to use. This PAM in addition to our previously used pin and ring configuration was used to compress a caudal rat disc. This calibrated setup was assessed on a previously frozen tail to test the ability for our LabView program and strain feedback system to maintain a stable force while the disc tissue undergoes viscoelastic creep. While results were only mildly successful, we believe that the use of two separate pressure regulating elements would allow for a more accurate feedback response.

The work completed up until now has only begun to explore the impact of load history. We have investigated changes in mechanical behavior and gene expression as a result of simple sequences of short term loading. The development of the PAM loading device will allow the application of loading regimes for longer periods of time on a live rat model. This will allow more relevant and complex sequences of loading be investigated, such as a daily loading routines for several weeks. This will allow for not only a look at changes in viscoelastic properties and gene expression, but also give enough time for histological changes. Further studies can also be pursued to reveal more specifically the cause for the gene expression changes observed. Measurements involving osmolarity of the NP as well as other cellular factors can monitored for changes under applied loads. Recently, a smaller and more robust pressure sensor was developed in Dr. Yu's lab and may be able to provide live *in vivo* readings while under loading. The more robust manufacturing method may allow for a wider array of tests to be performed. A number of paths can

be taken to further understand the role of hydration, and effects of load history on the behavior of the IVD; however, the work presented above uncovers another piece to complete the picture of disc function. We have opened to door to the role load history has in loading response. It impacts how the NP must be thought of, as an ever changing hydrated matrix. It may indicate beneficial loading regimes that may help build strength by inducing extracellular matrix production, or by simply suggest what a better option, a straight dead lift of a sofa bed, or a gradual warm-up of bookshelves and TV before the sofa bed. It is important that the knowledge gained about pressurization and hydration will be applied in future studies to further uncover the response of the disc.

These studies have contributed many things unique in this field. First, at the time of publication, the use of a pressure sensor inside a rat caudal disc to measure intradiscal pressure was the first of its kind. While past studies have investigated pressure generation within other animal models, our study helps bridge the gap between large and small animal models through the use of a novel fiber optic pressure sensor. The main significant contribution of this work has been the investigation of the effects of load history. Having been alluded to by several studies, our experiments explore mechanical and biological response of the disc towards prior loading. This has yet to be investigated in the past, specifically for the disc, and provides a foundation for disc behavior, given a specific load history. This research reiterated the importance of NP hydration and pressurization, and response due to small nuanced changes in the disc. Lastly, we hoped to improve on the effectiveness of a long term loading device for caudal motion segments on an *in vivo* rat model

through the use of PAMs. PAMs offered a variety of benefits as well as a lighter device that is fitted onto the rat. Our discovery helped better understand the workings of the NP, and will serve as a basis for future discovery. These contributions advanced the knowledge in the field of disc mechanobiology and took advantage of two novel technologies in this pursuit; however, much still needs to be learned before an effective and thorough therapy can be developed.

Appendix A [3]

International Journal of Pharmaceutics 368 (2009) 215–219

Contents lists available at ScienceDirect

International Journal of Pharmaceutics

journal homepage: www.elsevier.com/locate/ijpharm

Pharmaceutical nanotechnology

Influence of polymer structure and biodegradation on DNA release from silk–elastinlike protein polymer hydrogels

David Hwang[a,1], Vikas Moolchandani[b,1], Ramesh Dandu[b], Mohamed Haider[b,e], Joseph Cappello[c], Hamidreza Ghandehari[a,b,d,*]

[a] Department of Bioengineering, University of Maryland, College Park, MD, USA
[b] Center for Nanomedicine & Cellular Delivery and Department of Pharmaceutical Sciences, University of Maryland, Baltimore, Baltimore, MD, USA
[c] Protein Polymer Technologies, Inc., San Diego, CA, USA
[d] Departments of Pharmaceutics & Pharmaceutical Chemistry and Bioengineering, Nano Institute of Utah, University of Utah, Salt Lake City, UT, USA
[e] Department of Pharmaceutical Sciences, Cairo University, Cairo, Egypt

ARTICLE INFO

Article history:
Received 12 August 2008
Received in revised form 15 October 2008
Accepted 16 October 2008
Available online 5 November 2008

Keywords:
Hydrogels
Controlled release
Biodegradation
Elastase
Gene delivery
Naked DNA

ABSTRACT

Silk–elastinlike protein polymers (SELPs) of varying ratios and lengths of silk and elastin blocks capable of hydrogel formation were evaluated as matrices for controlled delivery of plasmid DNA. Influence of polymer structure, ionic strength of the media and gelation time on DNA release from two structurally related hydrogels, SELP-47K and SELP-415K, was evaluated. The influence of elastase-induced degradation on the swelling behavior and DNA release from these hydrogels was investigated. Results indicate that release is a function of polymer structure, concentration and cure time. SELP-415K which has twice the number of elastin units as that of SELP-47K demonstrated higher release than that of SELP-47K. DNA release from these hydrogels is an inverse function of polymer concentration and cure time, with higher release observed at lower polymer concentration and shorter cure time. Results indicate that ionic strength of the media governs the rate of release. An increase in swelling ratio was observed in the presence of elastase at 12 wt.% composition for both SELP analogs. Release in the presence of elastase was enhanced due to increased swelling ratio and loss of hydrogel integrity. These studies allude to the utility of recombinant techniques to control plasmid DNA release and biodegradation in SELP hydrogels.

© 2008 Elsevier B.V. All rights reserved.

1. Introduction

Progress made in gene therapy is severely undermined by transient and low transfection efficiency of non-viral vectors and the toxicity and immunogenicity of viral vectors (Verma and Somia, 1997). Several systemic and localized gene delivery platforms have been explored to improve the duration and localization of gene transfer (Shen et al., 2007; Cohen-Sacks et al., 2004; Wang et al., 2004). Encapsulation of naked DNA, non-viral vectors, or viral vectors in polymeric matrices provides several advantages. These include (i) protection from enzymatic degradation, (ii) prolonged delivery, and (iii) efficient localization of transgene expression thereby minimizing toxicity and maximizing therapeutic efficacy (Doukas et al., 2001; Wang et al., 2003; Wang et al., 2005).

Both natural and synthetic polymers have been applied as matrices for controlled gene delivery (Dang and Leong, 2006; Shen et al., 2007; Cohen-Sacks et al., 2004; Wang et al., 2005; Bellocq et al., 2004). Limited control over polymer sequence and structure or issues surrounding the biocompatibility and biodegradability of such polymers has reduced the viability of these delivery platforms for gene delivery applications (Van De Weert et al., 2000). Genetically engineered polymers couple the versatility of biocompatibility and biodegradability of natural polymers on one hand with the high degree of control over polymer structure achievable by recombinant synthesis on the other (Haider et al., 2004). Silk–elastinlike protein polymers (SELPs) are a class of genetically engineered polymers composed of repeating units of silk-like (GAGAGS) and elastin-like (GVGVP) peptide blocks in the polymer structure (Cappello et al., 1990). Silk provides crosslinking capability and renders mechanical strength, while elastin enhances aqueous solubility. By carefully controlling the ratio and length of silk and elastin units using recombinant techniques, SELPs of diverse functionalities (stimuli-sensitive, biocompatible and

* Corresponding author. Present address: Departments of Pharmaceutics & Pharmaceutical Chemistry and Bioengineering, Nano Institute of Utah, University of Utah, 383 Colorow Road, Room 343, Salt Lake City, UT 84108, USA. Tel.: +1 801 587 1566; fax: +1 801 585 0575.
E-mail address: hamid.ghandehari@pharm.utah.edu (H. Ghandehari).
[1] These authors contributed equally to this manuscript.

0378-5173/$ – see front matter © 2008 Elsevier B.V. All rights reserved.
doi:10.1016/j.ijpharm.2008.10.021

[3] In case nothing has piqued your interested so far…
As published in D Hwang, V Moolchandani, R Dandu, M Haider, J Cappello, and H Ghandehari. Influence of polymer structure and biodegradation on DNA release from silk-elastinlike protein polymer hydrogels. International Journal of Pharmaceutics (2009). 368(1-2): 215-219.

A. AGSGAGAGS [(GVGVP)$_4$ G<u>K</u>GVP (GVGVP)$_3$ (GAGAGS)$_4$]$_{12}$

(GVGVP)$_4$ G<u>K</u>GVP (GVGVP)$_3$ (GAGAGS)$_2$ GAG

B. AGSGAGAGS [(GVGVP)$_4$ G<u>K</u>GVP (GVGVP)$_{11}$ (GAGAGS)$_4$]$_7$

(GVGVP)$_4$ G<u>K</u>GVP (GVGVP)$_{11}$ (GAGAGS)$_2$ GAG

Fig. 1. Amino acid sequences of (A) SELP-47K; (B) SELP-415K. Lys (K) residues underlined. The elastin blocks are highlighted in gray. Head and tail sequences not shown.

biodegradable) can be produced (Megeed et al., 2002; Nagarsekar et al., 2003; Haider et al., 2005).

SELPs with two or more silk units in the monomer repeat and with favorable silk to elastin (S:E) ratio tend to form hydrogels with elevation of temperature from room temperature to 37 °C. Solutions of two SELP analogs, 47K and 415K (Fig. 1), which undergo irreversible sol-to-gel transition at 37 °C have been developed that are capable of matrix-mediated gene delivery (Megeed et al., 2004; Haider et al., 2005). SELP-47K has a higher S:E and forms hydrogels in the concentration range 4–12 wt.% where as SELP-415K forms hydrogels above 10 wt.% concentration due to its low S:E ratio (Haider et al., 2005). This allows the injection of aqueous polymer–DNA solutions that transform into solid hydrogel matrices within minutes in the body, enabling temporal and spatial control over gene release. Controlled plasmid DNA delivery can be beneficial in tissue engineering, vaccine delivery and a number of other biomedical applications (Doukas et al., 2001; Megeed et al., 2004). Controlled release of DNA from SELP-47K hydrogels is shown to be a function of polymer concentration and cure time (Megeed et al., 2002). SELP-415K which has eight more elastin repeats in its monomer sequence than that of SELP-47K has been shown to have higher swelling ratio (Haider et al., 2005) but its DNA release characteristics are unknown. The influence of length and sequence of elastin units (SELP-415K) on interaction with DNA and elastase-induced biodegradation in these polymers is also unexplored. The presence of elastin blocks in SELPs that can potentially be degraded by the endogenous elastase (released from leukocytes) can alter the network properties of the formed matrix and thereby the release of DNA from these systems. The current study reports the influence of SELP structure, composition, ionic strength of the media, and hydrogel cure time on controlled release of plasmid DNA. Also reported is the influence of elastase incorporation on the swelling behavior and DNA release from these matrices.

2. Materials and methods

2.1. Preparation of DNA-containing hydrogels

SELP-47K was provided by Protein Polymer Technologies, Inc. (San Diego, CA). SELP-415K was biosynthesized and characterized by procedures described previously (Haider et al., 2005). Leukocyte elastase was purchased from Sigma (St. Louis, MO). Plasmid pRL-CMV-*luc* 4.08 kbp (Promega, Madison, WI) was propagated in Novablue Singles Competent Cells (Novagen, San Diego, CA), and purified using an EndoFree Giga Kit (QIAGEN Sciences, Germantown, MD) according to manufacturer's instructions. Syringes containing frozen 12 wt.% (%,w/w) polymer solutions were thawed in a beaker containing 500 ml of water for 5 min at room temperature. Polymer solutions and plasmid DNA were gently mixed. The volume of the mixture was adjusted by addition of PBS and MilliQ ultrapurified water from Millipore (Billerica, MA) to yield 250 μg/ml plasmid DNA in 11.5 wt.% polymer. The mixtures were then transferred to disposable syringes (1 ml), incubated at 37 °C for 4 h and 48 h, respectively. After the appropriate cure time, the syringe tip was cut off, and the DNA containing hydrogels were extruded and cut into 50 mm^3 cylindrical discs (2.3 mm radius) using razor blade for swelling and release studies. The hydrogels were robust and did not deform.

2.2. Influence of ionic strength on DNA release

DNA-containing hydrogel discs were placed in 4 ml glass vials containing 3 ml of the release buffer. PBS (10 mM, pH 7.4, 0.01%, w/v NaN_3) buffer with total ionic strength (μ), adjusted with NaCl to 0.016 M, 0.16 M, and 1.6 M, respectively were used as release media. Vials containing hydrogels submerged in buffer were incubated at 37 °C in a shaking (120 rpm) incubator for the duration of the experiments. At predetermined time points, the buffer was sampled and replaced with fresh buffer. The amount of DNA in the release media was determined by Picogreen DNA Quantitation Kit (Molecular Probes, Eugene, OR) and cumulative released DNA was calculated by procedures described previously (Megeed et al., 2002).

2.3. Ionic interactions of SELP copolymers with plasmid DNA

The interaction of both polymers, 47K and 415K, containing one lysine residue per monomer repeat (Fig. 1) with plasmid DNA at various ionic strengths was evaluated by a turbidity assay (Megeed et al., 2002). DNA:polymer complexes were formed at the charge ratios of 2:1, 1:1, and 1:2 assuming full ionization of the lysine residues and DNA phosphates at pH 7.4 and room temperature. The upper limit concentration of polymer used in the complexes was 0.0094 μg/μL. Polymer solutions were added drop wise to solutions containing 50 μg of plasmid pRL-CMV-*luc* in PBS with ionic strengths adjusted to 0.016 M, and 0.16 M to a final volume of 137 μL. After incubation at room temperature for 30 min the absorbance at 400 nm was determined by spectrophotometric techniques.

2.4. Determination of swelling behavior

SELP-47K and 415K form hydrogels in the concentration range of 4–12 wt.%, and 10–12 wt.%, respectively (Haider et al., 2005). Hydrogels were prepared and allowed to reach equilibrium in a PBS solution (Table 1). Soluble polymer fractions remaining in the hydrogels post-gelation were removed by extensively washing the hydrogels for 1-week in 1X dPBS under mild agitation (120 rpm) at 37 °C. Fresh buffer was replaced daily throughout the washing period. Hydrogels were equilibrated for 24 h in PBS or PBS with 100 ng elastase. The weight equilibrium swelling ratio (q) was experimentally determined as a ratio of the weight of swollen

Table 1
Polymer composition and concentration and elastase effects on swelling.

SELP analog	SELP concentration (%)	Release media
47K	4	PBS
47K	8	PBS
47K	12	PBS
415K	12	PBS
47K	4	PBS with 100 ng elastase
47K	8	PBS with 100 ng elastase
47K	12	PBS with 100 ng elastase
415K	12	PBS with 100 ng elastase
47K	4	PBS with 10 ng elastase
47K	4	PBS with 50 ng elastase
47K	4	PBS with 150 ng elastase
47K	4	PBS with 200 ng elastase

hydrogel (W_s) over the weight of dry hydrogel (W_d) using procedures described previously (Dinerman et al., 2002; Dandu et al., 2008). Briefly, hydrogels were removed from test conditions after 1-week and gently blotted with a lint-free wipe to remove excess solvent from surfaces prior to determining the swollen (wet) weight. Dry weight was determined by weighing the hydrogels after desiccating the wet hydrogels using Drierite dessicant (Xenia, OH) for 5 days. Gel disks were then weighed and placed into a vacuum oven at 30 °C for 24 h and then re-weighed to ensure no change in dry hydrogel weight following vacuum drying.

2.5. Evaluation of polymer degradation and DNA release in the presence of elastase

Hydrogels were prepared as described above. Cylindrical SELP hydrogel analogs with 50 mm^3 volume were placed in 1 mL PBS or PBS containing physiological concentration of elastase (0.1 μg/mL) (Hind et al., 1991; Morrison et al., 1999). Media was collected at predetermined time points, and replenished with fresh media at each time point. The DNA concentration was then determined using the Quanti-It Picogreen assay kit.

Statistical analysis. Single factor analysis of variance (ANOVA) and student's *t*-test were carried out at $\alpha = 0.05$ to determine statistically significant differences between test samples. All studies were performed in triplicate.

3. Results and discussion

3.1. Effect of polymer structure and cure time on DNA release

Fig. 2 shows the release profile of plasmid DNA from both polymer constructs at 4 h and 48 h cure times, respectively. At 4 h cure time cumulative release from 415K hydrogels was higher than that of 47K up to day 28. Since there is an overall lower number of silk units in the polymer backbone than 47K, this is presumed to be due to the lower crosslinking density of 415K (Fig. 1). For both sets of hydrogels cured for 4 h, there was no significant DNA release beyond day 21 suggesting that the remainder of DNA is trapped in the matrices. An increase in cure time from 4 h to 48 h resulted in lower cumulative release for both polymers. This difference in release was more pronounced for hydrogels made from SELP-47K compared to SELP-415K.

Previous studies suggest that an increase in cure time for both polymers results in a decrease in their degree of swelling (Haider et al., 2005). These physically cross linked hydrogels are known to

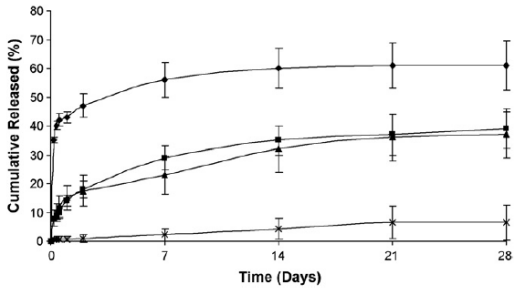

Fig. 2. Influence of polymer structure and cure time (CT) on DNA release from 12 wt.% SELP hydrogels at pH 7.4 and $\mu = 0.16$ M released over a 28-day period. Symbols represent SELP-415K at 4 h cure time (CT) (♦) and 48 h CT (■), and SELP-47K at 4 h CT (▲) and 48 h CT (×), respectively. Each symbol represents mean ± standard deviation for $n = 3$ samples.

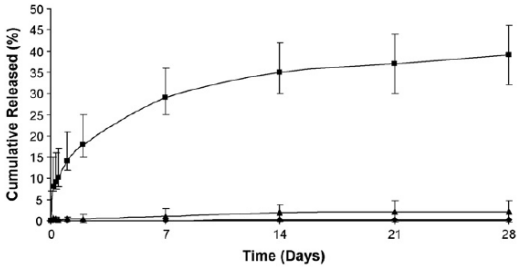

Fig. 3. Influence of ionic strength on DNA release from SELP-415 K hydrogels at pH 7.4. Symbols represent release at 0.016 M (♦), 0.16 M (■) and 1.6 M (▲). Each symbol represents mean ± standard deviation for $n = 3$ samples.

have a fraction of soluble polymer that does not participate in the hydrogel network (Dandu et al., 2008; Dinerman et al., 2002). With time there increased chances for more silk units in the vicinity to be recruited at the crosslinking site allowing the formation of a denser network therefore increased crosslinking density, resulting in decreased release. The reason for the pronounced effect of cure time for 47K is presumed to be the higher number of silk units in the polymer backbone that allows a higher degree of inter-polymer interactions compared to 415K.

3.2. Influence of ionic strength on DNA release

The release of DNA from hydrogels made from SELP-415K showed a strong dependence on the ionic strength of the medium with the highest release observed at 0.16 M (Fig. 3). Previously we had shown that an increase in ionic strength for SELP-415K hydrogels results in a decrease in their degree of swelling (Haider et al., 2005). The lower degree of swelling of SELP-415K at high ionic strength (1.6 M) explains the lower release of plasmid DNA at this ionic concentration compared to the physiologically relevant ionic strength of 0.16 M. At very low ionic strength (0.016 M) negatively charged plasmid DNA interacts with lysine residues of the polymer backbone which results in no release consistent with our previous observations (Megeed et al., 2002).

3.3. Influence of polymer structure and ionic strength on polymer–DNA interaction

Recombinant techniques allow the introduction of functional amino acid residues at precise locations in the polymer backbone. SELP-415K was designed such that it has a similar molecular weight as SELP-47K but with longer elastin-like units. Consequently there are five more lysine residues in 47K compared to 415K. This could reduce the interaction of negatively charged plasmid DNA with the 415K polymer backbone. To evaluate this phenomenon we measured the absorbance of DNA/polymer complexes at low non-gel forming concentrations. The absorbance of Polymer 47K mixture with plasmid DNA showed a substantial increase when prepared at low ionic strength compared to high ionic strength (Fig. 4). Mixtures of SELP-415K and plasmid DNA showed lower turbidity at both ionic strengths compared to their SELP-47K counterparts due to the presence of lower number of lysine residues.

3.4. Influence of elastase-induced biodegradation on swelling of SELP hydrogels

The elastin units in SELPs are susceptible to degradation by endogenous elastases providing a possible mechanism for their

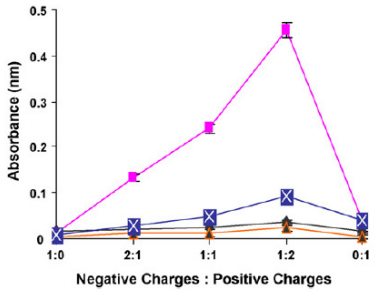

Fig. 4. Influence of polymer structure and ionic strength on the turbidity of DNA (at room temperature): Symbols represent absorbance of polymer complexes of SELP-415K at 0.016 M (♦) and 0.16 M (▲), and SELP-47K at 0.016 M (■) and 0.16 M (×). Each symbol represents mean ± standard deviation for $n = 3$ samples.

biodegradation in vivo. To investigate the nature and extent of biodegradation caused by elastase, studies were conducted in vitro using physiologically relevant concentrations of leukocyte elastase (Hind et al., 1991; Morrison et al., 1999). Results indicate an increase in the observed swelling ratio in the presence of elastase for both SELP analogs at 12 wt.% ($p < 0.05$) (Fig. 5). However, these differences were not significant at lower polymer concentration ($p = 0.05$). The greater swelling ratio of the elastase treated hydrogels at 12 wt.% concentration is likely due to a more loosely cross linked network probably as a result of chain cleavages by the protease. At this stage the extent to which elastase penetrates the hydrogel network is not known. The smaller polymer chains as a result of degradation likely elute from the hydrogel as soluble fraction thus reducing the dry weight (W_d) of the hydrogel and increasing the swelling ratio (q). At low polymer concentration, however, the difference is not significant probably because at low concentration the hydrogel network is already loosely cross linked that additional chain cleavages have lesser effect. It was also observed that in the presence of elastase, 4 wt.% SELP-47K hydrogels begin to breakdown into pieces and lose their hydrogel integrity within 10 days (data not shown) suggesting the potential utility of this polymer concentration for cases in which it is desirable to degrade the drug carrier within a week.

3.5. Influence of elastase-induced biodegradation on DNA release

Increased swelling ratio and loss of hydrogel network integrity suggest a larger pore size and greater release rate in the presence of

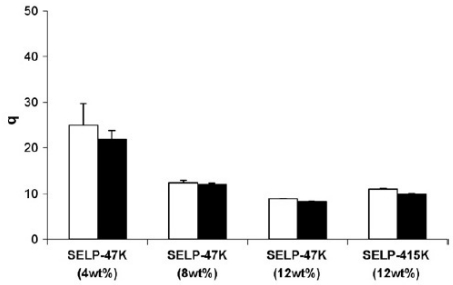

Fig. 5. Influence of elastase on the swelling behavior of SELP hydrogels as a function of polymer concentration and structure. The bars represent q of SELP hydrogels (i) in the presence (white) and absence (black) of elastase. Each bar represents mean ± standard deviation for $n = 3$ samples.

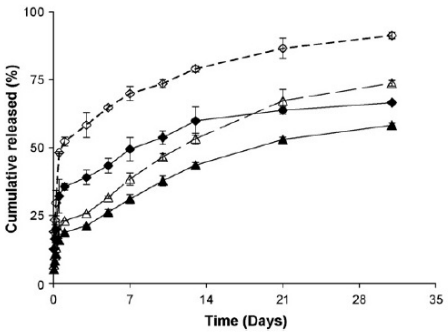

Fig. 6. Influence of elastase-induced degradation on release of DNA from SELP hydrogel analogs. Symbols represent cumulative percent release of DNA from 12 wt.% hydrogels of SELP-47K in the presence (△) and absence (▲) of elastase, and SELP-415K in the presence (◊) and absence (♦) of elastase. Each symbol represents mean ± standard deviation for $n = 3$ samples.

elastase. To understand the extent by which release is enhanced in the presence of elastase, DNA release was evaluated from both SELP hydrogels at similar polymer concentrations (12 wt.%) in the presence of elastase. As expected in the absence of elastase, SELP-47K, with its shorter elastin units, showed greater release than SELP-415K ($p < 0.05$) (Fig. 6). In the presence of elastase both polymers showed significantly higher release rates than in the absence of elastase ($p < 0.05$) (Fig. 6). For SELP-415K hydrogel, close to 100% DNA release was observed in the presence of elastase compared to 60% in the absence of elastase. These studies indicate that both release and biodegradation are a function of polymer concentration and structure and suggest that by controlling the sequence of the silk and elastin units, polymers of desirable release and biodegradation profiles can be developed for controlled gene delivery applications. Further research is necessary to characterize the pore size and mechanism of DNA release. In the design of polymeric matrices for gene delivery several important parameters need to be considered. These are ease of administration to the site where gene release is desired (e.g., intratumoral or intramuscular), their viscosity, the pore size of the hydrogels, interaction of plasmid DNA with the polymer backbone and its influence on gene release, biodegradation of the matrix and its biocompatibility and elimination from the body. By molecular engineering of SELPs these parameters may be controlled (Dandu and Ghandehari, 2007). In this report by increasing the length of the elastin unit while maintaining molecular weight constant, we demonstrated that polymer–DNA interaction, release and biodegradation can be modulated. Hence by design of polymer structure, matrix-mediated delivery of plasmid DNA from SELP hydrogels may be optimized. In addition, these studies can set the stage for utilization of such matrices for controlled release or incorporation of other bioactive agents such as viruses, cells, proteins and peptides.

4. Conclusion

Results indicate that polymer structure, concentration, ionic strength and hydrogel cure time govern the rate of DNA release from SELP hydrogels. The influence of the ratio of silk to elastin and the length of elastin units on release is demonstrated by the higher release rate observed in SELP-415K compared to SELP-47K. Treatment with elastase leads to the biodegradation of elastin units in SELPs. These studies provide a framework for the design and development of novel biodegradable and biocompati-

ble SELP-based matrix-mediated delivery systems for gene therapy applications.

Acknowledgement

Funding for this study was provided under NIH R01 CA107621.

References

Bellocq, N.C., Kang, D.W., Wang, X., Jensen, G.S., Pun, S.H., Schluep, T., Zepeda, M.L., Davis, M.E., 2004. Synthetic biocompatible cyclodextrin-based constructs for local gene delivery to improve cutaneous wound healing. Bioconjug. Chem. 15, 1201–1211.

Cappello, J., Crissman, J., Dorman, M., Mikolajczak, M., Textor, G., Marquet, M., Ferrari, F., 1990. Genetic engineering of structural protein polymers. Biotechnol. Prog. 6, 198–202.

Cohen-Sacks, H., Elazar, V., Gao, J., Golomb, A., Adwan, H., Korchov, N., Levy, R.J., Berger, M.R., Golomb, G., 2004. Delivery and expression of pDNA embedded in collagen matrices. J. Control Release 95, 309–320.

Dandu, R., Cappello, J., Ghandehari, H., 2008. Characterization of structurally related adenovirus-laden silk-elastinlike hydrogels. J. Bioact. Compat. Polym. 23, 5–19.

Dandu, R., Ghandehari, H., 2007. Delivery of bioactive agents from recombinant polymers. Prog. Polym. Sci. 32, 1008–1030.

Dang, J.M., Leong, K.W., 2006. Natural polymers for gene delivery and tissue engineering. Gene Deliv. Tissue Eng. 58, 487–499.

Dinerman, A.A., Cappello, J., Ghandehari, H., Hoag, S.W., 2002. Swelling behavior of a genetically engineered silk-elastinlike protein polymer hydrogel. Biomaterials 23, 4203–4210.

Doukas, J., Chandler, L.A., Gonzalez, A.M., Gu, D., Hoganson, D.K., Ma, C., Nguyen, T., Printz, M.A., Nesbit, M., Herlyn, M., Crombleholme, T.M., Aukerman, S.L., Sosnowski, B.A., Pierce, G.F., 2001. Matrix immobilization enhances the tissue repair activity of growth factor gene therapy vectors. Hum. Gene Ther. 12, 783–798.

Haider, M., Leung, V., Ferrari, F., Crissman, J., Powell, J., Cappello, J., Ghandehari, H., 2005. Molecular engineering of silk-elastinlike polymers for matrix-mediated gene delivery: biosynthesis and characterization. Mol. Pharm. 2, 139–150.

Haider, M., Megeed, Z., Ghandehari, H., 2004. Genetically engineered polymers: status and prospects for controlled release. J. Control Release 95, 1–26.

Hind, C.R., Joyce, H., Tennent, G.A., Pepys, M.B., Pride, N.B., 1991. Plasma leukocyte elastase concentrations in smokers. J. Clin. Pathol. 44, 232–235.

Megeed, Z., Cappello, J., Ghandehari, H., 2002. Controlled release of plasmid DNA from a genetically engineered silk-elastinlike hydrogel. Pharm. Res. 19, 954–959.

Megeed, Z., Haider, M., Li, D., O'Malley Jr., B.W., Cappello, J., Ghandehari, H., 2004. In vitro and in vivo evaluation of recombinant silk-elastinlike hydrogels for cancer gene therapy. J. Control Release 94, 433–445.

Morrison, H.M., Welgus, H.G., Owen, C.A., Stockley, R.A., Campbell, E.J., 1999. Interaction between leukocyte elastase and elastin: quantitative and catalytic analyses. Biochim. Biophys. Acta 1430, 179–190.

Nagarsekar, A., Crissman, J., Crissman, M., Ferrari, F., Cappello, J., Ghandehari, H., 2003. Genetic engineering of stimuli-sensitive silk–elastinlike protein block copolymers. Biomacromolecules 4, 602–607.

Shen, X., Tong, H., Jiang, T., Zhu, Z., Wan, P., Hu, J., 2007. Homogeneous chitosan/carbonate apatite/citric acid nanocomposites prepared through a novel in situ precipitation method. Compos. Sci. Technol. 67, 2238–2245.

Van De Weert, M., Hennink, W.E., Jiskoot, W., 2000. Protein instability in poly(lactic-co-glycolic acid) microparticles. Pharm. Res. 17, 1159–1167.

Verma, I.M., Somia, N., 1997. Gene therapy – promises, problems and prospects. Nature 389, 239–242.

Wang, Y., Hu, J.K., Krol, A., Li, Y.P., Li, C.Y., Yuan, F., 2003. Systemic dissemination of viral vectors during intratumoral injection. Mol. Cancer Ther. 2, 1233–1242.

Wang, Y., Li, C.Y., Yuan, F., 2004. Systemic virus dissemination during local gene delivery in solid tumors and its control with an alginate solution. In: International Conference of the IEEE Engineering in Medicine and Biology Society.IEEE Engineering in Medicine and Biology Society Conference, United States.

Wang, Y., Liu, S., Li, C.Y., Yuan, F., 2005. A novel method for viral gene delivery in solid tumors. Cancer Res. 65, 7541–7545.

Bibliography

1 M. A. Adams, and P. J. Roughley, 'What Is Intervertebral Disc Degeneration, and What Causes It?', *Spine (Phila Pa 1976),* 31 (2006), 2151-61.

2 K. Singh, K. Masuda, E. J. Thonar, H. S. An, and G. Cs-Szabo, 'Age-Related Changes in the Extracellular Matrix of Nucleus Pulposus and Anulus Fibrosus of Human Intervertebral Disc', *Spine (Phila Pa 1976),* 34 (2009), 10-6.

3 B. Shen, J. Melrose, P. Ghosh, and F. Taylor, 'Induction of Matrix Metalloproteinase-2 and -3 Activity in Ovine Nucleus Pulposus Cells Grown in Three-Dimensional Agarose Gel Culture by Interleukin-1beta: A Potential Pathway of Disc Degeneration', *Eur Spine J,* 12 (2003), 66-75.

4 M. A. Adams, D. S. McNally, and P. Dolan, "Stress' Distributions inside Intervertebral Discs. The Effects of Age and Degeneration', *J Bone Joint Surg Br,* 78 (1996), 965-72.

5 P. J. Roughley, M. Alini, and J. Antoniou, 'The Role of Proteoglycans in Aging, Degeneration and Repair of the Intervertebral Disc', *Biochem Soc Trans,* 30 (2002), 869-74.

6 F. Mwale, J. C. Iatridis, and J. Antoniou, 'Quantitative Mri as a Diagnostic Tool of Intervertebral Disc Matrix Composition and Integrity', *Eur Spine J,* 17 Suppl 4 (2008), 432-40.

7 C. P. Mullan, and B. E. Kelly, 'Magnetic Resonance (Mr) Imaging of Lumbar Spine: Use of a Shortened Protocol for Initial Investigation of Degenerative Disease', *Ulster Med J,* 74 (2005), 29-32.

8 T. J. Birney, J. J. White, Jr., D. Berens, and G. Kuhn, 'Comparison of Mri and Discography in the Diagnosis of Lumbar Degenerative Disc Disease', *J Spinal Disord,* 5 (1992), 417-23.

9 A. Borthakur, P. M. Maurer, M. Fenty, C. Wang, R. Berger, J. Yoder, R. A. Balderston, and D. M. Elliott, 'T1rho Mri and Discography Pressure as Novel Biomarkers for Disc Degeneration and Low Back Pain', *Spine (Phila Pa 1976)* (2011).

10 M. A. Adams, D. W. McMillan, T. P. Green, and P. Dolan, 'Sustained Loading Generates Stress Concentrations in Lumbar Intervertebral Discs', *Spine (Phila Pa 1976),* 21 (1996), 434-8.

11 J. J. MacLean, C. R. Lee, M. Alini, and J. C. Iatridis, 'The Effects of Short-Term Load Duration on Anabolic and Catabolic Gene Expression in the Rat Tail Intervertebral Disc', *J Orthop Res,* 23 (2005), 1120-7.

12 C. T. Ching, D. H. Chow, F. Y. Yao, and A. D. Holmes, 'The Effect of Cyclic Compression on the Mechanical Properties of the Inter-Vertebral Disc: An in Vivo Study in a Rat Tail Model', *Clin Biomech (Bristol, Avon),* 18 (2003), 182-9.

13 A. J. Walsh, and J. C. Lotz, 'Biological Response of the Intervertebral Disc to Dynamic Loading', *J Biomech,* 37 (2004), 329-37.

14 L. Ekstrom, A. Kaigle, E. Hult, S. Holm, M. Rostedt, and T. Hansson, 'Intervertebral Disc Response to Cyclic Loading--an Animal Model', *Proc Inst Mech Eng H,* 210 (1996), 249-58.

15 J. L. Gunning, J. P. Callaghan, and S. M. McGill, 'Spinal Posture and Prior Loading History Modulate Compressive Strength and Type of Failure in the Spine: A Biomechanical Study Using a Porcine Cervical Spine Model', *Clin Biomech (Bristol, Avon),* 16 (2001), 471-80.
16 J. J. MacLean, C. R. Lee, S. Grad, K. Ito, M. Alini, and J. C. Iatridis, 'Effects of Immobilization and Dynamic Compression on Intervertebral Disc Cell Gene Expression in Vivo', *Spine (Phila Pa 1976),* 28 (2003), 973-81.
17 D. M. Elliott, C. S. Yerramalli, J. C. Beckstein, J. I. Boxberger, W. Johannessen, and E. J. Vresilovic, 'The Effect of Relative Needle Diameter in Puncture and Sham Injection Animal Models of Degeneration', *Spine,* 33 (2008), 588-96.
18 A. G. Edwards, D. S. McNally, R. C. Mulholland, and A. E. Goodship, 'The Effects of Posterior Fixation on Internal Intervertebral Disc Mechanics', *J Bone Joint Surg Br,* 79 (1997), 154-60.
19 W. T. Edwards, N. R. Ordway, Y. Zheng, G. McCullen, Z. Han, and H. A. Yuan, 'Peak Stresses Observed in the Posterior Lateral Anulus', *Spine,* 26 (2001), 1753-9.
20 D. W. McMillan, D. S. McNally, G. Garbutt, and M. A. Adams, 'Stress Distributions inside Intervertebral Discs: The Validity of Experimental "Stress Profilometry", *Proc Inst Mech Eng [H],* 210 (1996), 81-7.
21 D. S. McNally, and M. A. Adams, 'Internal Intervertebral Disc Mechanics as Revealed by Stress Profilometry', *Spine,* 17 (1992), 66-73.
22 A. J. Lisi, C. W. O'Neill, D. P. Lindsey, R. Cooperstein, E. Cooperstein, and J. F. Zucherman, 'Measurement of in Vivo Lumbar Intervertebral Disc Pressure During Spinal Manipulation: A Feasibility Study', *J Appl Biomech,* 22 (2006), 234-9.
23 A. R. Meir, J. C. Fairbank, D. A. Jones, D. S. McNally, and J. P. Urban, 'High Pressures and Asymmetrical Stresses in the Scoliotic Disc in the Absence of Muscle Loading', *Scoliosis,* 2 (2007), 4.
24 D. J. Polga, B. P. Beaubien, P. M. Kallemeier, K. P. Schellhas, W. D. Lew, G. R. Buttermann, and K. B. Wood, 'Measurement of in Vivo Intradiscal Pressure in Healthy Thoracic Intervertebral Discs', *Spine,* 29 (2004), 1320-4.
25 H. Wilke, P. Neef, B. Hinz, H. Seidel, and L. Claes, 'Intradiscal Pressure Together with Anthropometric Data--a Data Set for the Validation of Models', *Clin Biomech (Bristol, Avon),* 16 Suppl 1 (2001), S111-26.
26 H. J. Wilke, P. Neef, M. Caimi, T. Hoogland, and L. E. Claes, 'New in Vivo Measurements of Pressures in the Intervertebral Disc in Daily Life', *Spine,* 24 (1999), 755-62.
27 K. Sato, S. Kikuchi, and T. Yonezawa, 'In Vivo Intradiscal Pressure Measurement in Healthy Individuals and in Patients with Ongoing Back Problems', *Spine,* 24 (1999), 2468-74.
28 A. Nachemson, and J. Morris, 'Lumbar Discometry. Lumbar Intradiscal Pressure Measurements in Vivo', *Lancet,* 1 (1963), 1140-2.
29 A. Nachemson, and J. M. Morris, 'In Vivo Measurements of Intradiscal Pressure. Discometry, a Method for the Determination of Pressure in the Lower Lumbar Discs', *J Bone Joint Surg Am,* 46 (1964), 1077-92.

30 G. R. Buttermann, B. P. Beaubien, and L. C. Saeger, 'Mature Runt Cow Lumbar Intradiscal Pressures and Motion Segment Biomechanics', *Spine J* (2007).
31 F. Unglaub, T. Guehring, H. Lorenz, C. Carstens, and M. W. Kroeber, 'Effects of Unisegmental Disc Compression on Adjacent Segments: An in Vivo Animal Model', *Eur Spine J,* 14 (2005), 949-55.
32 L. Ekstrom, S. Holm, A. K. Holm, and T. Hansson, 'In Vivo Porcine Intradiscal Pressure as a Function of External Loading', *J Spinal Disord Tech,* 17 (2004), 312-6.
33 M. Sasaki, T. Takahashi, K. Miyahara, and T. Hirose a, 'Effects of Chondroitinase Abc on Intradiscal Pressure in Sheep: An in Vivo Study', *Spine,* 26 (2001), 463-8.
34 A.H. Hsieh, D.A. Ryan, S.C. Nesson, and M. Yu, 'Measurement of Intradiscal Pressure in Rat Discs Using a Miniaturized Fiber Optic Sensor', in *International Society for the Study of the Lumbar Spine 31th Annual Meeting*, 2007).
35 S.C. Nesson, M. Yu, and A.H. Hsieh, 'Transient Pressure Measurements in Rat Intervertebral Discs During Stress Relaxation', in *Transactions of the 54th Annual Meeting of the Orthopaedic Research Society*, 2008), p. 46.
36 H. S. An, K. Takegami, H. Kamada, C. M. Nguyen, E. J. Thonar, K. Singh, G. B. Andersson, and K. Masuda, 'Intradiscal Administration of Osteogenic Protein-1 Increases Intervertebral Disc Height and Proteoglycan Content in the Nucleus Pulposus in Normal Adolescent Rabbits', *Spine,* 30 (2005), 25-31; discussion 31-2.
37 K. Masuda, and H. S. An, 'Prevention of Disc Degeneration with Growth Factors', *Eur Spine J,* 15 Suppl 3 (2006), S422-32.
38 K. Masuda, Y. Imai, M. Okuma, C. Muehleman, K. Nakagawa, K. Akeda, E. Thonar, G. Andersson, and H. S. An, 'Osteogenic Protein-1 Injection into a Degenerated Disc Induces the Restoration of Disc Height and Structural Changes in the Rabbit Anular Puncture Model', *Spine,* 31 (2006), 742-54.
39 A. J. Walsh, D. S. Bradford, and J. C. Lotz, 'In Vivo Growth Factor Treatment of Degenerated Intervertebral Discs', *Spine,* 29 (2004), 156-63.
40 K. Nishida, M. Doita, T. Takada, K. Kakutani, H. Miyamoto, T. Shimomura, K. Maeno, and M. Kurosaka, 'Sustained Transgene Expression in Intervertebral Disc Cells in Vivo Mediated by Microbubble-Enhanced Ultrasound Gene Therapy', *Spine,* 31 (2006), 1415-9.
41 M. W. Kroeber, F. Unglaub, H. Wang, C. Schmid, M. Thomsen, A. Nerlich, and W. Richter, 'New in Vivo Animal Model to Create Intervertebral Disc Degeneration and to Investigate the Effects of Therapeutic Strategies to Stimulate Disc Regeneration', *Spine,* 27 (2002), 2684-90.
42 K. Nishida, J. D. Kang, L. G. Gilbertson, S. H. Moon, J. K. Suh, M. T. Vogt, P. D. Robbins, and C. H. Evans, 'Modulation of the Biologic Activity of the Rabbit Intervertebral Disc by Gene Therapy: An in Vivo Study of Adenovirus-Mediated Transfer of the Human Transforming Growth Factor Beta 1 Encoding Gene', *Spine,* 24 (1999), 2419-25.

43 K. Nishida, J. D. Kang, J. K. Suh, P. D. Robbins, C. H. Evans, and L. G. Gilbertson, 'Adenovirus-Mediated Gene Transfer to Nucleus Pulposus Cells. Implications for the Treatment of Intervertebral Disc Degeneration', *Spine,* 23 (1998), 2437-42; discussion 43.
44 T. Iwashina, J. Mochida, D. Sakai, Y. Yamamoto, T. Miyazaki, K. Ando, and T. Hotta, 'Feasibility of Using a Human Nucleus Pulposus Cell Line as a Cell Source in Cell Transplantation Therapy for Intervertebral Disc Degeneration', *Spine,* 31 (2006), 1177-86.
45 D. Sakai, J. Mochida, T. Iwashina, T. Watanabe, T. Nakai, K. Ando, and T. Hotta, 'Differentiation of Mesenchymal Stem Cells Transplanted to a Rabbit Degenerative Disc Model: Potential and Limitations for Stem Cell Therapy in Disc Regeneration', *Spine,* 30 (2005), 2379-87.
46 Y. G. Zhang, X. Guo, P. Xu, L. L. Kang, and J. Li, 'Bone Mesenchymal Stem Cells Transplanted into Rabbit Intervertebral Discs Can Increase Proteoglycans', *Clin Orthop Relat Res* (2005), 219-26.
47 H. Bertram, M. Kroeber, H. Wang, F. Unglaub, T. Guehring, C. Carstens, and W. Richter, 'Matrix-Assisted Cell Transfer for Intervertebral Disc Cell Therapy', *Biochem Biophys Res Commun,* 331 (2005), 1185-92.
48 G. Crevensten, A. J. Walsh, D. Ananthakrishnan, P. Page, G. M. Wahba, J. C. Lotz, and S. Berven, 'Intervertebral Disc Cell Therapy for Regeneration: Mesenchymal Stem Cell Implantation in Rat Intervertebral Discs', *Ann Biomed Eng,* 32 (2004), 430-4.
49 K. Nishimura, and J. Mochida, 'Percutaneous Reinsertion of the Nucleus Pulposus. An Experimental Study', *Spine,* 23 (1998), 1531-8; discussion 39.
50 R. J. Hoogendoorn, P. I. Wuisman, T. H. Smit, V. E. Everts, and M. N. Helder, 'Experimental Intervertebral Disc Degeneration Induced by Chondroitinase Abc in the Goat', *Spine,* 32 (2007), 1816-25.
51 D. S. Lu, Y. Shono, I. Oda, K. Abumi, and K. Kaneda, 'Effects of Chondroitinase Abc and Chymopapain on Spinal Motion Segment Biomechanics. An in Vivo Biomechanical, Radiologic, and Histologic Canine Study', *Spine,* 22 (1997), 1828-34; discussion 34-5.
52 A. Ono, S. Harata, K. Takagaki, and M. Endo, 'Proteoglycans in the Nucleus Pulposus of Canine Intervertebral Discs after Chondroitinase Abc Treatment', *J Spinal Disord,* 11 (1998), 253-60.
53 J. S. Park, and J. I. Ahn, 'The Effect of Chondroitinase Abc on Rabbit Intervertebral Disc. Radiological, Histological and Electron Microscopic Findings', *Int Orthop,* 19 (1995), 103-9.
54 M. Sakuma, N. Fujii, T. Takahashi, J. Hoshino, S. Miyauchi, and H. Iwata, 'Effect of Chondroitinase Abc on Matrix Metalloproteinases and Inflammatory Mediators Produced by Intervertebral Disc of Rabbit in Vitro', *Spine,* 27 (2002), 576-80.
55 K. Sumida, K. Sato, M. Aoki, Y. Matsuyama, and H. Iwata, 'Serial Changes in the Rate of Proteoglycan Synthesis after Chemonucleolysis of Rabbit Intervertebral Discs', *Spine,* 24 (1999), 1066-70.
56 T. Takahashi, H. Kurihara, S. Nakajima, T. Kato, S. Matsuzaka, T. Sekiguchi, M. Onaya, S. Miyauchi, S. Mizuno, K. Horie, Y. Fujita, and T. Hirose,

'Chemonucleolytic Effects of Chondroitinase Abc on Normal Rabbit Intervertebral Discs. Course of Action up to 10 Days Postinjection and Minimum Effective Dose', *Spine,* 21 (1996), 2405-11.

57 R. J. Hoogendoorn, M. N. Helder, R. J. Kroeze, R. A. Bank, T. H. Smit, and P. I. Wuisman, 'Reproducible Long-Term Disc Degeneration in a Large Animal Model', *Spine,* 33 (2008), 949-54.

58 T. Tsuchida, 'A Pathological Study of Experimental Chemonucleolysis with Collagenase', *Nippon Seikeigeka Gakkai Zasshi,* 61 (1987), 1237-49.

59 J. I. Boxberger, J. D. Auerbach, S. Sen, and D. M. Elliott, 'An in Vivo Model of Reduced Nucleus Pulposus Glycosaminoglycan Content in the Rat Lumbar Intervertebral Disc', *Spine,* 33 (2008), 146-54.

60 J. P. Norcross, G. E. Lester, P. Weinhold, and L. E. Dahners, 'An in Vivo Model of Degenerative Disc Disease', *J Orthop Res,* 21 (2003), 183-8.

61 G. A. Tayrose, E. R. Costa, J. Hooker, and L. E. Dahners, 'Costal Cartilage Autografts to Simulated Degenerative Intervertebral Discs in the Rat', *Spine,* 31 (2006), E863-6.

62 F. Kato, H. Iwata, K. Mimatsu, and T. Miura, 'Experimental Chemonucleolysis with Chondroitinase Abc', *Clin Orthop Relat Res* (1990), 301-8.

63 J. I. Boxberger, S. Sen, C. S. Yerramalli, and D. M. Elliott, 'Nucleus Pulposus Glycosaminoglycan Content Is Correlated with Axial Mechanics in Rat Lumbar Motion Segments', *J Orthop Res,* 24 (2006), 1906-15.

64 E. Kaapa, X. Han, S. Holm, J. Peltonen, T. Takala, and H. Vanharanta, 'Collagen Synthesis and Types I, Iii, Iv, and Vi Collagens in an Animal Model of Disc Degeneration', *Spine,* 20 (1995), 59-66; discussion 66-7.

65 E. Kaapa, S. Holm, X. Han, T. Takala, V. Kovanen, and H. Vanharanta, 'Collagens in the Injured Porcine Intervertebral Disc', *J Orthop Res,* 12 (1994), 93-102.

66 J. Melrose, P. Ghosh, T. K. Taylor, B. Vernon-Roberts, J. Latham, and R. Moore, 'Elevated Synthesis of Biglycan and Decorin in an Ovine Annular Lesion Model of Experimental Disc Degeneration', *Eur Spine J,* 6 (1997), 376-84.

67 K. S. Kim, S. T. Yoon, J. Li, J. S. Park, and W. C. Hutton, 'Disc Degeneration in the Rabbit: A Biochemical and Radiological Comparison between Four Disc Injury Models', *Spine,* 30 (2005), 33-7.

68 S. J. Lipson, and H. Muir, '1980 Volvo Award in Basic Science. Proteoglycans in Experimental Intervertebral Disc Degeneration', *Spine,* 6 (1981), 194-210.

69 S. J. Lipson, and H. Muir, 'Experimental Intervertebral Disc Degeneration: Morphologic and Proteoglycan Changes over Time', *Arthritis Rheum,* 24 (1981), 12-21.

70 K. Masuda, Y. Aota, C. Muehleman, Y. Imai, M. Okuma, E. J. Thonar, G. B. Andersson, and H. S. An, 'A Novel Rabbit Model of Mild, Reproducible Disc Degeneration by an Anulus Needle Puncture: Correlation between the Degree of Disc Injury and Radiological and Histological Appearances of Disc Degeneration', *Spine,* 30 (2005), 5-14.

71 O. L. Osti, B. Vernon-Roberts, and R. D. Fraser, '1990 Volvo Award in Experimental Studies. Anulus Tears and Intervertebral Disc Degeneration. An Experimental Study Using an Animal Model', *Spine,* 15 (1990), 762-7.
72 S. Sobajima, J. F. Kompel, J. S. Kim, C. J. Wallach, D. D. Robertson, M. T. Vogt, J. D. Kang, and L. G. Gilbertson, 'A Slowly Progressive and Reproducible Animal Model of Intervertebral Disc Degeneration Characterized by Mri, X-Ray, and Histology', *Spine,* 30 (2005), 15-24.
73 M. A. Rousseau, J. A. Ulrich, E. C. Bass, A. G. Rodriguez, J. J. Liu, and J. C. Lotz, 'Stab Incision for Inducing Intervertebral Disc Degeneration in the Rat', *Spine,* 32 (2007), 17-24.
74 J. A. Ulrich, E. C. Liebenberg, D. U. Thuillier, and J. C. Lotz, 'Issls Prize Winner: Repeated Disc Injury Causes Persistent Inflammation', *Spine,* 32 (2007), 2812-9.
75 A. Race, N. D. Broom, and P. Robertson, 'Effect of Loading Rate and Hydration on the Mechanical Properties of the Disc', *Spine (Phila Pa 1976),* 25 (2000), 662-9.
76 Y. M. Lu, W. C. Hutton, and V. M. Gharpuray, 'The Effect of Fluid Loss on the Viscoelastic Behavior of the Lumbar Intervertebral Disc in Compression', *J Biomech Eng,* 120 (1998), 48-54.
77 K. B. Broberg, 'Slow Deformation of Intervertebral Discs', *J Biomech,* 26 (1993), 501-12.
78 Y. Schroeder, W. Wilson, J. M. Huyghe, and F. P. Baaijens, 'Osmoviscoelastic Finite Element Model of the Intervertebral Disc', *Eur Spine J,* 15 Suppl 3 (2006), S361-71.
79 A. H. Hsieh, D. R. Wagner, L. Y. Cheng, and J. C. Lotz, 'Dependence of Mechanical Behavior of the Murine Tail Disc on Regional Material Properties - a Parametric Finite Element Study', *J Biomech Eng,* 127 (2005).
80 W. Johannessen, E. J. Vresilovic, A. C. Wright, and D. M. Elliott, 'Intervertebral Disc Mechanics Are Restored Following Cyclic Loading and Unloaded Recovery', *Ann Biomed Eng,* 32 (2004), 70-6.
81 J. J. MacLean, J. P. Owen, and J. C. Iatridis, 'Role of Endplates in Contributing to Compression Behaviors of Motion Segments and Intervertebral Discs', *J Biomech,* 40 (2007), 55-63.
82 J. J. Cassidy, M. S. Silverstein, A. Hiltner, and E. Baer, 'A Water Transport Model for the Creep Response of the Intervertebral Disc', *Journal of Materials Science-Materials in Medicine,* 1 (1990), 81-89.
83 R. R. Sokal, and F. J. Rohlf, *Biometry*. 3rd ed. edn (New York City, NY: W. H. Freeman and Co., 1995), pp. 260-65.
84 M. A. Adams, and P. J. Roughley, 'What Is Intervertebral Disc Degeneration, and What Causes It?', *Spine,* 31 (2006), 2151-61.
85 W. Johannessen, J. M. Cloyd, G. D. O'Connell, E. J. Vresilovic, and D. M. Elliott, 'Trans-Endplate Nucleotomy Increases Deformation and Creep Response in Axial Loading', *Ann Biomed Eng,* 34 (2006), 687-96.
86 I. Cowgill, K. Sairyo, A. Biyani, and V. K. Goel, 'Biomechanical Alteration Initiates Intervertebral Disc Degeneration in the Needle Puncture Model', in *Transactions of the 52nd Orthopaedic Research Society*, 2006), p. 1223.

87 M. W. Kroeber, F. Unglaub, H. Wang, C. Schmid, M. Thomsen, A. Nerlich, and W. Richter, 'New in Vivo Animal Model to Create Intervertebral Disc Degeneration and to Investigate the Effects of Therapeutic Strategies to Stimulate Disc Regeneration', *Spine,* 27 (2002), 2684-90.
88 G. D. O'Connell, E. J. Vresilovic, and D. M. Elliott, 'Comparison of Animals Used in Disc Research to Human Lumbar Disc Geometry', *Spine,* 32 (2007), 328-33.
89 C. L. Korecki, J. J. Costi, and J. C. Iatridis, 'Needle Puncture Injury Affects Intervertebral Disc Mechanics and Biology in an Organ Culture Model', *Spine,* 33 (2008), 235-41.
90 M. A. Adams, B. J. Freeman, H. P. Morrison, I. W. Nelson, and P. Dolan, 'Mechanical Initiation of Intervertebral Disc Degeneration', *Spine (Phila Pa 1976),* 25 (2000), 1625-36.
91 H. J. Wilke, P. Neef, M. Caimi, T. Hoogland, and L. E. Claes, 'New in Vivo Measurements of Pressures in the Intervertebral Disc in Daily Life', *Spine (Phila Pa 1976),* 24 (1999), 755-62.
92 A. Nachemson, 'The Effect of Forward Leaning on Lumbar Intradiscal Pressure', *Acta Orthop Scand,* 35 (1965), 314-28.
93 C. R. Dennison, P. M. Wild, M. F. Dvorak, D. R. Wilson, and P. A. Cripton, 'Validation of a Novel Minimally Invasive Intervertebral Disc Pressure Sensor Utilizing in-Fiber Bragg Gratings in a Porcine Model: An Ex Vivo Study', *Spine (Phila Pa 1976),* 33 (2008), E589-94.
94 T. Guehring, F. Unglaub, H. Lorenz, G. Omlor, H. J. Wilke, and M. W. Kroeber, 'Intradiscal Pressure Measurements in Normal Discs, Compressed Discs and Compressed Discs Treated with Axial Posterior Disc Distraction: An Experimental Study on the Rabbit Lumbar Spine Model', *Eur Spine J,* 15 (2006), 597-604.
95 S. Nesson, M. Yu, X. Zhang, and A. H. Hsieh, 'Miniature Fiber Optic Pressure Sensor with Composite Polymer-Metal Diaphragm for Intradiscal Pressure Measurements', *J Biomed Opt,* 13 (2008), 044040.
96 J. J. Costi, T. C. Hearn, and N. L. Fazzalari, 'The Effect of Hydration on the Stiffness of Intervertebral Discs in an Ovine Model', *Clin Biomech (Bristol, Avon),* 17 (2002), 446-55.
97 D. Hwang, A. S. Gabai, M. Yu, A. G. Yew, and A. H. Hsieh, 'Role of Load History in Intervertebral Disc Mechanics and Intradiscal Pressure Generation', *Biomech Model Mechanobiol* (2011).
98 W. C. Hutton, T. M. Ganey, W. A. Elmer, E. Kozlowska, J. L. Ugbo, E. S. Doh, and T. E. Whitesides, Jr., 'Does Long-Term Compressive Loading on the Intervertebral Disc Cause Degeneration?', *Spine (Phila Pa 1976),* 25 (2000), 2993-3004.
99 D. M. Elliott, and J. J. Sarver, 'Young Investigator Award Winner: Validation of the Mouse and Rat Disc as Mechanical Models of the Human Lumbar Disc', *Spine (Phila Pa 1976),* 29 (2004), 713-22.
100 R. Hoogendoorn, B. Z. Doulabi, C. L. Huang, P. I. Wuisman, R. A. Bank, and M. N. Helder, 'Molecular Changes in the Degenerated Goat Intervertebral Disc', *Spine (Phila Pa 1976),* 33 (2008), 1714-21.

101 B. Jim, T. Steffen, J. Moir, P. Roughley, and L. Haglund, 'Development of an Intact Intervertebral Disc Organ Culture System in Which Degeneration Can Be Induced as a Prelude to Studying Repair Potential', *Eur Spine J* (2011).
102 J. Melrose, S. M. Smith, C. B. Little, R. J. Moore, B. Vernon-Roberts, and R. D. Fraser, 'Recent Advances in Annular Pathobiology Provide Insights into Rim-Lesion Mediated Intervertebral Disc Degeneration and Potential New Approaches to Annular Repair Strategies', *Eur Spine J,* 17 (2008), 1131-48.
103 E. Kaapa, X. Han, S. Holm, J. Peltonen, T. Takala, and H. Vanharanta, 'Collagen Synthesis and Types I, Iii, Iv, and Vi Collagens in an Animal Model of Disc Degeneration', *Spine (Phila Pa 1976),* 20 (1995), 59-66; discussion 66-7.
104 F. Mwale, K. Masuda, R. Pichika, L. M. Epure, T. Yoshikawa, A. Hemmad, P. J. Roughley, and J. Antoniou, 'The Efficacy of Link N as a Mediator of Repair in a Rabbit Model of Intervertebral Disc Degeneration', *Arthritis Res Ther,* 13 (2011), R120.
105 A. H. Hsieh, D. Hwang, D. A. Ryan, A. K. Freeman, and H. Kim, 'Degenerative Anular Changes Induced by Puncture Are Associated with Insufficiency of Disc Biomechanical Function', *Spine (Phila Pa 1976),* 34 (2009), 998-1005.
106 Q. Q. Liang, Q. Zhou, M. Zhang, W. Hou, X. J. Cui, C. G. Li, T. F. Li, Q. Shi, and Y. J. Wang, 'Prolonged Upright Posture Induces Degenerative Changes in Intervertebral Discs in Rat Lumbar Spine', *Spine (Phila Pa 1976),* 33 (2008), 2052-8.
107 A. J. Michalek, M. R. Buckley, L. J. Bonassar, I. Cohen, and J. C. Iatridis, 'The Effects of Needle Puncture Injury on Microscale Shear Strain in the Intervertebral Disc Annulus Fibrosus', *Spine J,* 10 (2010), 1098-105.
108 A. J. Michalek, K. L. Funabashi, and J. C. Iatridis, 'Needle Puncture Injury of the Rat Intervertebral Disc Affects Torsional and Compressive Biomechanics Differently', *Eur Spine J,* 19 (2010), 2110-6.
109 J. J. Cassidy, M. S. Silverstein, A. Hiltner, and E. Baer, 'A Water Transport Model for the Creep Response of the Intervertebral-Disk', *Journal of Materials Science-Materials in Medicine,* 1 (1990), 81-89.
110 X. Guo, Y. Lanir, and G. S. Kassab, 'Effect of Osmolarity on the Zero-Stress State and Mechanical Properties of Aorta', *Am J Physiol Heart Circ Physiol,* 293 (2007), H2328-34.
111 T. Saxena, J. L. Gilbert, and J. M. Hasenwinkel, 'A Versatile Mesoindentation System to Evaluate the Micromechanical Properties of Soft, Hydrated Substrates on a Cellular Scale', *J Biomed Mater Res A,* 90 (2009), 1206-17.
112 S. M. Han, S. Y. Lee, M. H. Cho, and J. K. Lee, 'Disc Hydration Measured by Magnetic Resonance Imaging in Relation to Its Compressive Stiffness in Rat Models', *Proc Inst Mech Eng H,* 215 (2001), 497-501.
113 A. H. Hoffman, D. R. Robichaud, 2nd, J. J. Duquette, and P. Grigg, 'Determining the Effect of Hydration Upon the Properties of Ligaments Using Pseudo Gaussian Stress Stimuli', *J Biomech,* 38 (2005), 1636-42.

114 G. M. Thornton, N. G. Shrive, and C. B. Frank, 'Altering Ligament Water Content Affects Ligament Pre-Stress and Creep Behaviour', *J Orthop Res,* 19 (2001), 845-51.
115 T. L. Haut, and R. C. Haut, 'The State of Tissue Hydration Determines the Strain-Rate-Sensitive Stiffness of Human Patellar Tendon', *J Biomech,* 30 (1997), 79-81.
116 W. Y. Gu, and H. Yao, 'Effects of Hydration and Fixed Charge Density on Fluid Transport in Charged Hydrated Soft Tissues', *Ann Biomed Eng,* 31 (2003), 1162-70.
117 E. Nimer, R. Schneiderman, and A. Maroudas, 'Diffusion and Partition of Solutes in Cartilage under Static Load', *Biophys Chem,* 106 (2003), 125-46.
118 G. Zernia, and D. Huster, 'Collagen Dynamics in Articular Cartilage under Osmotic Pressure', *NMR Biomed,* 19 (2006), 1010-9.
119 E. Wachtel, and A. Maroudas, 'The Effects of Ph and Ionic Strength on Intrafibrillar Hydration in Articular Cartilage', *Biochim Biophys Acta,* 1381 (1998), 37-48.
120 A. Barbir, A. J. Michalek, R. D. Abbott, and J. C. Iatridis, 'Effects of Enzymatic Digestion on Compressive Properties of Rat Intervertebral Discs', *J Biomech,* 43 (2010), 1067-73.
121 A. Antolic, R. Harrison, C. Farlinger, N. M. Cermak, S. J. Peters, P. LeBlanc, and B. D. Roy, 'Effect of Extracellular Osmolality on Cell Volume and Resting Metabolism in Mammalian Skeletal Muscle', *Am J Physiol Regul Integr Comp Physiol,* 292 (2007), R1994-2000.
122 P. G. Bush, and A. C. Hall, 'Passive Osmotic Properties of in Situ Human Articular Chondrocytes within Non-Degenerate and Degenerate Cartilage', *J Cell Physiol,* 204 (2005), 309-19.
123 P. G. Bush, and A. C. Hall, 'The Osmotic Sensitivity of Isolated and in Situ Bovine Articular Chondrocytes', *J Orthop Res,* 19 (2001), 768-78.
124 K. Masuoka, A. J. Michalek, J. J. MacLean, I. A. Stokes, and J. C. Iatridis, 'Different Effects of Static Versus Cyclic Compressive Loading on Rat Intervertebral Disc Height and Water Loss in Vitro', *Spine (Phila Pa 1976),* 32 (2007), 1974-9.
125 M. A. Adams, and W. C. Hutton, 'The Effect of Posture on the Fluid Content of Lumbar Intervertebral Discs', *Spine,* 8 (1983), 665-71.
126 I. Adamska, M. Lindahl, M. Roobol-Boza, and B. Andersson, 'Degradation of the Light-Stress Protein Is Mediated by an Atp-Independent, Serine-Type Protease under Low-Light Conditions', *Eur J Biochem,* 236 (1996), 591-9.
127 D. S. Pflaster, M. H. Krag, C. C. Johnson, L. D. Haugh, and M. H. Pope, 'Effect of Test Environment on Intervertebral Disc Hydration', *Spine (Phila Pa 1976),* 22 (1997), 133-9.
128 D. M. Elliott, C. S. Yerramalli, J. C. Beckstein, J. I. Boxberger, W. Johannessen, and E. J. Vresilovic, 'The Effect of Relative Needle Diameter in Puncture and Sham Injection Animal Models of Degeneration', *Spine (Phila Pa 1976),* 33 (2008), 588-96.

129 R. E. Seroussi, M. H. Krag, D. L. Muller, and M. H. Pope, 'Internal Deformations of Intact and Denucleated Human Lumbar Discs Subjected to Compression, Flexion, and Extension Loads', *J Orthop Res,* 7 (1989), 122-31.
130 J. R. Meakin, and D. W. Hukins, 'Effect of Removing the Nucleus Pulposus on the Deformation of the Annulus Fibrosus During Compression of the Intervertebral Disc', *Journal of Biomechanics,* 33 (2000), 575-80.
131 J. R. Meakin, T. W. Redpath, and D. W. Hukins, 'The Effect of Partial Removal of the Nucleus Pulposus from the Intervertebral Disc on the Response of the Human Annulus Fibrosus to Compression', *Clin Biomech (Bristol, Avon),* 16 (2001), 121-8.
132 S. Kumaresan, N. Yoganandan, F. A. Pintar, and D. J. Maiman, 'Finite Element Modeling of the Cervical Spine: Role of Intervertebral Disc under Axial and Eccentric Loads', *Medical Engineering and Physics,* 21 (1999), 689-700.
133 J. C. Lotz, O. K. Colliou, J. R. Chin, N. A. Duncan, and E. Liebenberg, 'Compression-Induced Degeneration of the Intervertebral Disc: An in Vivo Mouse Model and Finite-Element Study', *Spine,* 23 (1998), 2493-506.
134 D. Lacroix, and P. J. Prendergast, 'A Mechano-Regulation Model for Tissue Differentiation During Fracture Healing: Analysis of Gap Size and Loading', *J Biomech,* 35 (2002), 1163-71.
135 D. R. Carter, and M. Wong, 'Modelling Cartilage Mechanobiology', *Philos Trans R Soc Lond B Biol Sci,* 358 (2003), 1461-71.
136 D. S. McNally, and M. A. Adams, 'Internal Intervertebral Disc Mechanics as Revealed by Stress Profilometry', *Spine (Phila Pa 1976),* 17 (1992), 66-73.
137 A. H. Hsieh, A. L. Walsh, L. Y. Cheng, and J. C. Lotz, 'Apoptosis Corresponds with Disc Strain Environment During Dynamic Compression', in *Transactions of the 50th Annual Meeting of the Orthopaedic Research Society* (San Francisco, CA, 2004), p. 131.
138 C. L. Le Maitre, A. P. Fotheringham, A. J. Freemont, and J. A. Hoyland, 'Development of an in Vitro Model to Test the Efficacy of Novel Therapies for Ivd Degeneration', *J Tissue Eng Regen Med,* 3 (2009), 461-9.
139 C. L. Le Maitre, J. Frain, A. P. Fotheringham, A. J. Freemont, and J. A. Hoyland, 'Human Cells Derived from Degenerate Intervertebral Discs Respond Differently to Those Derived from Non-Degenerate Intervertebral Discs Following Application of Dynamic Hydrostatic Pressure', *Biorheology,* 45 (2008), 563-75.
140 M. Kasra, V. Goel, J. Martin, S. T. Wang, W. Choi, and J. Buckwalter, 'Effect of Dynamic Hydrostatic Pressure on Rabbit Intervertebral Disc Cells', *J Orthop Res,* 21 (2003), 597-603.
141 T. Handa, H. Ishihara, H. Ohshima, R. Osada, H. Tsuji, and K. Obata, 'Effects of Hydrostatic Pressure on Matrix Synthesis and Matrix Metalloproteinase Production in the Human Lumbar Intervertebral Disc', *Spine (Phila Pa 1976),* 22 (1997), 1085-91.
142 J. C. Beckstein, S. Sen, T. P. Schaer, E. J. Vresilovic, and D. M. Elliott, 'Comparison of Animal Discs Used in Disc Research to Human Lumbar Disc:

Axial Compression Mechanics and Glycosaminoglycan Content', *Spine (Phila Pa 1976),* 33 (2008), E166-73.

143 C. T. Ching, D. H. Chow, F. Y. Yao, and A. D. Holmes, 'Changes in Nuclear Composition Following Cyclic Compression of the Intervertebral Disc in an in Vivo Rat-Tail Model', *Med Eng Phys,* 26 (2004), 587-94.

144 J. J. Maclean, C. R. Lee, M. Alini, and J. C. Iatridis, 'Anabolic and Catabolic Mrna Levels of the Intervertebral Disc Vary with the Magnitude and Frequency of in Vivo Dynamic Compression', *J Orthop Res,* 22 (2004), 1193-200.

145 K. Wuertz, K. Godburn, J. J. MacLean, A. Barbir, J. S. Donnelly, P. J. Roughley, M. Alini, and J. C. Iatridis, 'In Vivo Remodeling of Intervertebral Discs in Response to Short- and Long-Term Dynamic Compression', *J Orthop Res,* 27 (2009), 1235-42.

146 C. R. Dennison, P. M. Wild, P. W. Byrnes, A. Saari, E. Itshayek, D. C. Wilson, Q. A. Zhu, M. F. Dvorak, P. A. Cripton, and D. R. Wilson, 'Ex Vivo Measurement of Lumbar Intervertebral Disc Pressure Using Fibre-Bragg Gratings', *J Biomech,* 41 (2008), 221-5.

147 A. J. Michalek, K. L. Funabashi, and J. C. Iatridis, 'Needle Puncture Injury of the Rat Intervertebral Disc Affects Torsional and Compressive Biomechanics Differently', *Eur Spine J* (2010).

148 M. V. Risbud, T. J. Albert, A. Guttapalli, E. J. Vresilovic, A. S. Hillibrand, A. R. Vaccaro, and I. M. Shapiro, 'Differentiation of Mesenchymal Stem Cells Towards a Nucleus Pulposus-Like Phenotype in Vitro: Implications for Cell-Based Transplantation Therapy', *Spine (Phila Pa 1976),* 29 (2004), 2627-32.

149 K. Wuertz, J. P. G. Urban, J. Klasen, A. Ignatius, H. J. Wilke, L. Claes, and C. Neidlinger-Wilke, 'Influence of Extracellular Osmolarity and Mechanical Stimulation on Gene Expression of Intervertebral Disc Cells', *Journal of Orthopaedic Research,* 25 (2007), 1513-22.

150 K. Wuertz, K. Godburn, J. J. MacLean, A. Barbir, J. S. Donnelly, P. J. Roughley, M. Alini, and J. C. Iatridis, 'In Vivo Remodeling of Intervertebral Discs in Response to Short- and Long-Term Dynamic Compression', *Journal of Orthopaedic Research,* 27 (2009), 1235-42.

151 W. C. Hutton, W. A. Elmer, S. D. Boden, S. Hyon, Y. Toribatake, K. Tomita, and G. A. Hair, 'The Effect of Hydrostatic Pressure on Intervertebral Disc Metabolism', *Spine (Phila Pa 1976),* 24 (1999), 1507-15.

152 H. Ishihara, D. S. McNally, J. P. Urban, and A. C. Hall, 'Effects of Hydrostatic Pressure on Matrix Synthesis in Different Regions of the Intervertebral Disk', *J Appl Physiol,* 80 (1996), 839-46.

153 T. T. Tsai, K. G. Danielson, A. Guttapalli, E. Oguz, T. J. Albert, I. M. Shapiro, and M. V. Risbud, 'Tonebp/Orebp Is a Regulator of Nucleus Pulposus Cell Function and Survival in the Intervertebral Disc', *J Biol Chem,* 281 (2006), 25416-24.

154 A. C. Hall, J. P. Urban, and K. A. Gehl, 'The Effects of Hydrostatic Pressure on Matrix Synthesis in Articular Cartilage', *J Orthop Res,* 9 (1991), 1-10.

155 J. J. MacLean, P. J. Roughley, R. D. Monsey, M. Alini, and J. C. Iatridis, 'In Vivo Intervertebral Disc Remodeling: Kinetics of Mrna Expression in Response to a Single Loading Event', *J Orthop Res,* 26 (2008), 579-88.
156 C. Speed, 'Low Back Pain', *BMJ,* 328 (2004), 1119-21.
157 D. L. Wang, S. D. Jiang, and L. Y. Dai, 'Biologic Response of the Intervertebral Disc to Static and Dynamic Compression in Vitro', *Spine (Phila Pa 1976),* 32 (2007), 2521-8.
158 A. Rastogi, P. Thakore, A. Leung, M. Benavides, M. Machado, M. A. Morschauser, and A. H. Hsieh, 'Environmental Regulation of Notochordal Gene Expression in Nucleus Pulposus Cells', *J Cell Physiol,* 220 (2009), 698-705.
159 T. Guehring, A. Nerlich, M. Kroeber, W. Richter, and G. W. Omlor, 'Sensitivity of Notochordal Disc Cells to Mechanical Loading: An Experimental Animal Study', *Eur Spine J,* 19 (2010), 113-21.
160 G. N. Kawchuk, A. M. Kaigle Holm, L. Ekstrom, T. Hansson, and S. H. Holm, 'Bulging of the Inner and Outer Annulus During in Vivo Axial Loading of Normal and Degenerated Discs', *J Spinal Disord Tech,* 22 (2009), 214-8.
161 H.F. Shulte, 'The Characteristics of the Mckibben Artificial Muscle', *The Application of External Power in Prosthetics and Orthotics, National Academy of Sciences Research Council* (1961), 94-115.
162 N.T. Yerkes, and N.M. Wereley, 'Pneumatic Artificial Muscle Activation for Trailing Edge Flaps', *Proceedings of American Institute of Aeronautics and Astronautics* (2007), 1-10.
163 F. Daerden, and D. Lefeber, 'Pneumatic Artificial Muscles: Actuators for Robotics and Automation', *European Journal of Mechanical and Environmental Engineering,* 47 (2002), 11.
164 B.S. Kang, C. S. Kothera, B. K. S. Woods, and N. M. Wereley, 'Dynamic Modeling of Mckibben Pneumatic Artificial Muscles for Antagonistic Actuation', *IEEE International Conference on Robotics and Automation* (2009), 182-87.
165 C. S. Kothera, M. Jangid, J. Sirohi, and N. M. Wereley, 'Experimental Characterization and Static Modeling of Mckibben Actuators', *Jounral of Mechanical Design,* 131 (2009), 091010-1 - 10-10.
166 R.M. Robinson, B. K. S. Woods, R.D. Vocke, C. S. Kothera, and N. M. Wereley, 'High Specific Power Actuators for Robotic Manipulators', *Proceedings of the ASME 2010 Conference on Smart Materials, Adaptive Structures and Intelligent Systems* (2010), 1-10.
167 G. Klute, J. Czerniecki, and B. Hannaford, 'Artificial Muscles: Actuators for Biorobotic Systems', *International Journal of Robotics Research,* 21 (2002), 295-309.
168 J. J. MacLean, C. R. Lee, M. Alini, and J. C. Iatridis, 'The Effects of Short-Term Load Duration on Anabolic and Catabolic Gene Expression in the Rat Tall Intervertebral Disc', *Journal of Orthopaedic Research,* 23 (2005), 1120-27.
169 C. S. Kothera, B. K. S. Woods, J. Sirohi, N. M. Wereley, and P. C. Chen, 'Fluid-Driven Artificial Muscles as Mechanisms for Controlled Actuation', in

Patent Application Publication US 2008/0035798 A1, ed. by U.S. Patent and Trademark Office (US: Techno-Sciences, Inc., Beltsville, MD, 2008).